9th Biennial Workshop on Japan-Kamchatka-Alaska Subduction Processes (JKASP 2016)

Understanding active subduction processes in North Pacific arcs

MAY 31 – JUNE 3, 2016

SCIENTIFIC PROGRAM & ABSTRACTS

GEOPHYSICAL INSTITUTE
UNIVERSITY OF ALASKA FAIRBANKS
FAIRBANKS, ALASKA

Conference Sponsors

Geophysical Institute, University of Alaska Fairbanks
College of Natural Science and Mathematics, University of Alaska Fairbanks

Local Organizing Committee

Jeff Freymueller, Geophysical Institute, University of Alaska Fairbanks
Pavel Izbekov, Geophysical Institute, University of Alaska Fairbanks
John Eichelberger, Graduate School, University of Alaska Fairbanks

Cheryl Cameron, Alaska Division of Geological & Geophysical Surveys
Michelle Coombs, Alaska Volcano Observatory, USGS
David Fee, Geophysical Institute, University of Alaska Fairbanks
Taryn Lopez, Geophysical Institute, University of Alaska Fairbanks
Jessica Larsen, Geophysical Institute, University of Alaska Fairbanks
Dmitry Nicolsky, Geophysical Institute, University of Alaska Fairbanks
John Power, Alaska Volcano Observatory, USGS
Natalia Ruppert, Geophysical Institute, University of Alaska Fairbanks
Janet Schaefer, Alaska Division of Geological & Geophysical Surveys
Elena Suleimani, Geophysical Institute, University of Alaska Fairbanks
Kristi Wallace, Alaska Volcano Observatory, USGS
Peter Webley, Geophysical Institute, University of Alaska Fairbanks
Michael West, Geophysical Institute, University of Alaska Fairbanks

Technical Support*

Lea Gardine (logistics)
Kimberly Cummins (visa support)

** all at the Geophysical Institute, University of Alaska Fairbanks*

TABLE OF CONTENTS Page

SCIENTIFIC PROGRAM

MONDAY, MAY 30

On-site registration and ice-breaker — **IARC lobby, 16:00-19:00**

Hosts: Jeff Freymueller and Pavel Izbekov; registration: Lea Gardine

16:00 Registration opens

17:00 Ice-breaker starts

TUESDAY, MAY 31

On-site registration and morning coffee — **REIC lobby, 07:00 – 08:00**

07:00 On-site registration continues

07:30 Breakfast

PLENARY SESSION

Welcoming remarks — **REIC 201, 08:00 – 08:40**

08:00 Introduction: Jeff Freymueller

08:10 Welcome: Robert McCoy, Director of the Geophysical Institute

08:20 Welcoming remarks from John Eichelberger (UAF), Evgenii Gordeev (Institute of Volcanology and Seismology), and Minoru Kasahara (Hokkaido University)

Keynote Talk — **REIC 201, 08:40 – 09:00**

08:40 David W. Scholl, Stephen H. Kirby, and Roland Von Huene BASED ON GLOBAL OBSERVATIONS, TWO REASONS WHY THE ALEUTIAN-ALASKA SUBDUCTION ZONE IS PRONE TO RUPTURE IN GREAT (> Mw8.0) MEGATHRUST EARTHQUAKES

TECHNICAL SESSIONS

Seismology (Oral presentations) — **REIC 201, 09:00 – 10:00**

Chairs: Mike West and Matt Haney

09:00 Stephen R. McNutt, Glenn Thompson, Jochen Braunmiller, and Stephen Holtkamp PEAK RATES AND LARGEST MAGNITUDE EVENTS IN EARTHQUAKE SWARMS FROM DIFFERENT TECTONIC SETTINGS

09:20 Hiroaki Takahashi, Mako Ohzono, Koji Minato, Noritoshi Okazaki, Takahiro Suzuki, Tetsuya Takahashi, Fujio Akita MAGMA, THERMAL STRUCTURE, STRAIN CONCENTRATION AND ACTIVE SEISMICITY IN KUSSHARO CALDERA, HOKKADIO, JAPAN

09:40 Nikolai Shapiro, Dmitry Droznin, Svetlana Droznina, Victor Chebrov, Evgeny Gordeev, William Frank THE REVEALING OF THE VOLCANIC ACTIVITY FOR KLYUCHEVSKAYA GROUP OF VOLCANOES FROM CONTINUOUS SEISMIC RECORDS

10:00 Coffee break

Seismology (Oral presentations), continued **REIC 201, 10:20 – 12:00**

Chairs: Hiroaki Takahashi and John Lyons

10:20 Alexandra K. Farrell and Stephen R. McNutt SEISMIC ATTENUATION, TIME DELAYS AND RAYPATH BENDING OF TELESEISMS BENEATH CERRO UTURUNCU, BOLIVIA

10:40 Matthew M. Haney, Victor C. Tsai, Kevin M. Ward WIDESPREAD IMAGING OF THE LOWER CRUST, MOHO, AND UPPER MANTLE BENEATH ALASKA FROM RAYLEIGH WAVES

11:00 Stephen Holtkamp USING EARTHQUAKES TO PROBE SUBDUCTION MEGATHRUST BEHAVIOR: A LOOK AT EARTHQUAKE SWARMS AND REPEATING EARTHQUAKES IN ALASKA

11:20 Anna Skorkina, Alexander Gusev CORNER FREQUENCIES OF SOURCE SPECTRA OF MODERATE SUBDUCTION-ZONE EARTHQUAKES OBSERVED NEAR THE AVACHA BAY, KAMCHATKA

12:00 Lunch

Seismology (Oral presentations), continued **REIC 201, 13:00 – 14:40**

Chairs: John Power and Hiroaki Takahashi

13:00 Mako Ohzono, Hiroaki Takahashi, Nikolay V. Shestakov, Guojie Meng, Mikhail. D. Gerasimenko ESTIMATION OF THE LONG-TERM EFFECT OF VISCOELASTIC RELAXATION INDUCED BY THE 2011 TOHOKU EARTHQUAKE AND OTHER INTERPLATE EARTHQUAKES AROUND NORTHEASTERN ASIA

13:20 John J. Lyons, Matthew M. Haney, Cynthia Werner, Peter Kelly, Matthew Patrick, Christoph Kern, and Frank Trusdell LONG PERIOD SEISMICITY AND VERY LONG PERIOD INFRASOUND DRIVEN BY SHALLOW MAGMATIC DEGASSING AT MOUNT PAGAN, MARIANA ISLANDS

13:40 Matthew M. Haney, Robin Matoza, David Fee, David F. Aldridge SEISMIC EQUIVALENTS OF INFRASONIC SCALING LAWS FOR VOLCANIC JETS AND ACOUSTIC MULTIPOLES

14:00 Cassandra M. Smith, Stephen R. McNutt, Glenn Thompson QUANTIFYING GROUND COUPLED AIR WAVES TO DETERMINE GAS FLUX AT PAVLOF VOLCANO, ALASKA, DURING THE 2007 ERUPTION

14:20 Michael West, Matt Gardine, Natalia Ruppert, Carl Tape, Jeffrey Freymueller, Stephen Holtkamp PERSPECTIVES ON THE M_W7.1 INISKIN EARTHQUAKE

14:40 Coffee break

Tectonics and experiments (Oral presentations) REIC 201, 15:00 – 16:20

Chair: Jeff Freymueller

15:00 Jeff Freymueller PLATE BOUNDARIES IN THE NORTH PACIFIC

15:20 Higashi Uchida STRAINMETER ARRAY OBSERVATION OF THE DIKE INTRUSION AT SAKURAJIMA VOLCANO ON 15 AUGUST 2015

15:40 Johan Gilchrist and Mark Jellinek SEDIMENT WAVES AND CLOUD LAYERING IN EXPLOSIVE VOLCANIC ERUPTIONS: EVIDENCE FROM ANALOGUE EXPERIMENTS

16:00 Shanshan Li, Jeff Freymueller, Natalia Ruppert, Jianjun Wang CORRELATION STUDY OF COULOMB STRESS CHANGE IMPARTED BY TWO NEW SLOW SLIP EVENTS AND SEISMIC RATE CHANGE IN LOWER COOK INLET OF THE ALASKA-ALEUTIAN SUBDUCTION ZONE

WEDNESDAY, JUNE 1

Morning coffee and informal discussions REIC lobby, 07:30 – 08:00

07:30 Breakfast.

TECHNICAL SESSIONS

Geology & Petrology & Geochemistry (Oral presentations) REIC 201, 08:00 – 10:00

Chairs: Michelle Coombs and Kirsten Nicolaysen

08:00 Izumi Yokoyama ORIGIN OF CALDERAS: COLLAPSES OR EXPLOSIONS?

08:20 Maxim Portnyagin, Kaj Hoernle, Reinhard Werner, Boris Baranov, Gene Yogodzinski and BERING participants BERING - A NEW INTERNATIONAL MARINE RESEARCH PROJECT TO INVESTIGATE THE MAGMATIC AND TECTONIC EVOLUTION OF THE BERING SEA AND ITS MARGINS

08:40 Kirsten Nicolaysen, Dixie West, Virginia Hatfield, Breanyn MacInnes, Mitsuru Okuno, Arkady Savinetsky, Olga Krylovich, Pavel Izbekov, Lyman Persico, John Lyons, Max Kaufman, Christina Neal, William E. Scott, John Power A CASE FOR INTEGRATED GEOSCIENCE AND ARCHEOLOGICAL STUDIES IN THE ALEUTIAN ARC

09:00 Owen K. Neill, Christopher J. Nye EVIDENCE FOR MAGMA MIXING AND RAPID MAGMATIC ASCENT IN GROUNDMASS GLASS COMPOSITIONS FROM THE 2008 ERUPTION OF KASATOCHI, CENTRAL ALEUTIAN ISLANDS

09:20 Taryn Lopez, Tobias Fischer, Andrea Rizzo ISOTOPIC CONSTRAINTS ON VOLATILE CYCLING WITHIN THE ALEUTIAN ARC

09:40 Alex M. Iezzi, Douglas M. Thompson, Beverly Chomiak LAHAR INUNDATION MODELING WITH THE AID OF HISTORIC FLOW DEPOSITS AT REDOUBT VOLCANO, COOK INLET, ALASKA

10:00 Coffee break

Geology & Petrology & Geochemistry (Oral presentations) **REIC 201, 10:00 – 12:00**

Chairs: Taryn Lopez and Pavel Izbekov

10:20 Michelle Coombs and Brian Jicha GEOLOGY AND $^{40}AR/^{39}AR$ GEOCHRONOLOGY OF LONG-LIVED AKUTAN VOLCANO, EASTERN ALEUTIAN ISLANDS

10:40 Daniel Rasmussen, Terry Plank, Amanda Lough, Pete Stelling, Diana Roman PETROLOGIC CHRONOLOGY OF THE 1999 SUB-PLINIAN ERUPTION OF SHISHALDIN VOLCANO

11:00 Sam H. Sheffer, Virginia Hatfield, Kirsten Nicolaysen, Thomas Bartlett III, Dixie West, Emily Deacon, Kale Bruner SOURCING PREHISTORIC OBSIDIAN TOOLS IN THE ISLANDS OF FOUR MOUNTAINS, ALASKA

11:20 Alexander Proussevitch, Pavel Izbekov, Dork Sahagian THE RELATION BETWEEN PRE- FRAGMENTATION BUBBLE SIZE DISTRIBUTION, ASH PARTICLE MORPHOLOGY, AND THEIR INTERNAL DENSITY: IMPLICATIONS TO VOLCANIC ASH TRANSPORT AND DISPERSION MODELS

11:40 O.V. Bergal-Kuvikas, V.L. Leonov, A.N. Rogozin, I.N. Bindeman, E.S. Kliapitskiy NEW DISCOVERED LATE MIOCENE VERCHNEAVACHINSKAY CALDERA ON EASTERN KAMCHATKA (UPSTREAM OF LEVAYA AVACHA AND KAVYCHA RIVERS): GEOLOGY, BOUNDARY AND COMPOSITION

12:00 Lunch

Geology & Petrology & Geochemistry (Oral presentations) **REIC 201, 13:00 – 13:40**

Chairs: Taryn Lopez and Pavel Izbekov

13:00 Cheryl Cameron, Katherine Mulliken, Janet Schaefer, Kristi Wallace, Scott Crass ALASKA TEPHRA DATABASE

13:20 Jessica F. Larsen, Janet R. Schaefer, James W. Vallance PETROLOGY AND GEOCHEMISTRY OF THREE EARLY HOLOCENE ERUPTIONS FROM MAKUSHIN VOLCANO, ALASKA

Interdisciplinary poster session **REIC lobby, 14:40 – 17:00**

Presiding: Jeff Freymueller and Pavel Izbekov

Coffee will be served at 14:40.

1 Celso R. Alvizuri and Carl Tape FULL MOMENT TENSOR AND SOURCE-TYPE ESTIMATION FOR VOLCANIC EVENTS

2 Ophelia George, Joan L. Latchman, Charles Connor, Stephen McNutt, Laura Connor GENERATING DYNAMIC VOLCANIC HAZARD MAPS FOR DOMINICA, LESSER ANTILLES BY USING GEOPHYSICAL DATA AS WEIGHTS IN SPATIAL INTENSITY MAPS

3 A.V. Kiryukhin, S.A. Fedotov, P.A. Kiryukhin GEOMECHANICAL INTERPRETATION OF LOCAL SEISMICITY CONCERNING ACTIVITY OF TOLBACHIK, KORYAKSKY AND AVACHINSKY VOLCANOES OF KAMCHATKA IN 2008-2012

4 Vipul Silwal and Carl Tape SEISMIC MOMENT TENSORS AND ESTIMATED UNCERTAINTIES IN SOUTHERN ALASKA SUBDUCTION ZONE

5 Michael West, Natalia Ruppert, Natalia Kozyreva, Sara Meyer, Dara Merz, Miriam Braun TRACKING GLACIERS WITH THE ALASKA SEISMIC NETWORK

6 Yusuke Yamashita, Masanao Shinohara, Tomoaki Yamada, Kazuo Nakahigashi , Hajime Shiobara, Kimihiro Mochizuki, Takuto Maeda, Kazushige Obara LONG-TERM OCEAN BOTTOM MONITORING OF SLOW EARTHQUAKES ON THE SHALLOW PLATE INTERFACE IN HYUGA-NADA, WESTERN PART OF THE NANKAI TROUGH

7 Noritoshi Okazaki, Ryo Takahashi, Makoto Tamura, Hiroaki Takahashi, Masayoshi Ichiyanagi, Teruhiro Yamaguchi, Ryo Honda, Yosuke Miyagi, Akimichi Takagi GRAVITY DECREASE AND VOLCANIC INFLATION AROUND THE ACTIVE CRATER AT TOKACHI-DAKE VOLCANO, HOKKAIDO, JAPAN

8 S.S. Serovetnikov, E.I. Gordeev, Hiroaki Takahashi, Pavel Izbekov THE KLUCHEVSKAYA VOLCANO GROUP OBSERVATION NETWORK 2006-2016. RUSSIA, KAMCHATKA.

9 Nikolay Shestakov, Grigory Nechaev, Nikolay Titkov, Mikhail Gerasimenko, Victor Bykov, Victor Pupatenko, Sergey Serovetnikov, Alexander Prytkov, Nikolay Vasilenko, Dmitry Sysoev, Alexey Sorokin, Hiroaki Takahashi and Mako Ohzono HAVE THE POSTSEISMIC MOTIONS DUE TO THE MAY 24, 2013 Mw 8.3 OKHOTSK DEEP FOCUS EARTHQUAKE BEEN DISCOVERED BY THE RUSSIAN FAR EAST GNSS NETWORKS?

10 Natalia Gorbach, Maxim Portnyagin, Tatiana Philosofova COMPOSITIONAL TRENDS OF AMPHIBOLE IN 2001-2013 YOUNG SHIVELUCH ANDESITES AS EVIDENCE OF MAGMA CHAMBER REPLENISHMENT AND SUBSEQUENT CONVECTION

11 Natalia Gorbach, Anastasiya Plechova , Dmitry Melnikov and Sergey Samoilenko LANDSLIDE AT ZHUPANOVSKY VOLCANO (KAMCHATKA) IN JULY 2015: DISTRIBUTION OF THE DEPOSITS AND POTENTIAL PRECURSORS

12 Kosuke Ishige, Mitsuhiro Nakagawa, Seiko Yamasaki, Akikazu Matsumoto GEOLOGY AND PETROLOGY OF TAISETSU VOLCANO GROUP, JAPAN; EVOLUTION OF MAGMA AND ACTIVITY AGES.

13 Olga Khubaeva and Antonina Nikolaeva THERMAL SUPPLY OF HYDROTHERMAL SYSTEM, A CASE STUDY OF THE BOGDANOVICH VOLCANIC CENTER HYDROTHERMAL SYSTEM (PARAMUSHIR ISLAND, THE KURIL ISLANDS)

14 Olga Khubaeva, Pavel Izbekov, Sergey Samoylenko, and John Eichelberger MUTNOVSKY AND GORELY VOLCANOES IN KAMCHATKA: A PERFECT CLASSROOM FOR TEACHING VOLCANOLOGY

15 Heather Miller, Jake Roush, Taryn Lopez, Tobias Fischer, Matt Schrenk FIRE AND LIFE: MICROBIAL MEDIATION OF DEEP CARBON CYCLING ALONG THE “RING OF FIRE”, A SUBDUCTING OCEANIC LITHOSPHERE, WESTERN ALEUTIAN ISLANDS

16 Mitsuhiro Nakagawa THE EFFECT OF THE AD 1611SANRIKU EARTHQUAKE ON VOLCANIC ACTIVITY IN HOKKAIDO, JAPAN

17 A.G. Nikolaeva, G.A. Karpov, A.F. Sashenkova SUMMARY OF 20-YEARS' SURVEY OF MINERAL COMPOSITION OF THE KARYMSKOYE CALDERA LAKE AFTER ITS 1996 HAZARDOUS ERUPTION

18 A.N. Rogozin, V.L. Leonov NEW DATA ON THE EOPLEISTOCENE CATASTROPHIC CALDERA-FORMING ERUPTION IN KAMCHATKA

19 Dmitry Savelyev, Olga Savelyeva , Maxim Portnyagin FRAGMENTS OF CRETACEOUS SEAMOUNTS IN ACCRETIONARY STRUCTURE OF THE KAMCHATSKY MYS PENINSULA (KAMCHATKA, RUSSIA)

20 Chiharu Tomijima, Mitsuhiro Nakagawa GEOLOGICAL STUDY ON CALDERA-FORMING ERUPTION OF SHIKOTSU VOLCANO, SOUTH-WESTERN HOKKAIDO : SPECIAL REFERENCE TO VENT FORMATION PROCESS AND MAGMA SYSTEM

21 Anna Volynets, Maria Pevzner, Andrey Babansky GEOCHEMISTRY OF NEOGENE-QUATERNARY MAGMATISM OF THE SOUTHERN PART OF SREDINNY RANGE, KAMCHATKA

22 Victor N. Chebrov, Anna A. Skorkina, Danila V. Chebrov, Dmitry V. Droznin, Dmitry A. Ototuk REAL-TIME EARTHQUAKE MONITORING FOR TSUNAMI WARNING IN KAMCHATKA DURING 2011-2015

23 Kei Ioki, Yuichiro Tanioka, Gentaro Kawakami, Yoshihiro Kase, Kenji Nishina, Wataru Hirose, Satoshi Ishimaru, Hideaki Yanagisawa TSUNAMI SIMULATION AND LANDSLIDE MODEL OF THE 1741 OSHIMA-OSHIMA ERUPTION

24 Yoshihiro Kase, Keiichi Hayashi, Gentaro Kawakami, Kenji Nishina, Atsushi Urabe, Yasuhiro Takashimizu CHARACTERIZATION OF ELECTRIC CONDUCTIVITY, PH, AND ORGANIC-WALLED MICROFOSSILS FOR IDENTIFYING TSUNAMI DEPOSITS: AN EXAMPLE OF MODERN TSUNAMI AND PALEOTSUNAMI DEPOSITS IN PACIFIC COAST LOWLANDS, HOKKAIDO AND TOHOKU, JAPAN

25 Olga Girina, Evgenii Gordeev, Alexander Manevich, Dmitry Melnikov, and Anton Nuzhdaev 2015-2016 ACTIVITY OF KAMCHATKAN AND NORTHERN KURILES VOLCANOES (RUSSIA) AND DANGER TO AVIATION

26 Hiroki Miyamachi, Koshun Yamaoka, Hiroshi Yakiwara, Yuta Maeda, Toshiki Watanabe, Takahiro Kunitomo, Takeshi Tameguri3, Masato Iguchi TEMPORAL VARIATION OF THE ACROSS SIGNALS DURING A PERIOD FROM JANUARY TO AUGUST, 2015 IN SAKURAJIMA VOLCANO, JAPAN.

27 Hugh Harper and Jeff Freymueller REVISITING COSEISMIC AND POSTSEISMIC DEFORMATION FROM THE 2002 DENALI, ALASKA EARTHQUAKE

THURSDAY, JUNE 2

EXCURSION

Field excursion to Chena Hot Springs	**09:00 – 22:00**

09:00 Bus picks up participants at the southern entrance to the Reichardt Building. Ride to the hot springs, on-bus discussions.

10:00 Arrival to the hot springs. Visit to hydrothermal power plant and other local attractions.

12:00 Lunch (boxes)
13:00 Discussions continue in the hot springs
17:30 Dinner at the Chena Hot Springs restaurant
20:30 Bus ride back to Fairbanks

FRIDAY, JUNE 3

TECHNICAL SESSIONS

Morning coffee **REIC lobby, 07:30 – 08:00**

07:30 Breakfast.

Volcano Monitoring (Oral presentations) **REIC 201, 08:00 – 10:00**

Chairs: Peter Webley and Taryn Lopez

08:00 John Lyons, Matthew Haney, David Fee, Cindy Werner, Christoph Kern, Diana Roman, and John Power RECENT ADVANCES IN GEOPHYSICAL MONITORING AT MOUNT CLEVELAND VOLCANO, ALASKA

08:20 Alex M. Iezzi, Hans F. Schwaiger, David Fee, Matthew Haney CONSTRAINING THE SPATIAL AND TEMPORAL VARIABILITY OF ATMOSPHERIC CONDITIONS TO EXPLORE THE INFRASOUND DETECTION OF VOLCANIC ERUPTIONS IN ALASKA

08:40 Kathleen McKee, David Fee, Akihiko Yokoo, Robin Matoza ANALYSIS OF FUMAROLE ACOUSTICS AT ASO VOLCANO, JAPAN

09:00 Jonathan Dehn, Peter Webley, and Anna Worden ERUPTION TRENDS IN THE KURILE, KAMCHATKA, AND ALASKAN ARCS

09:20 Shigeki Tasaka, Masaya Matsubara, Yasuhiro Asai, and Fumiaki Kimata INCREASING OF GAS BUBBLINGS AT WARIISHI FLOWING SPRING, CENTRAL JAPAN, PRIOR TO THE 2014 ONTAKE VOLCANO ERUPTION

09:40 P. W. Webley, O. Girina, J. S. Shipman REMOTE SENSING ANALYSIS OF THE 2015-2016 SHEVELUCH VOLCANO ACTIVITY

10:00 Coffee break

Volcano Monitoring (Oral presentations) continued **REIC 201, 10:20 – 12:00**

Chairs: Peter Webley and Taryn Lopez

10:20 David Fee, Matt Haney, Robin Matoza, Dave Schneider, Peter Cervelli, Alex Iezzi INFRASOUND AND SEISMIC OBSERVATIONS OF THE MARCH 2016 ERUPTION OF PAVLOF VOLCANO, ALASKA

10:40 P. Webley, J. Dehn, M. Harrild, A. Worden, D. McAlpin THERMAL REMOTE SENSING AND ASH DISPERSION MODELING OF THE 2016 ERUPTION OF PAVLOF VOLCANO

11:00 Taishi Yamada, Hiroshi Aoyama, Takeshi Nishimura, Masato Iguchi, Muhamad Hendrasto ESTIMATION OF VOLUME FLUX OF VOLCANIC ERUPTIONS WITH VERY-LONG-PERIOD ACOUSTIC SIGNALS

11:20 Ryo Tanaka, Takeshi Hashimoto, Tsuneo Ishido, Nobuo Matsushima NUMERICAL MODEL OF TEMPORAL CHANGES IN MAGNETIC TOTAL FIELD AND GROUND DEFORMATION DUE TO HYDROTHERMAL SYSTEM IN VOLCANOES (1). - A CASE STUDY ON TOKACHI-DAKE VOLCANO, JAPAN

11:40 Rui Fernandes, Machiel Bos, Rafael Couto, Jeff Freymueller, and Maksim Tretyakov EVALUATING THE INFLUENCE OF DATA GAPS IN THE ANALYSIS OF POSITION TIME-SERIES DERIVED FROM GPS CONTINUOUS STATIONS

12:00 Lunch

Tsunami (Oral presentations) REIC 201, 13:00 – 13:40

13:00 Dmitry Nicolsky, Elena Suleimani, Jeffrey Freymueller and Richard Koehler HYPOTHETICAL TECTONIC TSUNAMI SOURCES ALONG THE EASTERN ALEUTIAN ISLAND ARC AND ALASKA PENINSULA FOR INUNDATION MAPPING AND HAZARD ASSESSMENT

13:20 Elena Suleimani, Dmitry Nicolsky, Rich Koehler REGIONAL TSUNAMI HAZARD MAP FOR COMMUNITIES ON ALEUTIAN ISLANDS AND ALASKA PENINSULA

Discussion, concluding remarks and wrap up REIC 201, 13:40 – 14:40

Presiding: Jeff Freymueller, John Eichelberger, Minoru Kasahara, and Evgenii Gordeev

14:40 Coffee break

Additional time for focused group meetings and discussions REIC 201, 14:40 – 17:30

Farewell dinner on the Tanana Chief Riverboat 17:30 – 21:00

17:30 Depart for farewell dinner on the riverboat. Bus picks up participants at the southern entrance to the Reichardt Building. Local participants are encouraged to use their own transportation.

21:00 Bus ride back to the Reichardt Building.

Adjourn!

Katmai trip starts next morning!

ABSTRACTS

Keynote Talk

BASED ON GLOBAL OBSERVATIONS, TWO REASONS WHY THE ALEUTIAN-ALASKA SUBDUCTION ZONE IS PRONE TO RUPTURE IN GREAT (≥ Mw8.0) MEGATHRUST EARTHQUAKES

David W. Scholl[1,2], Stephen H. Kirby[1] Roland von Huene[1]
[1] U.S. Geological Survey, Emeritus, Menlo Park, California 94025, USA
[2] Department of Geology and Geophysics, Emeritus, University of Alaska Fairbanks, Fairbanks, Alaska 99775, USA

INTRODUCTION

Wonderments have long been expressed about the influence, if any, geologic factors have on the occurrence and non-occurrence areas of high-magnitude great (≥Mw8.0), giant (≥Mw8.5) and supergiant (≥Mw9.0) megathrust earthquakes. A large base of global observations, one that grew rapidly in the past 12 years, identifies two significant factors that respectively (1) inhibit and (2) favor high-magnitude rupturing. Both involve smoothness attributes of the subducting surface of the underthrusting oceanic plate. These are, respectively,

(1) **Inhibiting Factor**, the underthrusting of high, areally large bathymetric relief hinders rupture continuation and the generation of high-magnitude megathrust earthquakes (see, for example, *Wang, K., and Bilek, S.L., 2014, Fault creep caused by subduction of rough seafloor relief: Tectonophysics, v. 610, p. 1–24*), and,

(2) **Favoring Factor**, underthrusting thick sediment and/or bathymetric smooth seafloor promote rupture continuation and the generation of high-magnitude megathrust earthquakes. Based on a small and inaccurate data base, The smoothness factor was first explored by Ruff (*1989, Do trench sediments affect great earthquake occurrence in subduction zones?: Pure and Applied Geophysics, v. 129, p. 263–282*). A relationship was recognized but was not statistically compellingly.

CHECKING OUT THE SMOOTHNESS FACTOR

A newly compiled and much larger global base of well-vetted observations now statistically supports the posit that high-magnitude megathrust earthquakes are favored to occur where the underthrusting seafloor is:

(1) made smooth by a thick blanket of subducting, relief-smothering sediment or

(2) by an expanse of seafloor that is bathymetrically smooth (*Scholl et al., 2015. Great (≥Mw8.0) megathrust earthquakes and the subduction of excess sediment and bathymetrically smooth seafloor, Geosphere: v. 11, no. 2, p. 236–265*).

Smoothing is effected, perhaps dominantly, by the subduction of a trench-axis sediment section thicker than ~1km. Where the thickness is much thinner, smoothing can be produced by the underthrusting of low basement relief and where augmented by a subduction channel thickened by forearc subduction erosion (Fig. 1).

Figure 1: Megathrust Magnitude vs Thickness of Subducting Sediment

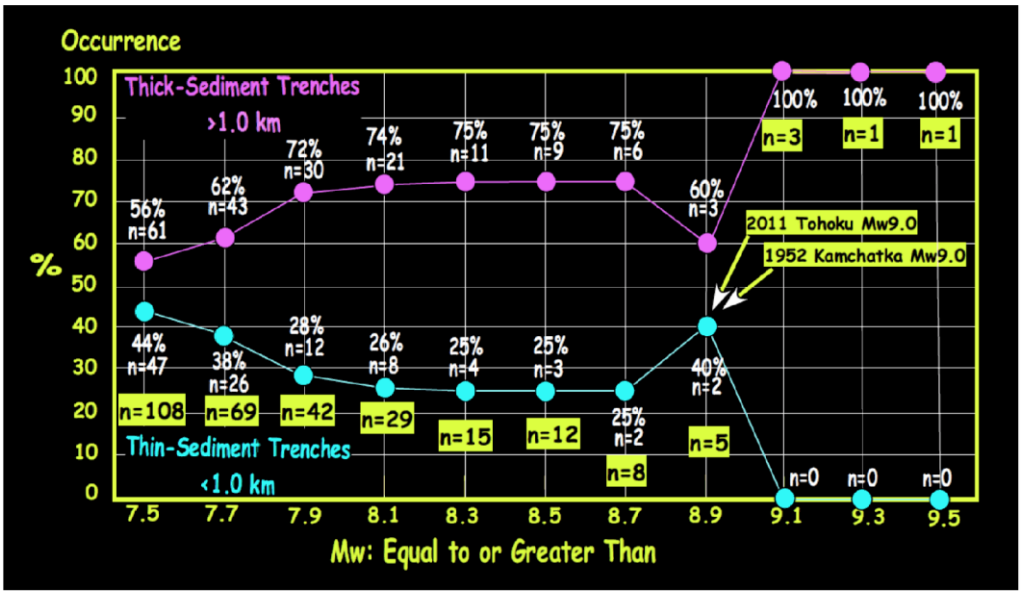

Relative occurrence percent of instrumentally recorded megathrust earthquakes of magnitude equal to or greater than Mw7.5 for thick- and thin-sediment trenches. Occurrence percent is ~normalized (corrected) for different global trench lengths (thin = ~19,000 km, thick =~7800 km). Tohoku and Kamchatka Mw9.0 events reflect regionally smooth subducting seafloor and active subduction erosion

IMPLICATIONS FOR ALEUTIAN-ALASKA SUBDUCTION ZONE

Both factors work together to favor the common rupturing of high-magnitude megathrust earthquake along the Aleutian-Alaska subduction zone. Inhibiting factor 1, subducting rupture-hindering relief, is principally located at widely spaced fracture zones and the seamount provinces of the Gulf of Alaska (Fig. 2). Favoring factor 2, subduction of thick sediment, is provided by glaciated Alaskan drainages that charged the trench axis with a ~2 km thick sediment body from the eastern end of the Alaska trench westward along much of the length of the Aleutian Trench. Active subduction erosion also further thickens and smooths the subduction channel separating the Pacific and North American plates.

It is worth noting that characteristically intra-oceanic subduction zones, e.g., the Izu-Bonin-Mariana (IBM) and Tonga-Kermadec arc-trench systems, are not prone to rupture in great megathrust earthquakes. The trenches of these subduction zones are only thinly sedimented and they are entered by large, rupture-inhibiting bathymetric elements, in particular the IBM system. The circumstance that the Aleutian-Alaska trench axis is charged with sediment between widely space bathymetric elements are prominent contributors to the repeated nucleation of great megathrust earthquakes that commonly generate destructive near and far-field tsunamis.

Figure 2. High-magnitude megathrust earthquakes repeatedly nucleate along the Aleutian-Alaska subduction zone, which is thickly charged with subducting sediment between widely spaced, large bathymetric elements entering the subduction zone.

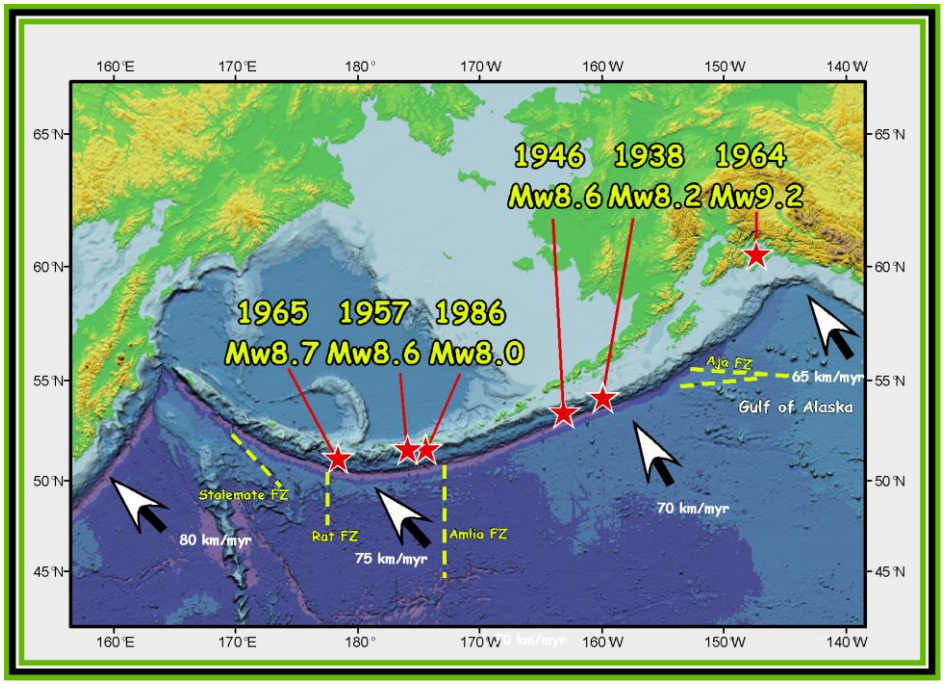

SEISMOLOGY

(Oral presentations)

PEAK RATES AND LARGEST MAGNITUDE EVENTS IN EARTHQUAKE SWARMS FROM DIFFERENT TECTONIC SETTINGS

Stephen R. McNutt[1], Glenn Thompson[1], Jochen Braunmiller[1], Stephen Holtkamp[2]
[1]*School of Geosciences, University of South Florida, Tampa, FL, USA*
[2]*Geophysical Institute, University of Alaska Fairbanks, Fairbanks, AK, USA.*

We present results of recent studies of earthquake swarms from local data at volcanoes, and teleseismic data from MOR and volcanic regions, with the focus on identifying diagnostics. One clear pattern for local volcanic swarms is that peak rates often occur early, whereas the largest M event occurs late. Using a dataset of 20 swarms from the literature, swarm durations ranged from 12 h to 180 d, measured from swarm onset to eruption onset. Data were normalized to % duration. Peak rates occurred from 1-42 % of the way through swarms (with 2 outliers), whereas the largest M event occurred from 32-99 % of the way through. Additional evidence from 4 cases suggests that the seismic source size grows systematically, especially for events with similar waveforms (families). This is revealed in plots of M or amplitude versus time for event families. For comparison, 19 cases of mid-ocean ridge swarms and 67 cases of teleseismic volcanic swarms were analyzed. The MOR data show durations of 1-42 d, with peak rates occurring 1-24 % of the way through and largest M occurring 1-87 % of the way through. In 6 cases largest M occurs before or at the same time as peak rate. The teleseismic volcanic data show durations of <1 to 577 d, with peak rates occurring 1 to 100 % of the way through and largest M occurring 1-100 % of the way through. Thus the patterns for MOR and teleseismic volcanic swarms are similar to each other but differ significantly from that for local volcanic swarms. Further work on volcanic swarms shows that the distribution of seismicity before the peak rate differs from after, suggesting two dominant processes. The durations of post-peak portions are roughly proportional to the peak rates. This is similar to the behavior of aftershock sequences and suggests that diffusion is a controlling process. The portions of the swarms prior to the peaks behave differently, however. These may represent the invasion of hot fluids and the opening or reopening of cracks prior to magma intrusion. We infer that the growth in event size reflects activation of a preferred magma pathway. Recognition of such patterns, linked to processes, may help to improve monitoring and reduce risks from eruptions. Comparison is recommended between the patterns observed here and those associated with induced seismicity from fracking and deep well injection.

MAGMA, THERMAL STRUCTURE, STRAIN CONCENTRATION AND ACTIVE SEISMICITY IN KUSSHARO CALDERA, HOKKADIO, JAPAN

Hiroaki Takahashi[1], Mako Ohzono[1], Koji Minato[2], Noritoshi Okazaki[3], Takahiro Suzuki[3], Tetsuya Takahashi[3], Fujio Akita[3]

[1]Institute of Seismology and Volcanology, Hokkaido University, Sapporo, Japan.
[2] Muroran Local Meteorological Office, Japan Meteorological Agency, Japan.
[3]Geological Survey of Hokkaido, Sapporo, Japan.

The Kussharo caldera in eastern Hokkaido is one of the largest active caldera of Japan with 26 by 20km diameters. Caldera formation had been occurred since 0.34 to 0.03Ma. Post-caldera volcanism of active doming and smaller caldera formation has been continued. Magneto-telluric surveys revealed magma body of about 10km diameter in uppermost crust of deeper than 7km (Honda et al., 2011). InSAR analysis detected unrest volcanic uplift of 25cm and successive subsidence with seismic activation during 1993-1998 (Geographical Survey Institute of Japan. 2006). Inflation and deflation of assumed magma body well explained this crisis. These facts suggested the magma have potential for future major activity.

Active seismicity inner caldera has been also recorded. Four tectonic M>6 events occurred concentrating in southwestern rim of caldera. Seismicity level of this caldera is highest in Hokkaido. Nationwide strain rate map estimated by the Japanese nationwide continuous GNSS network operated by Geospatial Information Authority of Japan (GEONET) clearly indicated this caldera is one of the highest strain rate zone over Japanese Islands with 3-07/yr. High density GNSS observation network deployed in caldera also suggested high strain rate and spatial complex strain field. Observed strain field might be due to multiple interaction of tectonic strain generated by plate coupling along Kuril trench and volcanic activity.

Separation of tectonic and volcanic factors is required to evaluate crustal activity. Inhomogeneous crustal structure might be one of control factor for heterogeneous strain field due to tectonic process. Caldera basin structure of 4km deep filled by soft volcanic sediments was confirmed by dense gravity surveys (Honda et al., 2011). Magma body in upper crust is also important inhomogeneous element. Effects of these physical foreign materials in crust for strain field were evaluated by FEM modeling. Boundary condition of regional strain field driven by plate coupling along Kuril trench was assumed. Simulation suggested a magma body in uppermost crustal medium generated little influence to strain field on earth's surface. Caldera basin, however, could cause strain concentration. These results suggested strain concentration observed on caldera surface might be primary due to caldera basin structure. Analysis with both caldera structure and a magma body implied stress concentration between caldera basin and a magma body.

Thermal structure could control deformation style of rock, brittle-ductile transition depth in upper crust and strength of rock failure. Subsurface temperature structure in this caldera had been evaluated using well-based thermal gradient data. Maximum 8degree/100m thermal gradient was observed in caldera center and 4degree/100m outside. Depth profile of brittle and creep strength under hydrostatic regime implied very thin elastic layer of less than 4km thick. Epicenters of past medium earthquakes were concentrated at the edge of caldera, and might suggest possible thermal structure controlling. Stress rate value estimated from FEM simulation was about 0.02MPa/yr, and significantly smaller than strength of rock failure. Mechanism for strength weakening, e.g. existence of high pressure liquid in uppermost crust, is required to explain active tectonic seismicity in this caldera.

THE REVEALING OF THE VOLCANIC ACTIVITY FOR KLYUCHEVSKAYA GROUP OF VOLCANOES FROM CONTINUOUS SEISMIC RECORDS

Nikolai Shapiro[1,2], Dmitry Droznin[3], Svetlana Droznina[3], Victor Chebrov[3], Evgeny Gordeev[2], William Frank[1]

[1] *Institute de Physique du Globe de Paris, Paris, France*

[2] *Institute of Volcanology and Seismology, Petropavlovsk- Kamchatsky, Russia*

[3] *Geophysical Survey, Petropavlovsk-Kamchatsky, Russia*

We analyze continuous seismic records from 18 permanent stations operated in vicinity of the Klyuchevskoy group of volcanoes (Kamchatka, Russia) during the period between 2009 and 2014. We explore the stability of the inter-station cross-correlation to detect different periods of sustained emission from seismic energy. The main idea of this approach is that cross-correlation waveforms computed from a wavefield emitted by a seismic source from a fixed position remain stable during the period when this source is acting. The detected periods of seismic emission correspond to different episodes of activity of volcanoes: Klyuchevskoy, Tolbachik, Shiveluch, and Kizimen. For Klyuchevskoy and Tolbachik whose recent eruptions are mostly effusive, the detected seismic signals correspond to typical volcanic tremor, likely caused by degassing processes. For Shiveluch and Kizimen producing more silicic lavas, the observed seismic emission often consists of many repetitive long period (LP) seismic events that might be related to the extrusion of viscous magmas. We develop an approach for automatic detection of these individual LP events in order to characterize variations of their size and recurrence in time.

SEISMIC ATTENUATION, TIME DELAYS AND RAYPATH BENDING OF TELESEISMS BENEATH CERRO UTURUNCU, BOLIVIA

Alexandra K. Farrell[1] and Stephen R. McNutt[1]
[1] *School of Geosciences, University of South Florida. Tampa, FL, USA*

Cerro Uturuncu (22° 16' 12" S, 67° 10' 48" W), Bolivia, is a Pleistocene-aged volcano which has attracted considerable scientific attention over the last few years. It was one of only four volcanic centers to show deformation based on an InSAR survey of over 900 South American volcanoes by Pritchard and Simons (2000). Mogi source modeling showed that the volcano was inflating 1.5-2 cm/yr centered ~3 km to the southwest of the volcano's summit and at mid-crustal depths of 17-20 km. A reconnaissance survey in 2004 showed a high rate of seismicity despite the volcano's quiescence during the past 270 K years (Sparks et al., 2008). Uturuncu also overlies the largest known crustal magma body in the world, the Altiplano-Puna Magma Body, which among other characteristics is a zone of low seismic velocities (Zandt et al., 2003). Determining the interaction between seismic waves and the seismic low-velocity zone (and possible magma body) beneath Cerro Uturuncu is important because such interactions affect the results of seismic imaging methods and can be used as additional sources of information to constrain the location and properties of partial melt.

A set of 14 teleseismic earthquakes sourced to the NE (1, Calabria Subduction Zone), NW (4, Japan Subduction Zone), SE (5, South Sandwich Subduction Zone), and SW (4, Kermadec-Tonga Subduction Zones) was studied to determine how wave propagation was affected by a presumed magma body beneath Uturuncu. The number of events is small but the events have good signal-to-noise ratios and very similar waveforms for each event so that reliable measurements could be made of arrival times and amplitudes. Attenuation of amplitudes occurs in a NW-SE trend beneath the volcano, 14 by 33 km, with calculated values of quality factor *Q* as low as 1.7, suggesting strong seismic attenuation. Relative time delays (between the theoretical and observed travel times) of up to 0.8 sec were also observed. The pattern of attenuation and relative time delays together showed four trends: fast and not attenuated (normal crust), slow and attenuated (partial melt), fast and attenuated (likely high fracture density), and slow but not attenuated (possible deep low Vp structure). Results suggest partial melt as high as 16-60% in a region of low Bouguer gravity, high Vp/Vs, persistent seismicity, and overlapping a locus of uplift. Realistically, percent partial melt values above 30% are unlikely and therefore, to account for this, the anomaly would need to have a greater thickness along the raypath for the stations showing 30% or more, thus giving a mean partial melt zone thickness of 24.7 km for an assumed uniform percent partial melt value of 20%.

WIDESPREAD IMAGING OF THE LOWER CRUST, MOHO, AND UPPER MANTLE BENEATH ALASKA FROM RAYLEIGH WAVES

Matthew M. Haney[1], Victor C. Tsai[2], Kevin M. Ward[3]
[1]*Alaska Volcano Observatory, U.S. Geological Survey, Anchorage, AK, USA*
[2]*California Institute of Technology, Seismological Laboratory, Pasadena, CA, USA*
[3]*University of Arizona, Department of Geoscience, Tucson, AZ, USA*

The inversion of surface-wave dispersion curves for a shear-wave velocity depth profile is a classic geophysical inverse problem. Recently, Haney and Tsai (2015; Geophysics) developed a new approach to this problem based on assumptions that are similar to those used in the formulation of the Dix equation in reflection seismology. In contrast to conventional surface-wave inversion, the Dix-type relation for surface waves does not require an initial model and solves directly for shear-wave velocity, not a perturbation in shear-wave velocity. Haney and Tsai (2015) demonstrated the method for both under- and over-parameterized cases and used under-parameterization to solve for Moho depth and crustal and mantle shear-wave velocity across the Western US from only three phase velocity maps.

Here we extend the under-parameterized method presented in Haney and Tsai (2015) to the over-determined case when more than three phase velocity maps are available. We apply the Dix technique to phase-velocity maps of the contiguous US and Alaska at periods between 12 and 45 s. We use the Dix inversion result as an initial model for subsequent nonlinear inversion. In the contiguous US, we image an apparent deepening of the Moho to the west of Cascade volcanic chain that we interpret as the waveguide interface transitioning to the slab due to the continental Moho becoming transparent above the mantle forearc. Our result in Alaska is the first regional Moho map explicitly derived from seismic waves. We find that crustal thickness is generally correlated with topography, with thicker crust beneath mountain ranges (Alaska Range, Talkeetna, Kenai, and Wrangell Mountains). North of the Denali Fault, the Moho is smoother than to the south and located at typical depths of 30-35 km. There are also indications that the waveguide interface we solve for beneath Prince William Sound is actually the subducting slab, as was also the case in the Cascades. The slab structure beneath Prince William Sound extends further east than the Pacific slab represented in the Slab1.0 model.

USING EARTHQUAKES TO PROBE SUBDUCTION MEGATHRUST BEHAVIOR: A LOOK AT EARTHQUAKE SWARMS AND REPEATING EARTHQUAKES IN ALASKA

Stephen Holtkamp[1]
[1]*Geophysical Institute, Univ. of Alaska. Fairbanks, AK, USA.*

Recent studies have proposed that analysis of smaller seismic events along a plate boundary can provide valuable insight regarding the state of stress, history of stress accumulation and release, and the segmentation potential of large faults. For example, analysis of background seismicity has allowed researchers to produce maps of stress accumulation and release at a very fine scale. Furthermore, the observation that earthquake swarms may be related to large earthquake rupture asperities and persistent segmentation boundaries worldwide suggests that cataloging these events may help characterize the rupture extent of future great earthquakes. Repeating earthquakes, which represent repeated rupture of the same asperity, are thought to occur within creeping sections of the fault. Repeating earthquakes can be used to map the creep history of faults before and after large earthquakes.

Here, I examine repeating earthquakes and megathrust earthquake swarms along the Alaskan/Aleutian subduction megathrust, where at least several dozen earthquake swarms have occurred over the past 50 years. Megathrust earthquake swarms in Alaska have occurred immediately prior larger megathrust earthquakes, such as the 2003 Mw 7.8 and 2006 Mw 6.6 Rat Islands earthquakes. Megathrust earthquake swarms also appear to delimit large earthquake rupture across a variety of spatial scales. Two sequences of earthquake swarms were associated with large geodetic signatures, which we interpret to be slow slip. In addition, we are able to find several families of repeating earthquakes in the Aleutians, despite the observational challenges. We hope that further analysis of repeating earthquake families and earthquake swarms will aid in understanding the state of stress and creep along the megathrust, and result in a better understanding of the relation between large earthquake rupture and earthquake swarms.

CORNER FREQUENCIES OF SOURCE SPECTRA OF MODERATE SUBDUCTION-ZONE EARTHQUAKES OBSERVED NEAR THE AVACHA BAY, KAMCHATKA

Anna Skorkina[1], Alexander Gusev[2,1]
[1]*Kamchatka Branch, Geophysical Survey, Russ.Ac.Sci., Petropavlovsk-Kamchatsky, Russia.*
[2]*Institute of Volcanology & Seismology, Russ.Ac.Sci., Petropavlovsk-Kamchatsky, Russia.*

Determination of parameters of earthquake source spectra are crucial for both understanding of earthquake source physics and solving problems of engineering seismology, strong ground motion prediction in particular.

The Fourier acceleration spectrum of a local earthquake, after correction for distance-related loss, is typically approximated with ω^2 low-frequency slope, a corner at frequency f_c (that often is split into double corner at f_{c1} and f_{c2}), and plateau (Aki, 1967; Brune, 1970). Later Hanks (1982) emphasized the "f_{max}" phenomenon: this plateau shows high-frequency cutoff at a certain frequency f_{max}. Gusev (1983) and Papageorgiou and Aki (1983) ascribed its origin to the source; later Aki (1988) noticed that f_{max} slowly decreases with magnitude, and treated this fact as supporting this idea. At the same period Anderson and Hough (1984) have shown that a near-site constant-Q attenuation layer of limited thickness commonly exists, that introduces distance-independent loss that can explain the f_{max} feature without any source-related effects.

However, evidence is accumulating that indicates that the "f_{max}" feature is a complex one, caused by both "source-controlled f_{max}" and "site-controlled f_{max}". Along this line Gusev and Guseva (2014) showed existence of "source-controlled f_{max}", relabeled as f_{c3}, for many Kamchatka subduction earthquakes using records of low-gain channel of IRIS BB station for 1993-2005.

In the present study, following (Gusev and Guseva, 2014), source spectra were approximated by a three-cornered shape. Data used are from 372 subduction earthquakes of 2011-2014, recorded by 6 rock-ground Kamchatka stations, including PET, equipped with accelerometers CMG5T or CMG5TD. The range of magnitudes $M_{w(L)}$ is 3.7–6.5 (calculated using equation $M_{w(L)} = ML - 0.32$ which works well for this region), the range of hypocentral distances is 50–250 km.

To enable reduction of a recorded spectrum to the source, loss parameters were estimated beforehand. Parameters of the attenuation model used are $Q_0 = 156$, $\gamma = 0.56$, $q = 0.08$ and $k_0 = 0.03$ s. The attenuation model used combined $\square_0 = 0.03$ s and $Q(r{=}100\text{km}) = 156\, f^{0.56}$, and included a gradual diminution of loss with distance (Gusev and Guseva, 2015). Spectral amplifications of individual stations due to site effects were estimated; and recorded spectra were reduced to conditions of the hard-rock PET station. Overall, 1252 S source spectra were analyzed; and corner frequency sets were obtained for each, consisting of $\{f_{c1}, f_{c2}, f_{c3}\}$ triples. Not all of them are the complete ones: there were cases when no reliable f_{c1} estimate was possible; and cases when no high-frequency cutoff (i.e. f_{c3}) was discernible. In total, 839, 1252 and 1028 estimates have been collected for f_{c1}, f_{c2} and f_{c3}, respectively.

Coefficients of variation (relative rms scatter) among several single-station estimates of f_{c1}, f_{c2} and f_{c3} are 0.17, 0.14 and 0.11, considered as acceptable. However, the question still arises if the estimates obtained reflect the source properties, not random fluctuations (noise), especially for f_{c3}, reality of which is not generally recognized.

For this purpose pair correlation analysis was used. From the data set we formed pairs of PET estimates and estimates of any other station, for the same event. The main interest was to check whether a f_{c3} estimate obtained at a station for a particular event matches to corresponding f_{c3} estimate at PET. The coefficient of correlation between such pairs of f_{c3} estimates (fig. 1c) occurred to be 0.62, with the lower bound of the 95% confidence interval

equal to 0.58, proving the match of estimates between stations, and demonstrating therefore that f_{c3} values are of source origin. Similar correlation coefficient for f_{c2} is 0.67 (fig. 1b), with the lower bound of the 95% confidence interval equal to 0.63.

The mass estimates of the first, f_{c1}, second, f_{c2} and third, f_{c3}, corner frequencies were also used to study their scaling properties, and in particular, scaling exponents $\gamma_k = d\lg f_{ck}/d\lg M_0$ (where k = 1, 2, 3). The assumption of similarity (γ = 1/3) is formally broken for f_{c1} (γ_1 = 0.26); but this result is unreliable because of significant incompleteness of low-f_{c1} values. Such data loss is related to the fact that on many spectra at their low-frequency edge, *S*-wave spectral level was evidently distorted by probable contribution of surface waves. Other data suggest that similarity is hardly significantly violated for f_{c1}. However, deviations from similarity are pronounced for f_{c2} (γ_2 = 0.22±0.01), and even more so for f_{c3} (γ_3 = 0.13±0.01). This information put significant constrains on possible rupture models for these earthquakes.

The study was supported by the grant from the Russian Science Foundation (project 14-17-00621), and was carried out at the Kamchatka Branch of the Geophysical Survey of Russian Ac. Sci.

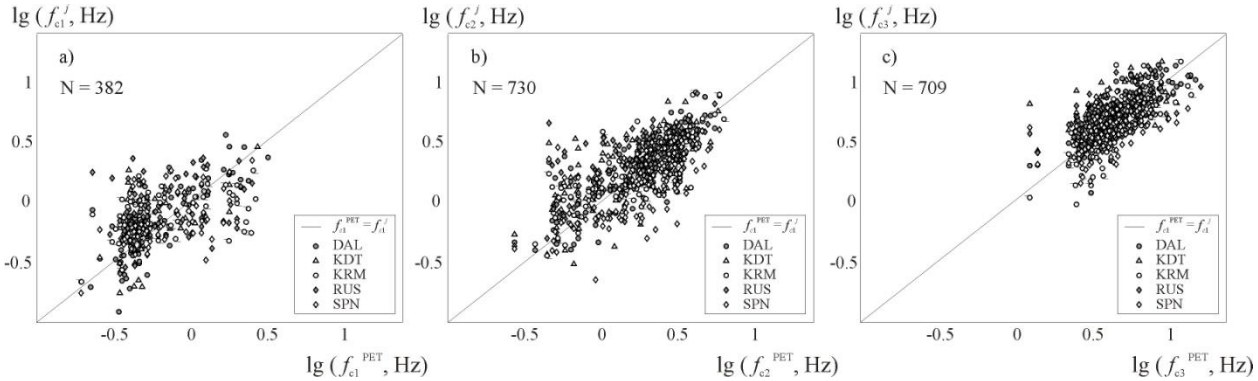

Fig. 1. Correlation between individual estimates of f_{c1} (a), f_{c2} (b), f_{c3} (c), obtained at the PET station (abscissa) and similar estimates obtained at each of other stations such as DAL, KDT, KRM, RUS and SPN (ordinate)

References

Aki, K. 1967. *J. Geophys. Res.*, v. 72. P. 1217-1231.

Aki, K. 1988. Physical theory of earthquakes // *Seismic Hazard in Mediterranean Region*, Kluwer Academic Publishers. P. 3-33.

Anderson, J. and *Hough, S.* 1984. *Bull. Seismol. Soc. Amer.*, v. 74. P. 1969-1993.

Brune, J. 1970. *J. Geophys. Res.*, v. 75. P. 4997-5009.

Gusev, A.A. 1983. *Geophys. J. Royal Astr. Soc.*, v. 74. P. 787-808.

Gusev, A.A. and *Guseva, E.M.* 2014. *Doklady Earth Sciences*, 458. P. 1112-1115.

Gusev, A.A. and *Guseva, E.M.* 2015. Splitting f_{max}: separating site-controlled and source-controlled contribution into the upper cutoff of acceleration spectrum of a local earthquake // 26th IUGG General Assembly, Prague.

Hanks, T. 1982. f_{max} // *Bull. Seismol. Soc. Amer.*, v. 72. P. 1867-1879.

Papageorgiou, A. and *Aki, K.* 1983. *Bull. Seismol. Soc. Amer.*, v. 73. P. 693-722.

ESTIMATION OF THE LONG-TERM EFFECT OF VISCOELASTIC RELAXATION INDUCED BY THE 2011 TOHOKU EARTHQUAKE AND OTHER INTERPLATE EARTHQUAKES AROUND NORTHEASTERN ASIA

Mako Ohzono[1], Hiroaki Takahashi[1], Nikolay V. Shestakov[2,3] Guojie Meng[4], Mikhail. D. Gerasimenko[3]

[1]*Institute of Seismology and Volcanology, Hokkaido University, Sapporo, Japan.*
[2]*Far Eastern Federal University, Vladivostok, Russia.*
[3]*Institute of Applied Mathematics, Far Eastern Branch, Russian Academy of Sciences, Vladivostok, Russia.*
[4]*Institute of Earthquake Science, China Earthquake Administration, Beijing, China.*

After the large earthquakes, postseismic deformation is induced by their stress disturbance. The large coseismic and postseismic deformation caused by the 2011 Tohoku-oki earthquake (magnitude 9.0) observed by GNSS not only in Japan, but also in the northeast Asia. Even though five years passed, the horizontal velocity at an IGS site, Changchun (CHAN), which is located ~1600 km away from the focal area, indicates faster velocity than that of interseismic period (~3mm/year). It means that the postseismic deformation has now been ongoing in the broad area.

Although there are several mechanisms of the postseismic deformation, the viscoelastic relaxation largely affects for long-term and widespread area around the focal area. Therefore, stable tectonic movement, such as plate motion, must be contaminated by this phenomenon. Quantitative estimation of this effect with preferable subsurface viscoelastic structure is important to understand the tectonic behavior with the earthquake cycle around the focal area.

In this study, we assume the long-term widespread postseismic deformation is mainly caused by the viscoelastic relaxation. Then, we predict the spatio-temporal evolution of the viscoelastic relaxation by the 2011 Tohoku-oki earthquake using VISCO-1d (Pollitz, 1997). Coseismic fault parameters are taken from several previous studies. The signal of surface displacement depends on subsurface structure, such as thickness of elastic layer and viscosity of the asthenosphere. We test several sets of those parameters. As an example, when we set 50 km thickness of elastic layer and 10^{18} Pa s of viscosity in the underlying viscoelastic layer, we find large and long-term deformation (~30 cm in horizontal, and ~5 cm in subsidence for 100 years).

Japan is a typical plate subduction zone, therefore many large interplate earthquakes have already occurred including the 2011 Tohoku-oki earthquake. In the historical record, there are 15 earthquakes over magnitude 8.0 have occurred since 869 in and around Japan. In order to check the effect of their possible postseismic deformation, we also estimate the long-term spatio-temporal surface displacement induced by the viscoelastic relaxation for those earthquakes. Preliminary result shows that five earthquakes may contaminate the displacement field around Vladivostok, Russia, when we set the 10^{18} Pa s of viscoelastic layer beneath 50 km thickness of elastic layer. The displacement signal from each postseismic deformation depends on the magnitude of earthquake, focal distance, fault mechanism, duration, and so on. From this estimation, it is considered that we are unable to ignore the effect of these postseismic deformation in extensive region of northeast Asia.

LONG PERIOD SEISMICITY AND VERY LONG PERIOD INFRASOUND DRIVEN BY SHALLOW MAGMATIC DEGASSING AT MOUNT PAGAN, MARIANA ISLANDS

John J. Lyons[1], Matthew M. Haney[1], Cynthia Werner[2], Peter Kelly[2], Matthew Patrick[3], Christoph Kern[2], and Frank Trusdell[3]
[1]Alaska Volcano Observatory, U.S. Geological Survey, Anchorage, Alaska, USA,
[2]Cascades VolcanoObservatory, U.S. Geological Survey, Vancouver,Washington, USA,
[3]Hawaiian Volcano Observatory, U.S. Geological Survey, Volcano, Hawaii, USA

Long period (0.5-5 Hz) seismicity is frequently observed at active volcanoes and has been attributed to both resonance in fluid-filled cavities and slow brittle failure. Identifying the location and source mechanism of long period (LP) seismicity is important for understanding and monitoring volcanic activity, but can be challenging because waveforms are often emergent, have low amplitudes, and may be affected by severe topography or an unknown shallow velocity structure. In this talk, I'll present results from a study of LP seismicity that highlights its utility in interpreting volcanic behavior and illuminating the geometry of shallow volcanic conduits, particularly when combined with other geophysical and geological data.

Mount Pagan produced LP seismicity and very long period (<0.5 Hz) infrasound (iVLP) during continuous degassing from July 2013 to January 2014. The frequency content of the LP and iVLP events and delay times between the two arrivals were remarkably stable and indicate nearly co-located sources. Full waveform inversion of a master LP event reveals a volumetric source 60 m below and 180 m west of the summit vent. The moment tensor reveals a volumetric source modeled as resonance of a subhorizontal sill intersecting a dike. We model the seismoacoustic wavefields with a coupled earth-air 3-D finite difference code. The ratios of pressure to velocity measured at the infrasound arrays are an order of magnitude larger than the synthetic ratios, so the iVLP is not the result of LP energy transmitting into the atmosphere at its epicenter. Based on crater shape and dimensions determined by structure from motion, we model the iVLP as acoustic resonance of an exponential horn. The source of the continuous plume from Multi-GAS and FLYSPEC data analysis is shallow magmatic degassing, which repeatedly pressurized the dike-sill portion of the conduit over the 7 months of observation. Periodic gas release caused the geologically controlled sill to partially collapse and resonate, while venting of gas at the surface triggered resonance in the crater. LP degassing only accounts for ~12% of total degassing, indicating that most degassing is relatively aseismic and that multiple active pathways exist beneath the vent.

Figure 1. Model of shallow magmatic degassing and LP generation at Mount Pagan. a) Mapped geology, elevation profile, and crack system modeled from LP seismicity in an east-west cross section through the summit crater. b,c) Schematic of degassing processes and sources of LP seismicity and iVLP (*from Lyons, J. J., M. M. Haney, C.Werner, P. Kelly, M. Patrick, C. Kern, and F. Trusdell (2016), Long period seismicity and very long period infrasound driven by shallow magmatic degassing at Mount Pagan, Mariana Islands, J. Geophys. Res. Solid Earth, 121, doi:10.1002/2015JB012490.*)

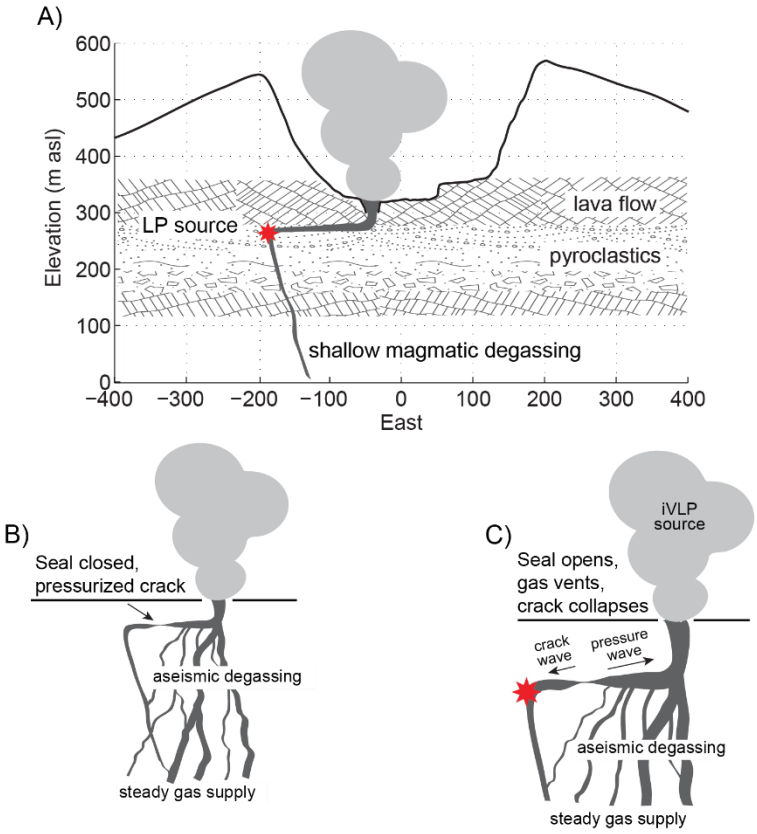
A)
600
500
400
300
200
100
0
Elevation (m asl)
LP source
lava flow
pyroclastics
shallow magmatic degassing
−400
−300
−200
−100
0
100
200
300
400
East
B)
Seal closed,
pressurized crack
aseismic degassing
steady gas supply
C)
iVLP
source
Seal opens,
gas vents,
crack collapses
crack
wave
pressure
wave
aseismic degassing
steady gas supply

SEISMIC EQUIVALENTS OF INFRASONIC SCALING LAWS FOR VOLCANIC JETS AND ACOUSTIC MULTIPOLES

Matthew M. Haney[1], Robin Matoza[2], David Fee[3], David F. Aldridge[4]
[1]*Alaska Volcano Observatory, U.S. Geological Survey, Anchorage, AK, USA*
[2]*University of California Santa Barbara, Department of Earth Science, Santa Barbara, CA, USA*
[3]*University of Alaska Fairbanks, Geophysical Institute/AVO, Fairbanks, AK, USA*
[4]*Sandia National Laboratories, Geophysics Department, Albuquerque, NM, USA*

Seismic and acoustic waves are manifestations of mechanical energy in the solid Earth and atmosphere, respectively. Here, we explore analogies between equivalent source theory in seismology (moment-tensor and single-force sources) and equivalent source theory in acoustics, i.e., monopoles, dipoles, and quadrupoles [e.g., Woulff and McGetchin, 1976]. Although infrasound from volcanic eruptions may be more complex than a simple monopole, dipole, or quadrupole assumption, these elementary sources are a logical place to begin to relate seismic and acoustic sources. Treating sources in such a unified way will be necessary in the application of seismo-acoustic waveform inversion at volcanoes, in which seismic and infrasound data are simultaneously reconciled for a common near-surface source (i.e., volcanic explosion).

By considering the radiated power of a harmonic force source at the surface of an elastic halfspace, we show that a volcanic plume modeled as a seismic force has the same scaling as an acoustic dipole. This is surprising since, in seismology, the equivalent force system is a widely-used representation of moment tensors in terms of force couples and dipoles. Here, we show from first principles that the seismic force source is in fact dipolar in nature, since it can be equivalently represented as an explosion dipole and a pair of torque dipoles in a particular configuration. This forges a deep connection between the multipole expansion in acoustics and the use of forces and moments in seismology and suggests that an alternative description of seismic sources is possible.

QUANTIFYING GROUND COUPLED AIR WAVES TO DETERMINE GAS FLUX AT PAVLOF VOLCANO, ALASKA, DURING THE 2007 ERUPTION

Cassandra M. Smith[1], Stephen R. McNutt[1], Glenn Thompson[1]
[1] *School of Geosciences, University of South Florida. Tampa, FL, USA*

An abnormally high number of explosion quakes were noted during the monitoring effort for the 2007 eruption of Pavlof Volcano on the Alaska Peninsula. This eruption lasted from August 14th to September 13th with the peak in activity between August 28th and September 2nd. In this study we manually catalogued the explosion quakes from their characteristic ground-coupled air waves. This study investigates how the ground-coupled air waves might be used in a monitoring or analysis effort by calculating energy release and gas mass release. Over $3x10^4$ quakes were recorded. Using Garces et al.'s (2000) equation for vertical ground velocity we calculated the energy release from the explosions to be $3x10^{11}$ J, and the total gas mass (assuming 100% water) released was 450 metric tons. We performed a sensitivity analysis in order to determine that our variable choices were reasonable and found that when our results are compared to other volcanoes in the literature they are found to be similar, but occasionally somewhat lower. Nevertheless, the tracking of explosion quakes has the potential to estimate relative eruption intensity as a function of time, and is thus a useful component of a seismic monitoring effort.

PERSPECTIVES ON THE Mw7.1 INISKIN EARTHQUAKE

Michael West[1], Matt Gardine[1], Natalia Ruppert[1], Carl Tape[1], Jeffrey Freymueller[1], Stephen Holtkamp[1]

[1]Alaska Earthquake Center, Geophys. Institute, Univ. Alaska Fairbanks, Fairbanks, AK, USA.

The M_w 7.1 earthquake on January 24, 2016 was the largest intermediate-depth earthquake ever recorded in mainland Alaska and produced the most significant shaking in the Cook Inlet region in half a century. The earthquake occurred in the subducting Pacific Plate at a depth of 125km. The earthquake ruptured a natural gas line resulting in an explosion and fire than consumed four homes. Additional structural damages were primarily the result of slumping soilsIt occurred at the edge of a long-recognized cluster of intermediate-depth earthquakes, with a similar down-dip minimum stress direction observed in prior earthquakes. It was larger however than any previously identified earthquake in this region. From 2001 to 2014 there were no intermediate-depth M6+ earthquakes in Alaska east of the Fox Islands. Since July 2014, there have been four including this one. The Iniskin earthquake aftershock zone extends ~60km northeast and abuts the hypocenter of M6.4 earthquake six months prior. Static displacements are largest 100 km east on the Kenai Peninsula. Ground motion were highly variable and consistent with the directionality of the source. Strong motion records corroborate felt reports of moderate shaking above the hypocenter and significant influences from regional structures including the Cook Inlet sedimentary basin. Significant population centers, and the limited damage, were all at least 100 km or more from the epicenter. This presents two significant public policy challenges. The first is the misperception that individuals experienced, and infrastructure survived, the near-field forces of a M7+ earthquake. Instrumental records and felt reports demonstrate clearly that this is not the case. Second, a M7.1 earthquake at intermediate depth, combined with comparable M6+ earthquakes in the past few years necessitate a re-evaluation of the maximum magnitude and frequency of intermediate depth earthquakes through the south-central region of Alaska.

TECTONICS AND EXPERIMENTS

(Oral presentations)

PLATE BOUNDARIES IN THE NORTH PACIFIC

Jeffrey T. Freymueller
Geophysical Institute, University of Alaska Fairbanks, Fairbanks, AK 99775

The North American and Eurasian plates diverge at spreading centers in the North Atlantic and Arctic Oceans, and converge in northeastern Asia. Because the pole of relative plate motion is located in the same area, relative plate motions are slow and deformation is diffuse. Overall, the region consists of a collage of small microplates or blocks moving relative to each other, with some of the microplate boundaries being uncertain or controversial, and some proposed microplates perhaps being regions of diffuse deformation rather than rigid plates. On the Alaska side of the North Pacific, additional complexity is driven by the collision of the Yakutat terrane at the eastern end of the Alaska-Aleutian subduction zone, and by the effects of oblique subduction. The Aleutian arc features an extreme variation in the obliquity of plate convergence, and the western part of the arc has long been recognized as an example of slip partitioning of highly oblique subduction. The direction of Pacific-North America relative motion is essentially trench-normal along the Alaska Peninsula in the eastern part of the arc, and reaches almost trench-parallel at the western end of the arc. Along much of the arc, a tectonic sliver of the overriding plate moves in a mostly trench-parallel direction with the rate of motion increasing to the west, and additional blocks or microplates (southern Alaska, Bering plate) accommodate eastward extrusion of material away from the Yakutat block collision. Here we examine the long-term velocities of sites in southern Alaska, the Aleutian arc and the Bering Sea region after removing the effects of recent earthquakes and postseismic deformation. We will re-examine the extent of the proposed Bering plate and evidence for block motions along the Aleutian arc in the light of an expanded and more precise data set, and recent seismicity and earthquake focal mechanisms. Our block models suggest a more complex pattern of deformation than previously proposed.

STRAINMETER ARRAY OBSERVATION OF THE DIKE INTRUSION AT SAKURAJIMA VOLCANO ON 15 AUGUST 2015

Higashi Uchida
Kagoshima Meteorological Office, Japan Meteorological Agency, Kagoshima, Japan.

On 15 August 2015, a rapid increase in the number of volcano-tectonic earthquakes and remarkable crustal deformation were observed at Sakurajima volcano in Japan. Strainmeter data from Arimura Station (Fig. 1), located 2km SSE of the volcano's Showa crater, showed crustal extension with more than 10 micro-strain (Fig. 2). The strain change was 1,000 times greater than those associated with typical explosions at the Showa crater, and was the largest ever observed at the station. The Japan Meteorological Agency (JMA) raised the Volcanic Alert Level from 3 to 4 at 10:15 on August 15 (Japan Standard Time (JST)) and expanded the hazard area from 2 to 3 km from the crater. JMA also issued its first residential area warning for Sakurajima, and around 80 residents living near the hazard area took refuge in evacuation centers.

No actual eruption occurred, and earthquake activity and crustal deformation subsided at 03:00 on August 17. Emergency observation by the Japan Aerospace Exploration Agency using the Daichi-2 satellite's Interferometric Synthetic Aperture Radar (InSAR) revealed deformation of up to about 16cm closer to the satellite on the eastern flank of Sakurajima. The Geospatial Information Authority of Japan (GSJ) analyzed these data and Global Navigation Satellite System data, and proposed a dike model to explain the observed deformation. The width, length and opening volume of the dike are 0.78km, 1.41km and $2x10^6m^3$, respectively.

InSAR data cover a wide area at very high spatial resolution, but are limited in terms of temporal sampling due to the orbital repeat period of the satellite. To elucidate the dike intrusion process, the time-continuous strain change observed by an array of three strainmeters (EX-R, EX-T and EX-D) was analyzed. As shown in Fig. 1, EX-R is aligned in the radial direction to the crater, and EX-T is aligned in the tangential direction. EX-D is at an angle of 45 degrees to the other strainmeters, and the array is installed at the end of a 200m horizontal tunnel to achieve a high signal-to-noise ratio. Each strainmeter has a baseline length of 28m. Ignoring local distortions of the strain field, three non-colinear strainmeters can be used to determine the principal strain.

The strain records (Fig. 2) are characterized by four points in the time-series representation: (A) Strain change began at 08:00 on August 15 JST. (B) The rate of strain change increased at 10:25. (C) The rate of EX-R component change turned from negative (contraction) to positive (extension) at 11:15. (D) Deformation ceased at 03:00 on August 17. The results show that the EX-D component exhibits the largest change among the three. We confirmed that the total strain change between A and D was consistent with the change predicted from the dike model proposed by GSJ.

To clarify the dike intrusion process, strain changes for the periods A-B, B-C and C-D were calculated as shown in Fig. 3. The contraction axis of the principal strain in the A-B period has a north-south orientation, and exhibits clockwise rotation during the B-C and C-D periods. This suggests that dike opening progressed from the SSW end to the NNE end as follows: The SSW end of the dike opened in the A-B period. The dike opening subsequently progressed to the NNE direction in the B-C period. Finally, the NNE part of the dike opened in the C-D period. We also found the migration of earthquake hypocenters, which also supports the NNE progression of the dike opening.

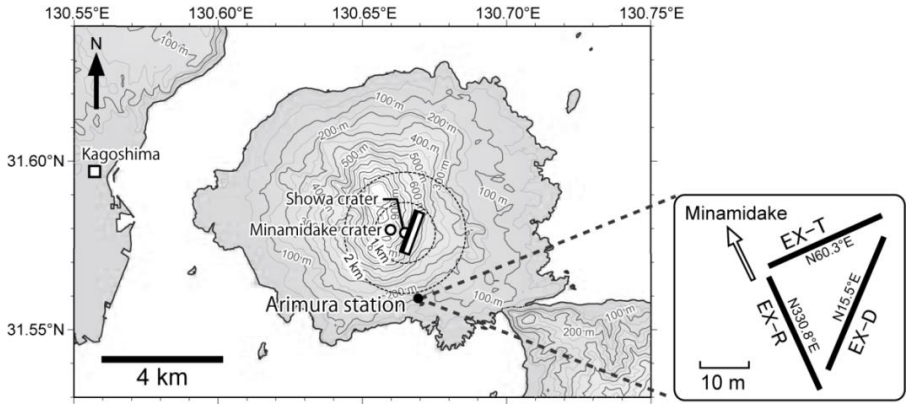

Fig. 1. Map of Sakurajima volcano. Location of Arimura station is denoted by solid circle. The dike model proposed by GSJ is represented by rectangle. The left shows strainmeter array in the observation tunnel complex at Arimura Station.

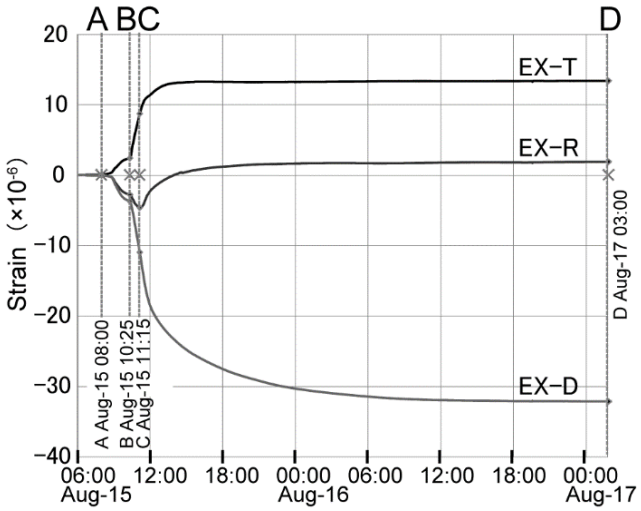

Fig. 2. Strain data recorded at Arimura Station in association with volcanic activity on 15 August 2015.

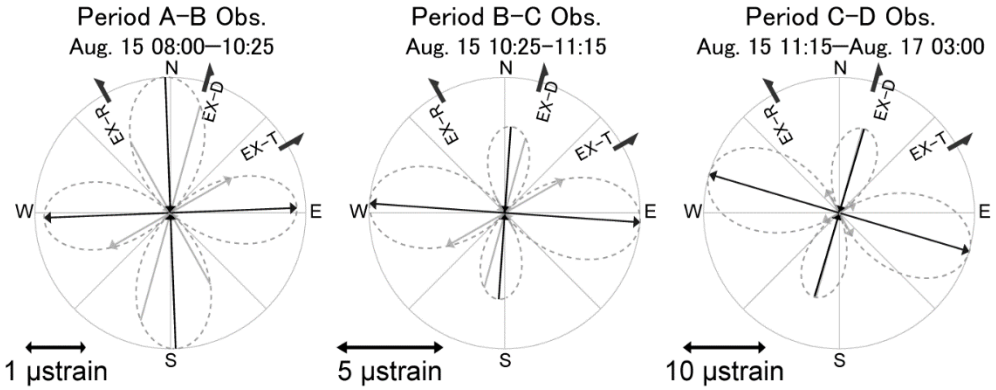

Fig. 3. Principal strain change observed at Arimura Station during the A-B, B-C and C-D periods. The black arrows indicate principal strain, and the gray arrows indicate strain observed at each strainmeter.

SEDIMENT WAVES AND CLOUD LAYERING IN EXPLOSIVE VOLCANIC ERUPTIONS: EVIDENCE FROM ANALOGUE EXPERIMENTS

Johan Gilchrist and Mark Jellinek
Earth, Ocean and Atmospheric Sciences, Univ. of British Columbia, Vancouver, BC, Canada

Introduction

Explosive volcanic eruptions inject (multiphase) mixtures of ash, volcanic gases and entrained air high into the atmosphere. On the basis of previous experiments (Veitch and Woods, 2000; Carazzo and Jellinek, 2012, CJ12 hereafter), eruptions apparently occur in "Buoyant Plume", "Total Collapse" and "Partial Collapse" regimes depending on source and environmental conditions (Fig. 1). Some Plinian eruptions, such as Soufriere Hills, Montserrat (February 11, 2010, Fig. 1a) and Mt. St. Helens (May 18, 1980), produce multiply-layered ash clouds and concurrent pyroclastic density currents (Wadge et. al, 2014, Hoblitt, 1986). Using analog experiments on multiphase volcanic jets we address three questions:

1. How do the differing dynamics of eruption and sedimentation interact to produce distinct BP, PC and TC regimes?
2. Over what range of source conditions do multiply-layered clouds occur?
3. How are the underlying processes governing sedimentation and cloud layering ultimately reflected in the structure and architecture of the resulting deposit?

Methods

Following CJ12, we inject dense, isothermal, sediment-laden water jets at a fixed rate into a 90 x 90 x 70 cm saltwater tank with a linear density stratification simulating the atmospheric density profile in the troposphere. We use 80 μm and 225 μm diameter silica particles to simulate fine and coarse ash, respectively. Two dimensionless parameters govern the regime of the jet: the source Richardson number, $-Ri_0$, is a measure of jet strength and expresses a balance between the driving inertial and stabilizing buoyancy forces acting at the source, and the particle volume fraction, ϕ_0, of the jet. We vary the source conditions to explore a $-Ri_0$-ϕ_0 parameter space appropriate to natural eruptions. We will define a PC jet as one where a modest fraction of the injected mixture collapses to the tank floor and the rest intrudes and spreads as an umbrella cloud (Figs. 1c and 2). TC jets, by contrast, are distinguished by a majority (>90%) of erupted material collapsing to the floor (Fig. 1b). BP jets produce an umbrella cloud with no jet fluid reaching the tank floor (Fig. 1d).

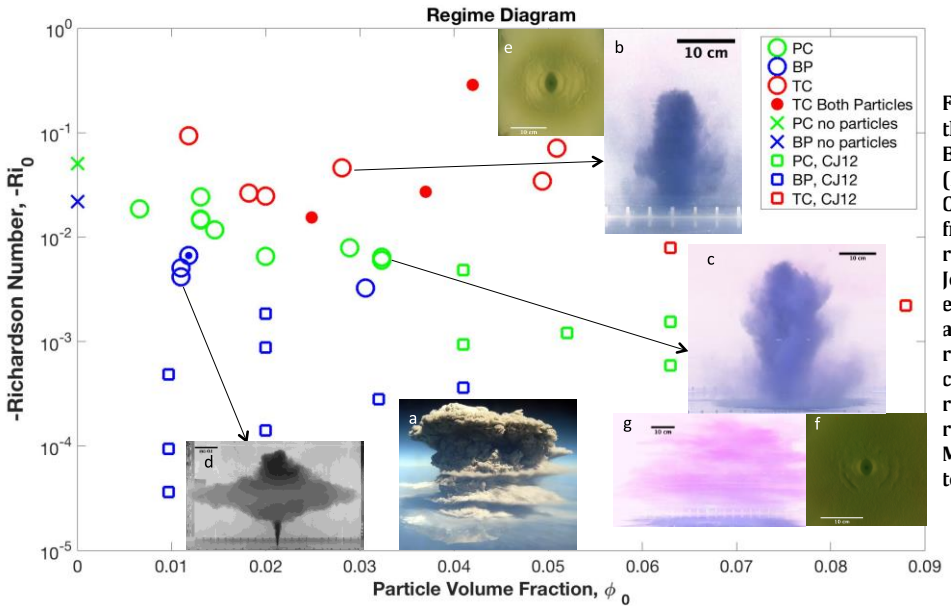

Figure 1: $-Ri_0$ vs. ϕ_0 regime diagram that partitions experiments into Buoyant Plume (BP), Partial Collapse (PC) and Total Collapse (TC) regimes. Circle and X markers represent data from this study while square markers represent data from Carazzo and Jellinek, 2012. (a) Feb. 11, 2010 eruption of Montserrat. (b), (c) and (d) are examples of TC, PC and BP regimes, respectively. (e) and (f) are deposits corresponding to (a) and (b), respectively, exhibiting concentric rings marking a terraced structure. (g) Multiply-layered cloud corresponding to (c). Scale bars are 10 cm long.

Results

In Fig. 1 we expand the parameter space initially explored by CJ12 to distinguish conditions for the BP, PC and TC regimes and for multiply-layered clouds. Qualitatively, we find:

- Multiply-layered clouds are a characteristic feature of PC jets (Figs. 1a and 1g)
- PC jets closer to the BP regime produce relatively thin multiply-layered clouds, while jets closer to the TC regime produce relatively thick multiply-layered clouds (cf. Figs. 2a and 2b)
- Axisymmetric, terraced deposits are produced by TC jets and PC jets with ϕ_0 > ~0.02 (Figs. 1e and 1f), while BP jets produce deposits decreasing in thickness monotonically from the vent
- Sediment waves occur in all PC and TC regimes and are discrete, periodic collapse events in which annular, radially tapered, dense waves fall from the plume top to the tank floor, or some height above it depending on $-Ri_0$ and ϕ_0 (e.g. Figs. 1b, 1c and 2).
- In PC and TC jets, sediment waves carry entrained buoyant jet fluid to the tank floor, deposit their sediment load and release the initially entrained jet fluid to intrude at a Level of Neutral Buoyancy (LNB)

Quantitatively, our results indicate:

- Transitions from the BP to TC regimes are marked by increases in the wavelength, size and velocity of sediment waves, as well as the production of terraced deposits.
- Transitions from the TC to BP regimes are marked by the sediment wave velocity approaching the value of the individual particle settling velocity and by the release of jet fluid from sediment waves above the tank floor

Conclusion

Our results support the following conclusions:

1. Multiply-layered clouds are a distinctive feature of PC jets
2. The periodic release and rise of entrained buoyant fluid from sediment waves coming to rest on the tank floor leads to the production of multiply-layered clouds.
3. PC and TC regimes with pronounced sediment waves produce terraced deposits. BP regimes are more typically characterized by deposits that vary smoothly in thickness with radius.
4. Transitions between BP, PC and TC regimes are continuous: These regimes are marked by changes in sediment wave properties that vary smoothly with $-Ri_0$ and ϕ_0 and are not sharply distinguished

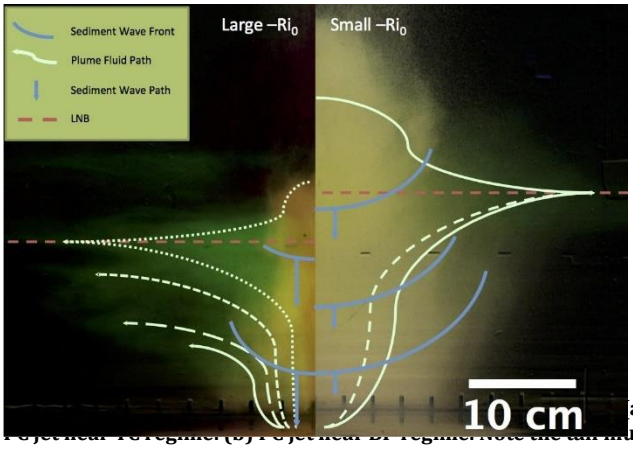

a) PC jet near TC regime. (b) PC jet near BP regime. Note the tall multi-layered cloud, lower LNB, larger wavelength and faster velocity of sediment waves in (a) as opposed to (b). More solid lines indicate younger intrusions.

Our work suggests a comparison of experimental deposits to natural near-vent deposits may provide insight into the eruption column dynamics of ancient eruptions.

CORRELATION STUDY OF COULOMB STRESS CHANGE IMPARTED BY TWO NEW SLOW SLIP EVENTS AND SEISMIC RATE CHANGE IN LOWER COOK INLET OF THE ALASKA-ALEUTIAN SUBDUCTION ZONE

Shanshan Li[1], Jeff Freymueller[1], Natalia Ruppert[1], Jianjun Wang[2]
[1]University of Alaska Fairbanks, Fairbanks, AK, United States,
[2]Wuhan University, Wuhan, Hubei, China

We identified two long-term slow slip events (SSEs) in Lower Cook Inlet, southcentral Alaska (1995.0-2004.8 and 2009.85-2011.81) by inverting the GPS site velocities (Li et al. 2016). The earlier SSE lasted at least 9 years (observations in that area began in 1995) with Mw~7.8 and average slip magnitude as ~82 mm/yr. The latter SSE had almost the same area as the earlier one, which is within 40-60 km depth range, and a duration of ~2 years with Mw~7.2 and average slip magnitude as ~91 mm/yr.

The estimated time-dependent slip behaviors of these two SSEs allow us to track the corresponding Coulomb stress changes and associate them with seismic activity and non-tectonic tremor in Lower Cook Inlet. We will use our slip models to calculate the Coulomb stress change induced by the time-dependent slip (SSEs) on Alaska-Aleutian subduction zone plate interface. We are interested to see whether the observations of the seismicity in Lower Cook Inlet are consistent with stress triggering outside the slowly slipping region. We will test whether the temporal evolution of earthquakes are explained by increased stressing caused by SSEs, implying that the earthquakes are triggered and probability changes for large earthquakes in southcentral Alaska. If this hypothesis can be tested, it can lead to a useful method to quantify the increasing the potential hazard during SSEs since the triggered earthquakes have the potential to be large and destructive ones.

GEOLOGY & PETROLOGY & GEOCHEMISTRY

(ORAL PRESENTATIONS)

ORIGIN OF CALDERAS: COLLAPSES OR EXPLOSIONS?

Izumi Yokoyama
Usu Volcano Observatory, Hokkaido University. Sapporo, Japan

Origins of calderas may be different depending on their subsurface structure that may be characterized by such features as high-density deposits and low ones that may be observed as high and low gravity anomalies. First, our discussion is focused on four calderas that were seen forming during the period from 1815 to 1991, before our eyes, including Novarupta, Alaska. Coincidently, these four calderas are all low-gravity-anomaly type. Some details of the four calderas are shown in Table 1.Their formation processes and subsurface structure are summarized by the existing data analyzed by various authors. And these results are confirmed by results of drillings at some other calderas. Then caldera formation of the both types is discussed: The high-gravity-anomaly type calderas usually originate from collapse of erupted ejecta to the summit magma reservoirs although their creative eruptions have not been identified, and so some historical eruptions accompanied by collapses on the calderas of this type are mentioned briefly. Next, low-gravity-anomaly type calderas are discussed from standpoints of both the models of collapses and explosions. To confirm the possibility that volcanic fragments collapse into magma reservoirs, we discuss stress propagation from a crushed reservoir toward the earth surface. It is emphasized that dynamic pressure of explosions is an important factor in the caldera formations, not only volume of the ejecta. Lastly, formation mechanisms of large calderas of this type are speculated. Large calderas measuring more than 10 km may be completed by amalgamation of componential calderas in geological times.

Table 1: The four calderas observed during their formation

Caldera	Diameter & depth (km)	Previous eruption	Earthq. before the event	Max. earthq. magnitude	Duration climactic eruption	Ejecta volume (km^3 DRE) + missing volume
Tambora 1815	6 0.6~0.7	?	3 yrs	7 (?)	3 days	(12~60) + 46
Krakatau 1883	5 0.25	1680 AD	99 days	5	23 hrs	(9~19) + 8
Novarupta 1912	2 ca. 0.25	?	7 days	7.0	14 hrs	15 + 0.7
Pinatubo 1991	2.5 0.2	ca.1490 AD	71 days	5.7	9 hrs	4.5 + 2.5

BERING - A NEW INTERNATIONAL MARINE RESEARCH PROJECT TO INVESTIGATE THE MAGMATIC AND TECTONIC EVOLUTION OF THE BERING SEA AND ITS MARGINS

Maxim Portnyagin[1], Kaj Hoernle[1], Reinhard Werner[1], Boris Baranov[2], Gene Yogodzinski[3] and BERING participants

[1]GEOMAR Helmholtz Centre for Ocean Research Kiel, Kiel, Germany.
[2] P.P. Shirshov Institute of Oceanology RAS, Moscow, Russia.
[3] University of South Carolina, Columbia, USA.

The BERING project is a new large project lead by the GEOMAR institution in Kiel and focused on marine and on-land investigations in Kamchatka, the Kurile and Aleutian Arcs, the Bering Sea, and the NW-Pacific. BERING is funded by the German Ministry of Education and Research with contributions from Russian and U.S. institutions. The overarching goal of BERING is to elucidate the magmatic and tectonic evolution of the Bering Sea and its margins over the past ≥50 m.y. In particular, BERING investigates the physical and chemical conditions that control the development of subduction zones, including subduction initiation, evolution of mature arc systems, and the impact of subduction volcanism on the environment. To achieve this goal BERING will address the following major scientific questions in four major directions of study:

(1) Early (pre-Aleutian) subduction history of the Bering Sea: What is the nature of the Beringian and Chukotka Margins and their junction?

(2) Aleutian arc inception and evolution: What is the age and composition of the oldest rocks in the western Aleutian Arc?

(3) Modern Aleutian arc system: What is the origin and occurrence of recent magmatic activity in the Western Aleutian Arc?

(4) Arc Input: What is the spatial and temporal compositional variability of the subducting Pacific lithosphere offshore the Aleutian Arc and Kamchatka?

A central part of the project is the R/V SONNE expedition SO-249, which will be conducted in June – August 2016 in the framework of the Russian-German Agreement on Marine and Polar Research and in close cooperation with U.S. American colleagues. The two legs of cruise SO-249 aim to map and sample magmatic structures in the Aleutians, the Pacific seafloor subducting beneath the Aleutians and northern Kamchatka, and in the western margin of the Bering Sea (Fig. 1). The on shore work program at GEOMAR and cooperating institutions will include geochronological, petrological and geochemical studies on igneous samples obtained during the cruise. The results of BERING will be integrated with those of previous campaigns (e.g. KOMEX and KALMAR projects), and work carried out within the World Oceans and GeoPRISMS initiatives.

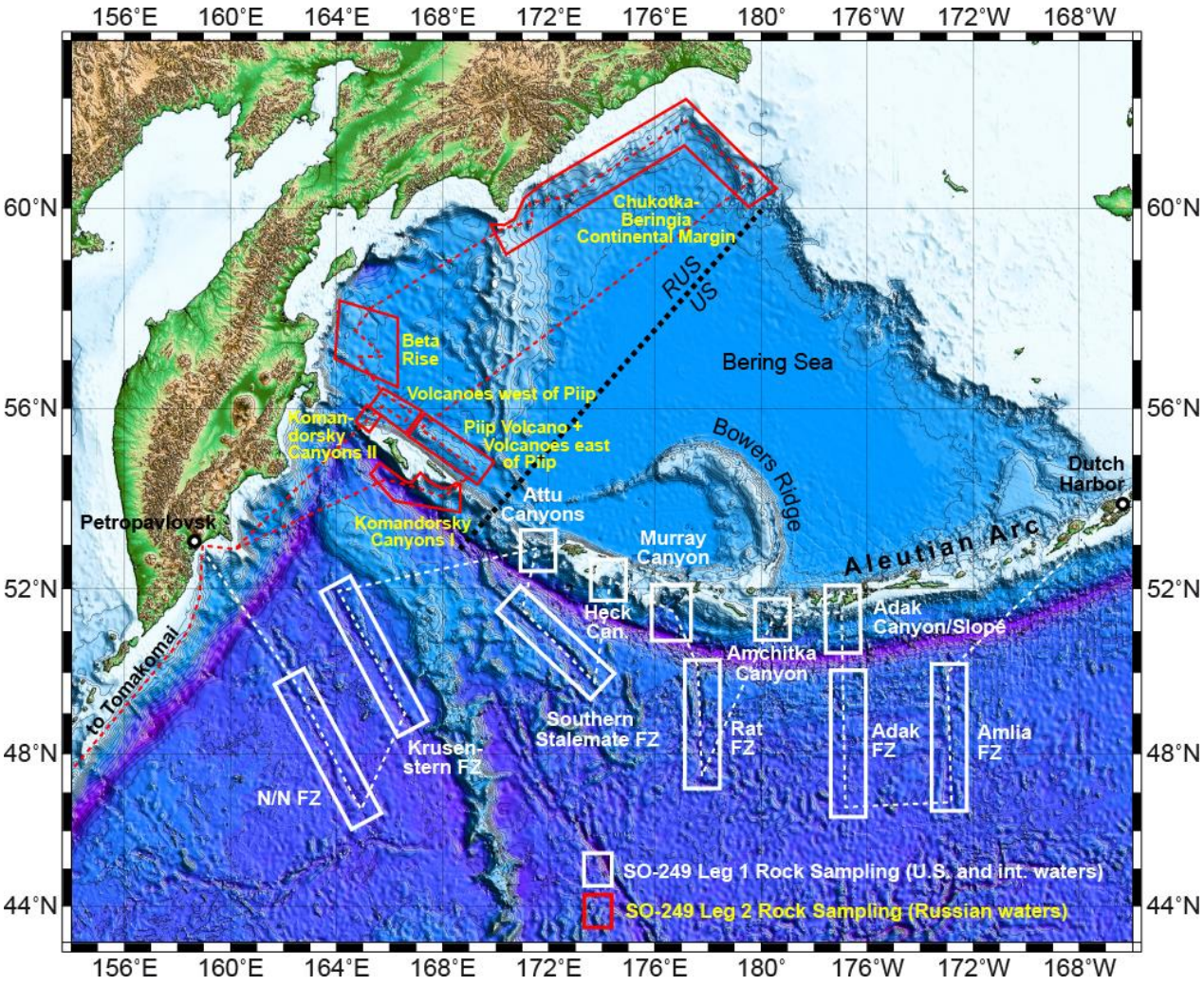

Fig. 1. The working areas of the R/V SONNE SO-249 BERING expedition Legs 1& 2.

A CASE FOR INTEGRATED GEOSCIENCE AND ARCHEOLOGICAL STUDIES IN THE ALEUTIAN ARC

Kirsten Nicolaysen[1], Dixie West[2], Virginia Hatfield[2], Breanyn MacInnes[3], Mitsuru Okuno[4], Arkady Savinetsky[5], Olga Krylovich[5], Pavel Izbekov[6], Lyman Persico[1], John Lyons[7], Max Kaufman[6,7], Christina Neal[8], William E. Scott[9], John Power[7]

[1] *Whitman College, Walla Walla, WA, USA.*
[2] *Biodiversity Institute, Univ. Kansas, Lawrence, KS, USA.*
[3] *Central Washington University, Ellensburg, WA, USA.*
[4] *Fukuoka University, Fukuoka, Japan.*
[5] *Russian Academy of Sciences, Moscow, Russia.*
[6] *Geophysical Institute, Univ. Alaska, Fairbanks, AK, USA.*
[7] *U.S. Geological Survey, Alaska Volcano Observatory, Anchorage, AK, USA.*
[8] *U.S. Geological Survey, Hawaiian Volcano Observatory, Hawaii National Park, HI, USA.*
[9] *U.S. Geological Survey, Cascades Volcano Observatory, Vancouver, WA, USA.*

The daunting array of cost, logistical equipment, difficult transportation, and hazardous summer weather has limited both exploratory and geographically focused research for the Aleutian arc, which offers a unique combination of millennia of human history and a broad array of geological problems including current geologic hazards. Worldwide, stakeholders, scientists, policy makers, and the public are experiencing and studying a rapidly changing circumpolar North. In the last ~120 years, our global society has experienced (1) declines in key marine mammals and arctic birds, (2) rising sea level and erosion swallowing coastal villages, (3) rapid ocean warming and ice melt, and (4) ocean acidification, 5) tsunamis generated by large subduction zone earthquakes, and 6) impacts of volcanic ash and tephra, particularly on air transportation. As we study this current climatic furor, react to geologic disasters locally and regionally, and attempt to predict what is in store for Earth's future, it is vital to recognize that the Aleutian arc offers an important record of geologic hazards and of how humans reacted locally to such events. This region experienced slow (climatic) and rapid (geological and human induced) impacts that influenced indigenous peoples and the North Pacific ecosystem. Supported by the National Science Foundation, the U.S. Geological Survey, the Alaska Department of Geological and Geophysical Surveys, and the Alaska Volcano Observatory, our unique partnership of professional and academic scientists and students includes those who study archeology, paleoecology, paleotsunamis, establishing the recent earthquake record, the tephra record, magmatic evolution of volcanoes, and the geomorphology of glacial and mass wasting events was. Shared resources and integration of scientific results greatly magnify our insights into particular disciplinary questions, our understanding of the relationships between the team's disciplinary results, and our ability to offer meaningful results to regional stakeholders, scientists, and policy makers.

EVIDENCE FOR MAGMA MIXING AND RAPID MAGMATIC ASCENT IN GROUNDMASS GLASS COMPOSITIONS FROM THE 2008 ERUPTION OF KASATOCHI, CENTRAL ALEUTIAN ISLANDS

Owen K. Neill[1], Christopher J. Nye[2]
[1]Peter Hooper GeoAnalytical Lab, School of the Environment, Washington State University, P.O. Box 642812, Pullman, WA 99164-2812.
[2]Alaska Volcano Observatory, State of Alaska, Division of Geological and Geophysical Surveys, 3354 College Road, Fairbanks, AK 99709 (retired).

Despite its small size (~3 km in subaerial diameter) and lack of historic eruptive history, the 7-8 August, 2008, eruption of the central Aleutian Kasatochi Island volcano was one of the most violent eruptions in recorded Alaskan history. This eruption lasted 21 hours, and included one earthquake with a magnitude of 5.9 and ~12 earthquakes with a magnitude of 4 or greater, releasing more cumulative seismic energy than any eruption ever monitored in the 28-year history of the Alaska Volcano Observatory (AVO) (Ruppert et al., 2011). The eruption also produced ~1.7 Tg of SO_2, the largest point source emission of sulfur during an eruption since the 1991 eruption of Cerro Hudson, Chile (Kristiansen et al., 2011), and a total volume of eruptive material of ~0.2 km^3 (Waythomas et al., 2011).

Previous studies of the petrology of the 2008 Kasatochi eruption have found that the eruptive products were dominated by two major lithologies; a white, pumiceous andesite containing ~58-62 wt% SiO_2, and a brown-grey, scoriaceous basaltic andesite containing ~52-55 wt% SiO_2 (Neill et al., 2015). Both lithologies are co-linear on many whole-rock element-element variation diagrams, but significant differences in some elements and ratios indicate that the two magmas were petrogenetically distinct, and that pre-eruptive mixing between the two was limited [4]. Groundmass glass compositions support this inference (Figure 1): at a given SiO_2 content, andesite glass compositions have significantly lower K_2O concentrations and K_2O/SiO_2 ratios. Trends in SiO_2 vs. TiO_2 and vs. P_2O_5 may indicate separate evolution of the andesite and basaltic andesite, with only late mixing between the two magmatic components.

All melt inclusions and groundmass glass from both the andesite and basaltic andesite record Cl concentrations of >1800 ppm, with the majority of concentrations >3000 ppm (Figure 2). Chlorine compositions show no significant correlation with either S or any major or minor oxide. Also, while Cl concentrations in melt inclusions appear slightly, albeit systematically, higher than those of the groundmass glass in the andesite, the range in melt inclusion and groundmass glass Cl concentrations overlap substantially in the basaltic andesite, thus magmatic ascent must have been sufficiently rapid for only minimal Cl loss via degassing to take place. By contrast, S concentrations in melt inclusions reach ~600 ppm in andesite melt inclusions and ~700 ppm in basaltic andesite melt inclusions, while groundmass glass S concentrations from both andesite and basaltic andesite samples are <250 ppm. This reflects the lower solubility and more rapid degassing of S (relative to Cl) in silicic magmas.

References:

Ruppert *et al.*, J. Geophys. Res. **116** (2011), pp. B00B07
Kristiansen *et al.*, J. Geophys. Res.-Atm. **115** (2010), pp. D00L16
Waythomas *et al.*, J. Geophys. Res. **115** (2010), pp. B00B05
Neill *et al.*. Am. Mineral. **100** (2015), pp. 722-737

Figures:

Figure 1: Andesite and Basaltic Andesite Groundmass Glass Compositions

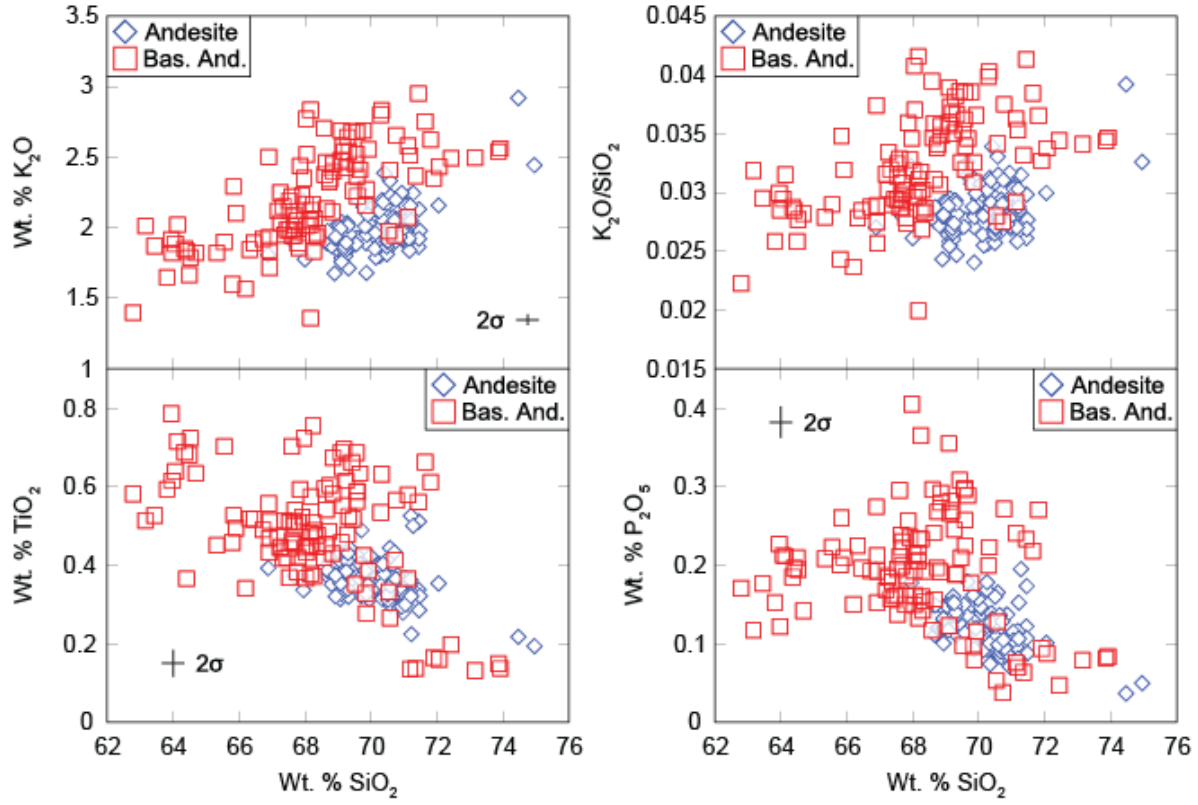

Figure 2: Melt inclusion and groundmass glass Cl concentrations

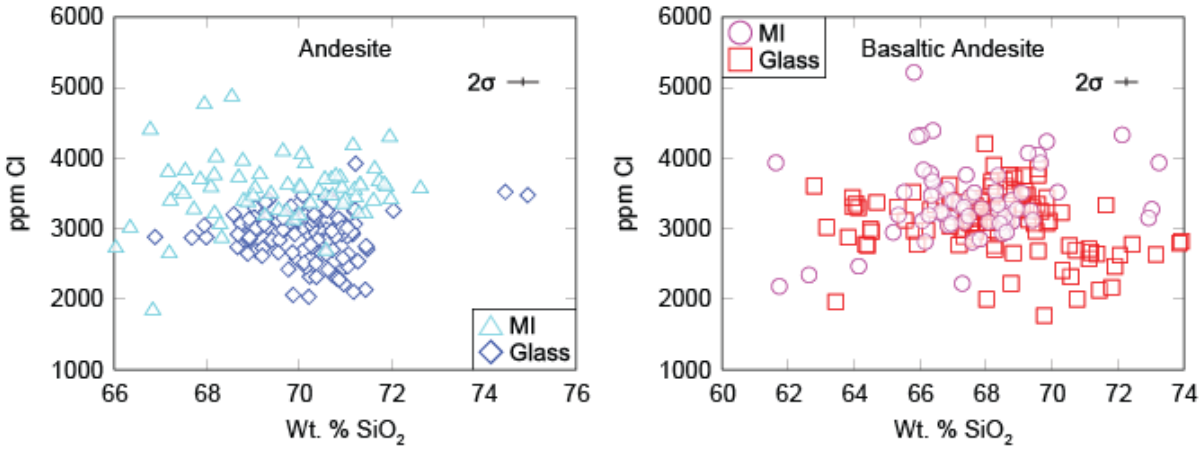

ISOTOPIC CONSTRAINTS ON VOLATILE CYCLING WITHIN THE ALEUTIAN ARC

Taryn Lopez[1], Tobias Fischer[2], Andrea Rizzo[3]
[1]*University of Alaska Fairbanks, Geophysical Institute, Fairbanks, AK, U.S.A.*
[2]*University of New Mexico, Albuquerque, NM, U.S.A.*
[3]*Istituto Nazionale di Geofisica e Vulcanologia (INGV), Palermo, Italy*

Volatiles are cycled between the Earth's interior and the exosphere primarily through the processes of subduction and arc volcanism. Volatiles released from arc volcanoes can originate from three sources: the subducted slab, mantle wedge and crust, each of which has a somewhat characteristic isotopic signature. For most well-studied volcanic arcs the subducted slab has been identified as the primary volatile source. The Aleutian Arc is home to some of the most poorly-studied volcanoes in the world, due to their remote location. For this reason, volatile cycling within this region is currently poorly constrained. To add to its intrigue, the Aleutian Arc is also known for significant along-strike variations in subduction features including convergence angle and rate, and subducted sediment flux, that we suspect strongly influence volatile cycling. The western portion of the Aleutian Arc in particular is known for low subducted sediment fluxes [Kelemen et al., 2003] and oblique convergence angles [DeMets et al., 1990], which we hypothesize results in its volatiles being sourced primarily from the mantle. Here we present new measurements of carbon and helium isotopes from volcanic gas emissions from four Western Aleutian volcanoes collected during a field expedition in September 2015. We compare the isotopic compositions of volcanic gases measured from our target volcanoes to the expected compositional ranges of the three potential volatile sources, and present preliminary interpretations of volatile provenance for the Western Aleutian Arc segment.

The volcanoes targeted in this study (from west to east) include: Kiska, Little Sitkin, Gareloi and Kanaga. Because each volcano has a different degassing manifestation, not all measurements were possible at each volcano. At Kiska, Little Sitkin and Kanaga we collected plume samples for analysis of $\delta^{13}C\text{-}CO_2$; while at Little Sitkin, Gareloi and Kanaga we collected fumarole samples for $^3He/^4He$ analyses, using the following methods. Plume gases were drawn into a lockable syringe, transferred into Tedlar bags, and then analyzed for CO_2 concentration and $\delta^{13}C\text{-}CO_2$ composition on board the Maritime Maid Research Vessel using a Thermo Scientific Delta Ray Isotope Analyzer. Between five and 20 samples were collected from each target volcano to ensure a variety of sample compositions reflecting mixtures between plume and ambient air. Then linear mixing trends between $\delta^{13}C\text{-}CO_2$ and $1/CO_2$ (ppmv) were used to extrapolate to the volcanic $\delta^{13}C\text{-}CO_2$ source following the methods of Chiodini et al. [2011] and Rizzo et al. [2014]. More details of this method can be found in Fischer and Lopez [2016]. Fumarole gases for He isotopic analysis were directly sampled by inserting a Titanium tube into the fumarolic vent and then connecting this tube to a copper tube, via silicon tubing. Once the sampling stream had thermally equilibrated with the fumarolic gases, the up-stream and down-stream ends of the copper tube were crimped to preserve the samples. These samples were then analyzed at the Noble Gas Isotope Laboratory at the Istituto Nazionale di Geofisica e Vulcanologia (INGV), Palermo, Italy. He concentration and isotope ratio were measured using a Helix SFT-GVI mass spectrometer following the methods of Rizzo et al., [2015]. The ^{20}Ne concentration, used to recalculate $^4He/^{20}Ne$ and to correct the $^3He/^4He$ for atmospheric contamination, was measured in a Helix MC plus-Thermo mass spectrometer. Extrapolated $\delta^{13}C\text{-}CO_2$ values of -5.1‰, -1.99‰, and -4.3‰ (in comparison to the reference PDB) are found for Kiska, Little Sitkin and Kanaga volcanoes, respectively (Fig. 1). The average measured $^3He/^4He$ ratios, first corrected for air contamination and normalized to the same ratio in air

(Rc/R_A), yield 7.02, 7.72, and 8.01 R_A for Little Sitkin, Gareloi and Kanaga volcanoes, respectively (Fig. 1). Considering that these values largely fall within the range of typical mantle $\delta^{13}C\text{-}CO_2$ and R_c/R_A values of 6.5±2.5‰ and 8±1, respectively, we propose that the mantle is the primary volatile source for these Western Aleutian volcanoes. The exception to this trend is Little Sitkin, whose $\delta^{13}C\text{-}CO_2$ is heavier than typical MORB, which could potentially reflect a carbonate source and/or isotopic fractionation. Complete geochemical analysis of the sampled gases is currently underway, which will help provide broader context to test and refine the interpretations presented here.

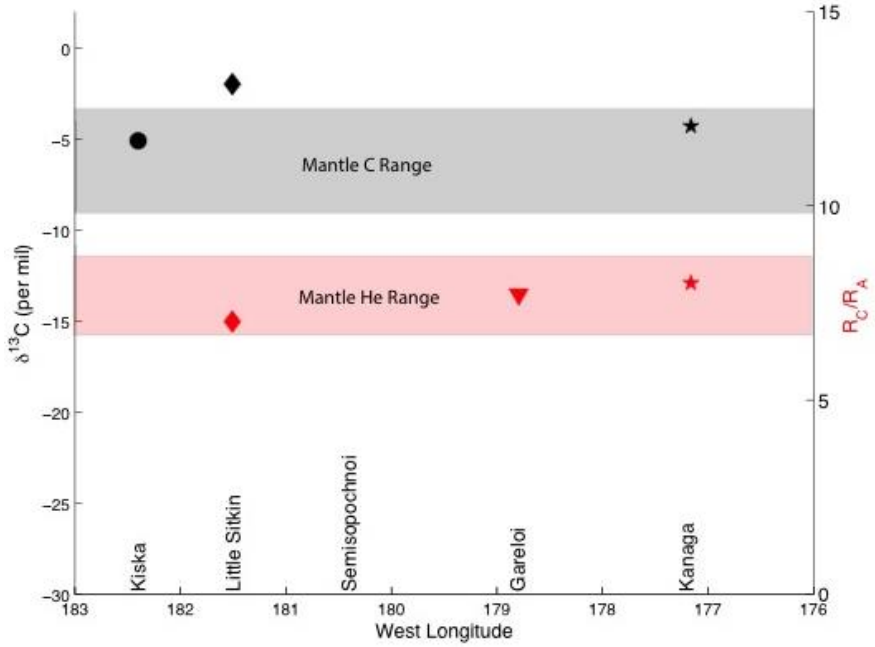

Figure 1: Measured $\delta^{13}C\text{-}CO_2$ (black symbols, left axis) and R_c/R_A (red symbols, right axis) isotopic compositions for Western Aleutian volcanoes, plotted by longitude. Typical mantle C and He isotopic compositions are shown for reference, in gray and red, respectively.

References:

DeMets, C., R. G. Gordon, D. F. Argus, and S. Stein (1990), Current plate motions, *Geophysics Journal International*, *101*, 425-478.

Chiodini, G., Caliro, S., Aiuppa, A., Avino, R., Granieri, D. and Moretti, R. (2011). First $^{13}C/^{12}C$ isotopic characterisation of volcanic plume CO_2, *Bulletin of Volcanology*, 73 (5): 531-542.

Fischer, T.P. and T.M. Lopez (2016), First airborne samples of a volcanic plume for $\delta^{13}C$ of CO_2 determinations, *Geophysical Research Letters*, 43, doi:10.1002/2016GL068499.

Kelemen, P. B., G. M. Yogodzinski, and D. W. Scholl (2003), Along-strike variations in the Aleutian Island Arc: Genesis of high Mg# andesite and implications for continental crust, *Inside the Subduction Factory, Geophysical Monograph*, *138*, 223-276.

Rizzo, A.L., Jost, H.-J., Caracausi, A., Paonita, A., Liotta, M. and Martelli, M. (2014), Real-time measurements of the concentration and isotope composition of atmospheric and volcanic CO_2 at Mount Etna (Italy), *Geophysical Research Letters*, 41: 2382-2389.

Rizzo, A., F. Barberi, M.L. Carapezza, A. Di Piazza, L. Francalanci, F. Sortino and W. D'Alessandro (2015), New mafic magma refilling a quiescent volcano: Evidence from He-Ne-Ar isotopes during the 2011–2012 unrest at Santorini, Greece, *Geochemistry Geophysics Geosystems*, doi:10.1002/2014GC005653.

LAHAR INUNDATION MODELING WITH THE AID OF HISTORIC FLOW DEPOSITS AT REDOUBT VOLCANO, COOK INLET, ALASKA

Alex M. Iezzi [1, 2], Douglas M. Thompson [2], Beverly Chomiak [2]
[1] *Geophysical Institute, Alaska Volcano Observatory, University of Alaska Fairbanks*
[2] *Department of Physics, Astronomy, and Geophysics, Connecticut College*

Redoubt Volcano is a 3108 m tall stratocone located in Cook Inlet, Alaska that explosively erupts roughly every 20 years. The five eruptions since 1900 all share the common characteristic of being accompanied by multiple large to very large lahars (10^8 to 10^9 m^3), as well as many that are smaller in magnitude (10^4 to 10^6 m^3). About 35 km from the crater of Redoubt Volcano lies the Drift River Marine Terminal that, if inundated, has the potential to cause an oil spill comparable in size to the Exxon Valdez spill of 1989. Non-Newtonian lahar flows evolve as they move down valley as a result of their bulking and debulking processes. The aim of this project was to model the largest lahars from the three most recent eruptions of Redoubt to better predict the area of inundation during future eruptions. Using GIS and the lahar simulation program Laharz_py, inundation models were created and compared with the known mapped area of post-eruption inundation done by the USGS for the seven most extensively studied lahars spanning the three most recent eruptions (1966-68, 1989-90, and 2009). The input data for these simulations consisted of a ten-meter resolution DEM and estimates of glacial meltwater volume as a measure of initial lahar volume proposed by both Dorava and Meyer (1994) and Waythomas et al. (2013). To capture the specific characteristics of the Redoubt Volcano lahars, a retrospective manipulation of the calibration factors was performed, such as the starting coordinates of the lahars, using the previously mapped areas of inundation.

Dorava, J. M., & Meyer, D. F. (1994). Hydrologic hazards in the lower Drift River basin associated with the 1989–1990 eruptions of Redoubt Volcano, Alaska. *Journal of Volcanology and Geothermal Research*, 62 (1), 387-407.

Waythomas, C. F., Pierson, T. C., Major, J. J., & Scott, W. E. (2013). Voluminous ice-rich and water-rich lahars generated during the 2009 eruption of Redoubt Volcano, Alaska. *Journal of Volcanology and Geothermal Research*, 259, 389-413.

GEOLOGY AND ^{40}AR/^{39}AR GEOCHRONOLOGY OF LONG-LIVED AKUTAN VOLCANO, EASTERN ALEUTIAN ISLANDS

Michelle Coombs[1] and Brian Jicha[2]
[1] *Volcano Science Center–Alaska Volcano Observatory, U.S. Geological Survey, Anchorage, AK 99508, USA.*
[2] *Department of Geoscience, University of Wisconsin, Madison, Wisconsin, 53706, USA.*

^{40}Ar/^{39}Ar dating and new whole-rock geochemical data expand the eruptive chronology for Akutan volcano, Akutan Island, in the eastern Aleutian island arc. Akutan Island (166° W, 54.1° N) is the site of long-lived volcanism and the entire island comprises volcanic rocks as old as 3.3 Ma (Richter et al., 1998, USGS Open-File 98-135). Our current focus is on the 225 km^2 western half of the island, where the Holocene active cone, Holocene to latest Pleistocene satellite vents, and underlying middle Pleistocene volcanic basement rocks are situated. Eruptive products span the tholeiitic–calc-alkaline boundary, are medium-K, and range from basalt to dacite. Incremental heating experiments on groundmass separates of 69 samples resulted in 55 ^{40}Ar/^{39}Ar plateau ages. The oldest ages (2075±9 and 2323±40 ka) are from two ridges southeast of the Holocene cone; these likely represent the volcanic basement that underlies the entire island. Above a major unconformity lie deeply eroded lavas from a several older satellite vents/volcanoes including Open Bight (765–752 ka), Lava Peak (605–595 ka), and Long Valley (678–522 ka). Two younger eruptive centers, Flat Top (155–98 ka) and Cascade Bight (63–43 ka) are located 3.5 km southwest and 4.5 km southeast of the current cone. Akutan edifice spans the last 286 kyr and has had two Holocene caldera forming eruptions. Our results show that the focus of volcanism has shifted within the western half of Akutan Island over the last ~700 ka, and that on occasion, multiple volcanic centers have been active over the same time period, including within the Holocene.

Holocene lavas, including those from Cascade Bight and Lava Point satellite vent on the NW coast, all fall along a single tholeiitic, basalt-to-dacite evolutionary trend that has lower K than Pleistocene lavas. Most "calc-alkaline" lavas show evidence consistent with their formation by mixing of mafic and evolved rocks, not through crystallization-derived differentiation through the calc-alkaline trend. Earliest lavas are mafic, have high La/Yb ratios consistent with broadly dispersed low degrees of partial melting throughout the mantle wedge. These magmas erupted prior to the development of Pleistocene fluctuations in glacial cover. Similar magmas erupted from Flat Top during MIS5, a time of rapid glacial unloading.

PETROLOGIC CHRONOLOGY OF THE 1999 SUB-PLINIAN ERUPTION OF SHISHALDIN VOLCANO

Daniel Rasmussen[1], Terry Plank[1], Amanda Lough[2], Pete Stelling[3], Diana Roman[2]
[1]*Lamont-Doherty Earth Observatory of Columbia University, Palisades, NY, USA.*
[2] *Department of Terrestrial Magnetism, Carnegie Institution of Washington, Washington, DC, USA.*
[3]*Geology Department, Western Washington University, Bellingham, WA, USA.*

On April 19, 1999 Shishaldin volcano burst to life, ejecting over 43 million cubic meters of basaltic ash into the atmosphere in a sub-Plinian eruption. InSAR images reveal a surprising lack of deformation preceding or accompanying the VEI 3 eruption (Moran et al., 2006 JVGR). Here we study olivine from this eruption to constrain subsurface magma movements and explore the causes of this unusual behavior. One possibility is that deep (>10 km) magma ascends relatively rapidly (i.e., within months) to shallow depths just prior to eruption (Moran et al., 2006 JVGR). This interpretation is consistent with the onset of long period seismic events suggesting the initiation of upward magma migration from depths of >15 km as early as July of 1998 (Moran et al., 2002 BV). By early February of 1999, at least some magma had reached the near-surface, as evidenced by a remotely-sensed thermal anomaly in the summit crater and vigorous steam venting. We can test the proposed open-vent behavior by determining precise locations of magmas and timing of pre-eruptive magmatic events (e.g., mixing) through petrologic analysis. This will serve both to inform our interpretation of precursory signals used to evaluate volcanic risks and aid in our understanding of open-vent volcanism.

We investigate chemical zonation and melt inclusions in olivines from the 1999 ash. Olivine core compositions are bimodal, with a broad mode centered on Fo_{62} and a much smaller mode of more primitive compositions near Fo_{78}. Most low-Fo olivines are reversely zoned, whereas high-Fo olivine are normally zoned, which provides strong evidence of magma mixing. The mixing-to-eruption timescale can be recovered from chemical gradients frozen in crystals that are erupted during partial diffusive equilibration, following a mixing event. Preliminary results of diffusion modeling suggest mixing occurred months to days prior to eruption. Such a large range of timescales implies that recharge did not occur at a single point in time, rather it was a prolonged event, which is consistent with seismic observations. Spatial constraints for this process can be provided by the study of melt inclusions, which act as pressure gauges because the dissolved volatile contents recorded by inclusions are strongly dependent on the pressures of entrapment. The majority of inclusions are found within the cores of low-Fo olivines. These inclusions have low volatile contents (0.2-2.1 wt.% H_2O, 0-164 ppm CO_2) and lack vapor bubbles. Vapor saturation pressures suggest maximum entrapment depths of 2.7 km, meaning the bulk of the more evolved mixing endmember was located within the edifice of Shishaldin. A second population of melt inclusions are entrapped within the reversely zoned rims of low-Fo olivine. These inclusions have higher volatile contents (0.6-2.4 wt.% H_2O, 199-330 ppm CO_2) and contain vapor bubbles. Entrapment occurred at depths of at least 3.5 km, which is likely to be consistent (after accounting for vapor bubbles) with the maximum depth of volcanic tremor at 5-6 km that occurred in the month leading up to the eruption (Thompson et al., 2002 BV). Thus, olivines record a rich history of the eruption that may relate closely to geophysical observations and bear on the causes of open-vent volcanism.

SOURCING PREHISTORIC OBSIDIAN TOOLS IN THE ISLANDS OF FOUR MOUNTAINS, ALASKA

Sam H. Sheffer[1], Virginia Hatfield[2], Kirsten Nicolaysen[1], Thomas Bartlett III[3], Dixie West[2], Emily Deacon[1], Kale Bruner[2]
[1] *Whitman College, Walla Walla, WA, USA.*
[2] *Biodiversity Institute, University of Kansas, Lawrence, KS, USA.*
[3] *Colgate University, Hamilton, NY, USA.*

Unlike lavas and jaspers, obsidian possesses more homogeneous compositions amenable to analysis by portable X-Ray Fluorescence (pXRF). Fractured obsidian produces thin, sharp edges ideal for knives and projectiles, though prehistoric Aleutians sites also include tools made of conchoidally fracturing aphyric lavas and jasper/opal. In the Islands of the Four Mountains (IFM), obsidian artifacts are found within cultural layers rich in datable organic matter and interbedded with distinctive tephra deposits (Hatfield et al., 2016). Because it offers rapid non-destructive analysis, pXRF is used to characterize and compare the chemical signatures of possible volcanic source materials available for tool-making and the tools themselves. A comparison of the compositions of 121 artifact fragments reveals similarities and differences for lithic resource use among six sites on three of the Islands of Four Mountains.

The isolated, windswept islands of Chuginadak, Carlisle, and Herbert lie in the transition from the eastern to the central Aleutian arc. Although these islands are currently uninhabited, the Unangax (Aleut) lived here for millennia (e.g., Laughlin, 1963; McCartney, 1984; West et al., 1999; Dumond and Knecht, 2001). ^{14}C dates of occupation by the IFM research team span as far back as 3632-3724 calibrated years BP (100% probability, 2□). In 2014 and 2015, obsidian artifacts especially tiny flakes or debitage (debris from making stone tools) were recovered from three prehistoric sites on Chuginadak Island and two prehistoric sites on Carlisle Island. In Unit 4 within a Carlisle Island site, the stratigraphy revealed many tools or tool fragments within multiple occupation horizons.

An investigation, using scatter plots of calibrated elemental data of obsidian identifies a unique signature for most IFM obsidian artifacts. Three replicate analyses of each sample and interspersed analytical standards produced accurate and precise measurements of elements Zr, Zn, Ca, Pb, K, and Nb. Use of the obsidian standards SPHM-1 and GBO plus powdered GSP-2, also provided calibration curves to correct the accuracy for precise elements Sr, Rb, Th, Fe, Mn, Ti, Ba, Al, and Si. Trace element ratios show most IFM obsidian artifacts cluster at consistent values such as Zr/Nb (24-26ppm), Fe/Mn (27-32ppm), and Ba/Rb (12-20ppm) shows that prehistoric IFM occupants primarily utilized one obsidian source. The discovery of a single lithic source suggests information sharing and cultural interaction among different IFM villages and islands. Zr/Nb, Fe/Mn and Ba/Rb clusters are distinct from previously characterized obsidian sources on Okmok and Akutan. However, one deeply buried artifact within a site on Carlisle Island matches Okmok obsidian elemental signature. Additionally, artifacts collected from Carlisle Island Unit 4 show that the same obsidian type was used consistently among stratigraphically-related different cultural horizons, i.e., through time.

THE RELATION BETWEEN PRE-FRAGMENTATION BUBBLE SIZE DISTRIBUTION, ASH PARTICLE MORPHOLOGY, AND THEIR INTERNAL DENSITY: IMPLICATIONS TO VOLCANIC ASH TRANSPORT AND DISPERSION MODELS

Alexander Proussevitch[1], Pavel Izbekov[2], Dork Sahagian[3]
[1]*Earth Systems Research Center, University of New Hampshire, Durham, NH 03824, USA*
[2]*Geophysical Institute, University of Alaska Fairbanks, Fairbanks, AK 99775, USA*
[3]*Lehigh University, Bethlehem, PA 18015, USA*

Parameterization of volcanic ash transport and dispersion (VATD) models strongly depends on particle morphology and their internal properties. Shape of ash particles affects terminal fall velocities (TFV) and, mostly, dispersion. Internal density combined with particle size has a very strong impact on TFV and ultimately on the rate of ash cloud thinning and particle sedimentation on the ground.

Unlike other parameters, internal density of vesicular ash particle cannot be measured directly because of the micron scale sizes of fine ash particles and the presence of vesicles, but we demonstrate that it varies greatly depending on the particle size. Small *simple* type ash particles (fragments of bubble walls, 5-20 micron size) do not contain whole large magmatic bubbles inside and their internal density is almost the same as that of volcanic glass matrix. On the other side, the larger *compound* type ash particles (>16 microns for silicic fine ashes) always contain some bubbles or the whole spectra of bubble size distribution (BSD), i.e. bubbles of all sizes, bringing their internal density down as compared to simple ash. So, density of the larger ash particles is a function of the void fraction inside them (magmatic bubbles) which, in turn, is controlled by BSD. Volcanic ash is a product of the fragmentation of magmatic foam formed by pre-fragmentation bubble population and characterized by BSD. The latter can now be measured from bubble imprints on ash particle surfaces using stereo-scanning electron microscopy (SSEM) and BubbleMaker software developed at UNH, or using traditional high-resolution computed X-Ray tomography (HR-XCT).

In this work we present the mathematical and statistical formulation for this problem connecting internal ash density with particle size and BSD, and demonstrate how the TFV of the ash population is affected by variation of particle density.

Theoretical formulations have been preliminarily validated with direct particle density measurements using Scanning Electron Microscope (SEM) and Back Scattered Electron (BSE) imagery analysis of particle cross-sections. We have used fine ash samples of explosive eruptions of Augustine Volcano in 1986, Redoubt Volcano in 2009. Loose micron-scale ash particle mounts have been mapped by SEM imagery, then impregnated in epoxy, polished, and examined using BSE analysis. The ratio of void to matrix area in individual ash particles has been used to measure each particle density. Our results are consistent with the theoretically predicted ash particle density distribution.

NEW DISCOVERED LATE MIOCENE VERCHNEAVACHINSKAY CALDERA ON EASTERN KAMCHATKA (UPSTREAM OF LEVAYA AVACHA AND KAVYCHA RIVERS): GEOLOGY, BOUNDARY AND COMPOSITION

O.V. Bergal-Kuvikas[1,2], V.L. Leonov[2], A.N. Rogozin[2], I.N. Bindeman[3], E.S. Kliapitskiy[2]
[1]Earth Observatory of Singapore, Nanyang Technological University, Singapore
[2]Institute of Volcanology and Seismology, Petropavlovsk-Kamchatsky, Russia
[3]University of Oregon, USA

During 2009, 2010, 2014 field works the new obtained caldera complex descripted in springheads of Levaya Avacha and Kavycha rivers (Eastern Range, Kamchatka) (Kuvikas & Rogozin, 2009; Leonov et al., 2011). Natural outcrops represented by thick interbedded layers of welded tuffs and ignimbrite (>500 meters thickness). The interbedded layers cover nearly 10 km area (Fig. 1). Volume of pyroclastic deposits was calculated as 220-230 km^3, based on size of caldera (Mason et al., 2004). These ejected volumes correspond to strong explosive eruptions with VEI 7 or more. The age of caldera-forming eruption was determined by Ar-Ar method to be of Late Miocene (5.78~5.58 Ma BP).

Detailed descriptions of the numerous thin sections and whole-rock geochemistry allows us to correlate sections of exposed outcrops from Verhneavachinskaya caldera (Fig. 2). We distinguished four main types of the rocks, which are characterized by different major and trace element composition, colors, textures, mineralogical and geochemical compositions. First types of the layers is ignimbrite of basaltic andesitic composition. Columnar jointing occurs at the most of the ignimbrite, exposed by active erosion process. Pyroclastic texture characterize most ignimbrite layers: microtexture represents by fragments of plagioclase, pyroxene phenocrystalls, and matrix of the rocks contains lithified welded tuffs with numerous fiammes. Second type of the layers is black, dense basaltic andesite less-changed ignimbrite layers. Structure of rocks contents fragments of plagioclase, pyroxene phenocrysts. Matrix of rocks represents by oriented plagioclase microlites. Third type is altered tuffs with yellow-orange tone. These rocks characterized by significant secondary hydrothermal alteration of rock`s matrix with quartz micro veins. Fourth type of the layers is volcanic breccias, which composed of broken different sizes rocks fragments with cemented tuffs matrix.

Whole-rock geochemistry of ignimbrite changes from basalt to andesite (SiO_2 51.2-59.5 wt. %), with corresponding natural decreasing FeO*, CaO, MgO, TiO_2. Across the outcrops from lower to upper ignimbrite layers the decreasing contents of SiO_2, MgO, Na_2O are observed with minimum on the top of outcrop. In comparing with another ignimbrite fields on Kamchatka the rocks from Verhneavachinskaya caldera characterized by higher contents of Nb, Ta, TiO_2 and MgO, lower contents of Na_2O, SiO_2 (Kliapitskiy, 2014).

New discovery of the Late Miocene Verhneavachinskaya caldera is as one of the older and mafic complex on Kamchatka opens many questions for origin and evolution magma in active island arc system: which are features of Late Miocene volcanism and how it correlate with geodynamic setting, e.g. with slab jumping and originated transform faults (Avdeiko, Bergal-Kuvikas, 2015).

Reference

Avdeiko, Bergal-Kuvikas. The geodynamic conditions for the generation of adakites and Nb-rich basalts... JVS, 2015. 9(5), 295-306.
Kliapitskiy. New data of geochemistry of ignimbrites…. XIII Regional young scientist conference. 2014. p. 81-90 p.
Kuvikas, Rogozin. First results of study 500-meters section...VII Regional conference for young scientists. 2009. p. 39-49.
Leonov et al. Determination of new caldera on Kamchatka… Material of conference to volcanologist day. 2011. 53-56 p.
Mason et al. The size and frequency of the largest explosive eruptions on Earth. Bull. Volcanol. 2004. V.66. p. 735-748.

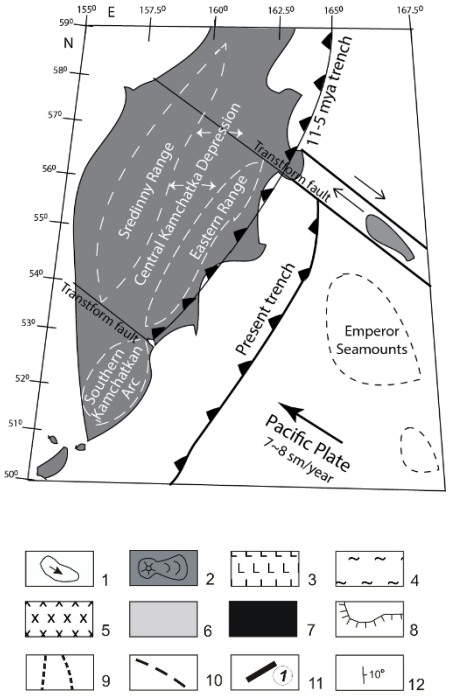

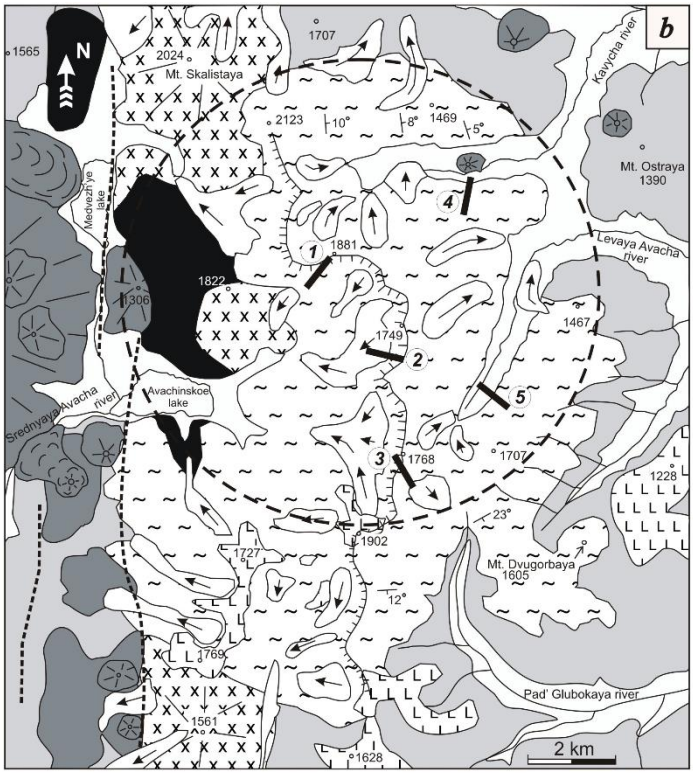

Fig. 1 a) General plate tectonic position of the Kamchatka and location of the Verhneavachinskaya caldera (black square).

b) Scheme of geological structure of springheads of Levaya Avacha and Kavycha rivers (Leonov et al., 2011). Note: 1 - Late Pleistocene-Holocene alluvium, glacial and debris deposits, arrows indicate movement of landslides, 2 - Pleistocene cinder comes and related lava flows, 3 – Pliocene-Early Pleistocene andesitic lava flows, 4 – Late Miocene ignimbrite deposits, 5 – Latter Miocene diorite intrusions, 6 – Miocene porphyritic basalts, agglomerate tuff, 7 - Late Cretaceous siltstones, argillites, 8 – cliffs of Avachinsky range, 9 - faults which are boundary graben of Srednyaya Avacha river, 10 - boundary of new-discovered caldera, 11- location of studied outcrops of ignimbrites (1-L-2010, 2-L-2014, 3-L-2012, 4- R-2009, 5-L-2009, please see details on Fig. 2), 12 – dip of the ignimbrite layer.

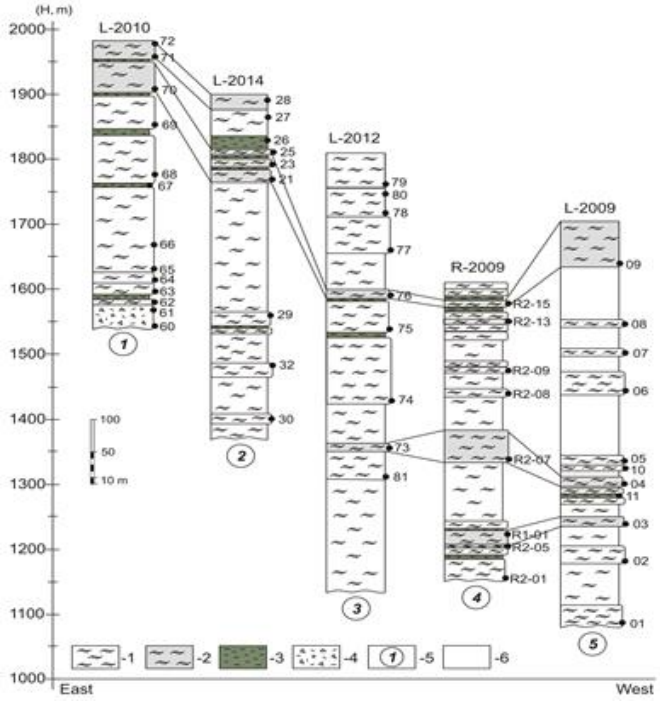

Fig. 2. Correlation of stratigraphic sections. Note: 1- ignimbrite layers, 2- marked ignimbrite layers, which are correlated on the sections, 3- altered tuffs with yellow-orange tones, 4-volcanic breccia, 5- numbers of the section are showed on Fig. 1, 6 – sodded outcrop area.

ALASKA TEPHRA DATABASE

Cheryl Cameron[1], Katherine Mulliken[1], Janet Schaefer[1], Kristi Wallace[2], Scott Crass[1]
[1]Alaska Division of Geological & Geophysical Surveys, Fairbanks AK.
[2] U.S. Geological Survey, Anchorage AK.

The Alaska Volcano Observatory (AVO) began construction of an Alaska tephra (volcanic ash) database in 2014. This project is a joint effort between staff at the Alaska Division of Geological & Geophysical Surveys (DGGS) and the USGS Alaska Tephra Lab. The Alaska tephra database houses all pertinent information on Alaska tephras, necessary for sample processing, archiving, and scientific research, and is fully integrated within AVO's larger Geologic Database of Information on Volcanoes in Alaska (GeoDIVA).

Tephra studies are a key component in understanding the process, magnitude, and frequency of volcanic eruptions, and improve volcanic ashfall hazard assessments and ashfall modeling efforts. Tephrostratigraphy is an integral part of linking marine, lacustrine, and terrestrial records critical to research of paleoclimate and archaeology. Developing correlations of tephra records across Alaska and the northern hemisphere requires an understanding of the age, chemistry, and character of tephra deposits. Currently, chemical, stratigraphic, and age data for Alaska tephra are dispersed in hundreds of publications and unpublished lab results, making efficient querying of data for specific research purposes impossible.

Our tephra database, with its associated web portals, will strive to alleviate this difficulty and make Alaska tephra data easily accessible for scientists. We are constructing the database in stages. The current database population and query focus is: basic sample information, sample age, and calculated averages from electron microprobe (EMPA) chemical analyses of glass. We have prioritized key marker-horizon tephras and have now entered sample information and EMPA glass averages for nearly 1,900 samples across Alaska, including those from Aniakchak and Hayes volcanoes, the Ahklun mountains area, Dawson tephra, Sheep Creek tephra, Old Crow tephra, and the White River Ash. We are about halfway through the available published data for EMPA glass averages from Alaska tephra.

We have also built an internal web portal to query sample metadata and geochemical data by geologist, author, publication, location, or known source volcano. After retrieving geochemical results a user may calculate a correlation coefficient using their desired parameters.

For the next phase, we plan improvements to the web portal, including search by possible source volcano, age, and spatial map query as well as improvements to the output to include number of analyses, standard deviation, and standards used in the analysis. When the web portal is robust, it will become available on the AVO public website.

Further steps to expand tephra data stored in the database include storing sample processing details and individual grain-point and mineral analyses as well as creating a laboratory interface for post-field sample workflow. We welcome feedback, comments, and questions from potential database users or dataset contributors.

PETROLOGY AND GEOCHEMISTRY OF THREE EARLY HOLOCENE ERUPTIONS FROM MAKUSHIN VOLCANO, ALASKA

Jessica F. Larsen[1], Janet R. Schaefer[2], James W. Vallance[3]
[1]*Geophysical Institute, Alaska Volcano Observatory, Univ. of Alaska. Fairbanks, AK, USA.*
[2] *Alaska Division of Geological and Geophysical Surveys, Fairbanks, AK, USA.*
[3]*U.S. Geological Survey, Cascades Volcano Observatory, Vancouver, WA, USA.*

Makushin volcano is a XX m stratovolcano with ice-filled caldera/crater, located 25 km west of Dutch Harbor and Unalaska village, Unalaska Island, Alaska. Makushin has produced on average one VEI 2-4 eruption every 200 years in the past 5000 C^{14} years (Bean, 1999). Tephra fall deposits exist in and around the Dutch Harbor/Unalaska area, with individual layer thicknesses from < 1 to ~20 cm locally. The three largest, most explosive Holocene eruptions from Makushin occurred within a ~1000-year time period: "CFE", (median radiocarbon age of 9048 BP), "Nateekin" (8743 BP), and "Driftwood" (8198 BP). The CFE unit produced thick scoria fall deposits to the northeast and east of the volcano and pyroclastic flow deposits in upper Makushin and "Waterfall" valleys to the east and north. The Nateekin eruption produced finer grained (fine ash to fine lapilli) deposits that are up to 20 cm in the Unalaska town area. The Driftwood eruption produced thick tan pumice and dense, black scoriaceous fall deposits primarily in the Driftwood valley and Lava Ramp area on the northeast flanks of the volcano.

Whole rock major and trace element compositions of 40 samples from the CFE and Driftwood eruptions were collected using XRF and LA-ICPMS analyses through the Washington State University Geoanalytical Lab. Samples from the Nateekin unit were not analyzed for whole rock geochemistry because they are too fine grained (typically <1cm lapilli to fine ash). Electron probe microanalyses of glass, phenocryst, and microlite phases from all three units were collected at UAF using the JEOL XX field emission electron microcprobe, using standard conditions for glass and mineral phases.

The CFE and Driftwood eruptions produced medium K_2O, tholeiitic (Miyashiro, 1974) andesites: CFE = 56 to 60 wt. % SiO_2; Driftwood = 60 to 63 wt. % SiO_2. The three units have andesite to rhyodacite glass compositions, as follows: CFE= 57 to 64 wt. % SiO_2; Nateekin = 59 to 61 wt. % SiO_2; Driftwood = 67 to 70 wt. % SiO_2. The CFE and Driftwood scoria and pumice samples have plagioclase, clinopyroxene and orthopyroxene as the primary mineral phases, with minor olivine in the CFE fall deposit scoria. The pyroxenes in the CFE and Driftwood samples are uniform in composition with orthopyroxenes = $Wo_{4.6}En_{58.7}Fs_{36.7}$ (n=58) and clinopyroxenes = $Wo_{39.7}En_{41.9}Fs_{18.4}$ (n=132). Plagioclase phenocrysts from Driftwood pumice have $An_{52\text{-}54}$ cores and slightly more sodic rims of $An_{48\text{-}49}$. CFE plagioclase phenocrysts are not as uniform, with a lower $An_{50\text{-}54}$ group and a higher $An_{70\text{-}89}$ group.

The Nateekin glass compositions are very similar to those from CFE scoria samples from the middle to top of the unit. Thus, the Nateekin eruption may have tapped the same magma body as the CFE, indicating the magma system did not change significantly in the ~300-year time period between the two eruptions. The Driftwood eruption produced an andesite with higher SiO_2, Al_2O_3, FeO, and lower MgO magma than the CFE. It is unlikely to be related to the CFE magma by simple fractionation of pyroxenes and plagioclase, indicating a significant change in the magma stored beneath Makushin in the ~700 years between the Nateekin and Driftwood eruptions.

INTERDISCIPLINARY POSTER SESSION

(Abstracts are listed sequentially according to the Scientific Program)

FULL MOMENT TENSOR AND SOURCE-TYPE ESTIMATION FOR VOLCANIC EVENTS

Celso R. Alvizuri, Carl Tape
Geophysical Institute and Department of Geosciences, Univ. of Alaska Fairbanks, Fairbanks, Alaska

The seismic full moment tensor is a general representation of any seismic point source, and can represent double-couple (DC) but also non-DC mechanisms such as isotropic and CLVD. We present a catalog of full seismic moment tensors for 63 small (Mw < 3) events from Uturuncu volcano in Bolivia. The events were recorded by up to 24 broadband stations during an array deployment by the PLUTONS project between 2010-2012. Most events had magnitudes between 0.5 < Mw < 2.0 and did not generate discernible surface waves. We estimate each event from a grid-search over the six-dimensional space of moment tensors. For each event we computed the misfit between observed and synthetic waveforms, and we also used first- motion polarity measurements to reduce the number of possible solutions. Each moment tensor solution was obtained using a grid search over the six-dimensional space of moment tensors. For each event we characterize the variation of moment tensor source type by plotting the misfit function in eigenvalue space, represented by a lune. We identify three main types of events in the catalog: (1) 6 isotropic events, (2) 5 tensional crack events, and (3) a swarm of 14 events that appear to be double-couples. The occurrence of positively isotropic events is consistent with other published results from volcanic and geothermal regions. Several of these previous results, as well as our results, cannot be interpreted within the context of either an oblique opening crack or a crack-plus-double-couple model; instead they require a multiple-process source model. Our study emphasizes the importance of characterizing uncertainties for full moment tensors, and it provides strong support for isotropic events at Uturuncu volcano.

GENERATING DYNAMIC VOLCANIC HAZARD MAPS FOR DOMINICA, LESSER ANTILLES BY USING GEOPHYSICAL DATA AS WEIGHTS IN SPATIAL INTENSITY MAPS

Ophelia George[1], Joan L. Latchman[2], Charles Connor[1], Stephen McNutt[1], Laura Connor[1]
[1] School of Geosciences, University of South Florida, Tampa, Florida, 33620
[2] Seismic Research Center, University of the West Indies, Port of Spain, Trinidad, West Indies

Risk posed by volcanic eruptions are generally quantified in a few ways; in the short term geophysical data such as seismic activity or ground deformation are used to assess the state of volcanic unrest while statistical approaches such as spatial density estimates are used for long term hazard assessment. Spatial density estimates have been used in a number of monogenetic volcanic fields for hazard map generation and utilize the age, location and volumes of previous eruptions to calculate the probability of a new event occurring at a given location within this field. In a previously unpublished study, spatial density estimates of the Lesser Antilles volcanic arc showed the island of Dominica to have the highest likelihood of future vent formation. In this current study, this technique was used in combination with the SRC catalog of seismic events occurring beneath Dominica within the last ~ 20 years to generate a hazard map which not only takes into consideration the past events but also the current state of unrest. Here, geophysical data serve as a weighting factor in the estimates with those centers showing more vigorous activity receiving stronger favorability in the assessment for future activity. In addition to this weighting, the bandwidth utilized in the 2D-elliptical kernel density function was optimized using the SAMSE method so as to find the value which best minimizes the error in the estimate. The end results of this study are dynamic volcanic hazards maps which will be readily updatable as changes in the geophysical data occur.

GEOMECHANICAL INTERPRETATION OF LOCAL SEISMICITY CONCERNING ACTIVITY OF TOLBACHIK, KORYAKSKY AND AVACHINSKY VOLCANOES OF KAMCHATKA IN 2008-2012

A.V. Kiryukhin, S.A. Fedotov, P.A. Kiryukhin
Institute of Volcanology & Seismology FEB RAS, Piip 9, P-Kamchatskii, Russia, 683006
Exigen Services, Pulkovskoe 40-1, Saint-Petersburg, Russia, 196158

Local seismic activity during 2012 eruption of Tolbachik volcano and 2008-2009 steam-gas eruption of Koryaksky volcano is considered as a result of the injection of magma forming plane-oriented zones: dykes, sills and activation of existing faults. To identify these zones the plane-oriented clusters of earthquakes were distinguished with the catalogs of Kamchatka Branch of Geophysical Survey RAS, their subsequent spatial-temporal analysis allows the following interpretation. 27.11.2012. Tolbachik volcano eruption was preceded by the injection of magma with the introduction of a series of dikes of west-north-west striking in the depth range -4 - +3 km abs. in the area to the southeast of the Plosky Tolbachik volcano. The indicated fractures dissection of a subhorizontal permeable zone at an altitude near zero lead to the formation of sills and magma discharge injection dike (dip angle of 50°, dip azimuth 300^{o}) at 5.5 km from the epicenter of the initial magma injection. 2008-2009 summit steam-gas eruption of Koryaksky volcano was preceded by the crustal chamber being saturated with magma (the depth of the roof -3 km abs, width 2.5 km) at the south-western foot of the Koryak volcano, further injection of magma in submeridional area (7.5 x 2.5 km, depth range -2 - -5 km abs.) of the northern sector of Koryaksky volcano occurred in parallel with the summit steam-gas eruption. The injection of magma into the cone of Avacha volcano (2010) took place with the cone being saturated with sills (in the range of marks +1600 - +1900 masl) and dikes (mostly of NW-trending).

SEISMIC MOMENT TENSORS AND ESTIMATED UNCERTAINTIES IN SOUTHERN ALASKA SUBDUCTION ZONE

Vipul Silwal and Carl Tape
Department of Geosciences, University of Alaska Fairbanks, Alaska, USA

We present a moment tensor catalog of 106 earthquakes in southern Alaska, and we perform a conceptually based uncertainty analysis for 21 of them. For each earthquake, we use both body waves and surface waves to do a grid search over double couple moment tensors and source depths. For smaller events we also include the first-motion polarity information to further constrain the solution. The combination of waveform and polarity misfit gives the total misfit function, at the minimum of which lies the solution. For our purposes, the inclusion of polarity misfit proved immensely beneficial when performing source inversion of small events around Cook Inlet and could possibly help in delineating unknown faults. The uncertainty parameter or, rather, our confidence parameter is the average value of the curve P(V), where P(V) is the posterior probability as a function of the fractional volume V of moment tensor space surrounding the minimum-misfit moment tensor. As a supplemental means for characterizing and visualizing uncertainties, we generate moment tensor samples of the posterior probability. We perform a series of inversion tests to quantify the impact of certain decisions made within moment tensor inversions and to make comparisons with existing catalogs. For example, using an L1 norm in the misfit function provides more reliable solutions than an L2 norm, especially in cases when all available waveforms are used. Using body waves in addition to surface waves, as well as using more stations, leads to the most accurate moment tensor solutions. These choices will be important when implementing real-time moment tensor inversion in Alaska. Our estimation of uncertainties will be important for identifying the style of faulting within yet-to-be-discovered fault zones.

TRACKING GLACIERS WITH THE ALASKA SEISMIC NETWORK

Michael West[1], Natalia Ruppert[1], Natalia Kozyreva[1], Sara Meyer[1], Dara Merz[1], Miriam Braun[1]
[1]Alaska Earthquake Center, Geophys. Institute, Univ. Alaska Fairbanks, Fairbanks, AK, USA.

More than 40 years ago it was known that calving glaciers in Alaska created unmistakable seismic signals that could be recorded tens and hundreds of kilometers away. Their long monochromatic signals invited studies that foreshadowed the more recent surge in glacier seismology. Beyond a handful of targeted studies, these signals have remained a seismic novelty. No systematic attempt has been made to catalog and track glacier seismicity across the years. Recent advances in understanding glacier sources, combined with the climate significance of tidewater glaciers, have renewed calls for comprehensive tracking of glacier seismicity in coastal Alaska. The Alaska Earthquake Center has included glacier events in its production earthquake catalog for decades. Until recently, these were best thought of as bycatch—accidental finds in the process of tracking earthquakes. Processing improvements a decade ago, combined with network improvements in the past five years, have turned this into a rich data stream capturing hundreds of events per year across 600 km of the coastal mountain range. Though the source of these signals is generally found to be iceberg calving, there are vast differences in behavior between different glacier termini. Some glaciers have strong peaks in activity during the spring, while others peak in the late summer or fall. These patterns are consistent over years pointing to fundamental differences in calving behavior. In several cases, changes in seismic activity correspond to specific process changes observed through other means at particular glacier. These observations demonstrate that the current network is providing a faithful record of the dynamic behavior of several glaciers in coastal Alaska. With this as a starting point, we examine what is possible (and not possible) going forward with dedicated detection schemes.

LONG-TERM OCEAN BOTTOM MONITORING OF SLOW EARTHQUAKES ON THE SHALLOW PLATE INTERFACE IN HYUGA-NADA, WESTERN PART OF THE NANKAI TROUGH

Yusuke Yamashita[1], Masanao Shinohara[2], Tomoaki Yamada[2], Kazuo Nakahigashi[3] , Hajime Shiobara[2], Kimihiro Mochizuki[2], Takuto Maeda[2], Kazushige Obara[2]
[1] Miyazaki Obs. Disaster Prevention Research Institute (DPRI), Kyoto University, Japan.
[2] Earthquake Research Institute (ERI), the Univ. of Tokyo, Japan.
[3] Tokyo University of Marine Science and Technology, Japan.

The Hyuga-nada region, western part of the Nankai Trough in Japan, is one of the most active areas of shallow slow earthquakes in the world. Recently, ocean-bottom observation of offshore seismicity near the trench have succeeded to detect shallow tremor as a complete episode lasting for one month exhibiting similar migration property of deep tremor for the first time [Yamashita *et al*., 2015 *Science*]. This activity was also associated with shallow very-low-frequency earthquake (VLFE) activity documented by land-based broadband seismic network. The coincidence between tremor and VLFE and their migration pattern show strong resemblance with deep tremors during ETS episodes; this similarity suggests that the tremor activity in the shallow plate boundary may also be coupled with VLFE and short-term slow slip events (SSEs) in this area. However, the shallow SSEs have not been detected to date, probably due to the lack of dense broadband seismic and/or geodetic observations in offshore. To clarify the relationship among these slow earthquakes is important to improve the assessments of the potential of tsunamigenic megathrust earthquake that is anticipated to occur at the Nankai Trough.

Motivated by these issues, we have started long-term ocean-bottom monitoring of them in this area from May 2014 using three kinds of sensors: broadband seismometer with pressure gauge (BBOBSP) and short-period seismometer (LTOBS). This project is the first of the long-term continuous observation over several years in this area. During the first observation (March 2014 to January 2015), minor shallow tremor and VLFE activity occurred just under the OBS network. In addition, we confirmed that seismicity of ordinary earthquake was very low within the focal area of shallow slow earthquake. The second observation started from January 2015 using 3 BBOBSPs and 10 LTOBSs, and all sensors were retrieved in January 2016. From the monitoring using land-based seismic observation, many shallow tremors and VLFEs occurred just under the OBS network during second observation period, which started from early in May 2015 and continued approximately 2 months. We confirmed the existence of these signals in the data recorded by each OBSs. Although the source locations are still not located, they were probably migrated within the OBS network, which reached at off Cape Ashizuri area where shallow VLFEs have been occurred every 6-7 years associated with long-term SSE at Bungo channel. This off Cape Ashizuri's activity (tremor and VLFE) started at the end of May, especially increased activity after the large deep-focused earthquake at Ogasawara region (Mw7.8, 30 May 2015).

In the presentation, we will introduce the review of shallow slow earthquake observation in Hyuga-nada and preliminary result of second observation, in particular focus on the migration of shallow tremor.

GRAVITY DECREASE AND VOLCANIC INFLATION AROUND THE ACTIVE CRATER AT TOKACHI-DAKE VOLCANO, HOKKAIDO, JAPAN

Noritoshi Okazaki[1], Ryo Takahashi[1], Makoto Tamura[1], Hiroaki Takahashi[2], Masayoshi Ichiyanagi[2], Teruhiro Yamaguchi[2], Ryo Honda[3], Yosuke Miyagi[4], Akimichi Takagi[5]
[1]Geological Survey of Hokkaido, Hokkaido Research Organization, Sapporo, Japan.
[2]Institute of Seismology and Volcanology, Hokkaido University, Sapporo, Japan.
[3]Tono Research Institute of Earthquake Science, Mizunami, Japan.
[4]National Research Institute for Earth Science and Disaster Prevention, Tsukuba, Japan.
[5]Meteorological Research Institute, Japan Meteorological Agency, Tsukuba, Japan.

Magmatic mass monitoring is one of fundamental parameter for activity forecasting. Recent development in portable gravity meter and high precision GPS positioning techniques have allowed us to make gravity observation on active volcano repeatedly. Simultaneous observation of gravity and ground deformation at same point will provide valuable information for deformation source material, e.g. magma or water.

Tokachi-dake volcano is one of the most active volcano in southwestern Kuril subduction zone. Three magmatic eruptions had been recorded in a recent hundred years. We installed the continuous GPS station in 2003 near the active crater in order to observe the ground deformation that associated with the active volcanic activity. The local inflation continues around the active crater from 2006. In order to investigate the cause of the inflation, we started the relative microgravity measurement at 27 benchmarks from 2008. Scintrex CG-3M and CG-5 gravity-meters, and dual-frequency GPS receiver for three dimensional positioning has been simultaneously in operation at benchmarks.

Figure shows 5 results of the relative gravity measurement using GSH's CG-5 from 2010 to 2015. The gravity change is a tendency to decrease at active crater area, and reaches -0.12 to -0.14 mGal in 2015. On the other hand, the ground uplift in our GPS station (G016) reaches a maximum of 0.2 m. Assuming a free air gradient (-0.3086mGal/m), if the ground is 0.2 m uplift, the gravity value is decreased by -0.062 mGal. Even includes measurement errors, the gravity decrease cannot be explained only ground uplift. Excessive decrease of such gravity values for ground uplift has also been observed in the Izu-Oshima volcano (Takagi et al., 2010). In order to explain this excessive decrease, it is necessary to consider such as the changes in the density structure in the shallower part of under the active crater.

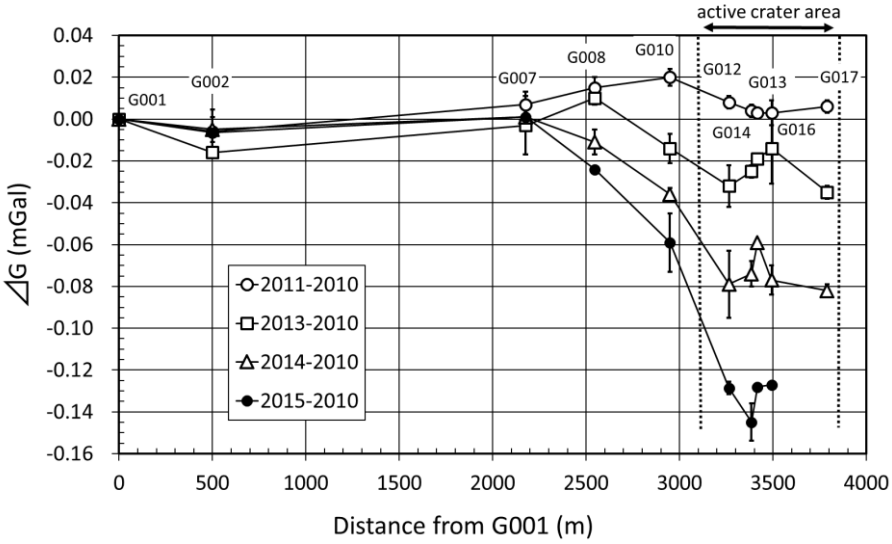

THE KLUCHEVSKAYA VOLCANO GROUP OBSERVATION NETWORK 2006-2016. RUSSIA, KAMCHATKA.

S.S. Serovetnikov[1], E.I. Gordeev[2], Hiroaki Takahashi[3], Pavel Izbekov[4]

[1] *Kamchatka Branch Geophysical Service, (KBGS RAS, Russia)* sssu@emsd.ru
[2] *Science Institute of Volcanology and Seismology (IVS FEB RAS, Russia)* aifgf@mail.ru
[3] *Hokkaido University (Japan)* hiroaki@mail.sci.hokudai.ac.jp
[4] *Geophysical Institute, UAF (USA)* peizbekov@alaska.edu

Last 10 years of the Russian and international projects was actively developed the networks of continuous geodynamic observations in various local parts of the Kluchevskoy volcanic center. As a result, in 2011 was generated the geodynamic network over all Kluchevskaya volcano group. The constant geodynamic stations of local observations over separate volcanoes, was unite to Kluchevskaya volcano group observation network. Further the network is extended constantly.

During the observations (2006-2016) have been registered the deformation processes caused by activity volcanoes Bezimianny, Kuchevskoy and Tolbachik. Now the geodynamic observations network includes 12 GNSS continuous stations, 5 Tiltmeter points and more than 50 points for periodic GNSS observations.

The Kluchevskaya volcano group observation network is created as a work result by projects “PIRE” (2006-2010) – Geophysical Institute (UAF,USA), “KAKENY” (2010-2015) – Hokkaido University (Japan), (2013-2015) the Russian fund of basic researches (RFBR RAS Russia), with assistance of Science Institute of Volcanology and Seismology (IVS FEB RAS, Russia) and Kamchatka Branch Geophysical Service, (KBGS RAS, Russia).

The poster describes formation stages of the geodynamic Kluchevskaya volcano group observation network, some results of observations and the further prospects of observation system development.

HAVE THE POSTSEISMIC MOTIONS DUE TO THE MAY 24, 2013 Mw 8.3 OKHOTSK DEEP FOCUS EARTHQUAKE BEEN DISCOVERED BY THE RUSSIAN FAR EAST GNSS NETWORKS?

Nikolay Shestakov[1,2], Grigory Nechaev[1,2], Nikolay Titkov[3], Mikhail Gerasimenko[1,2], Victor Bykov[4], Victor Pupatenko[4], Sergey Serovetnikov[3], Alexander Prytkov[5], Nikolay Vasilenko[5], Dmitry Sysoev[1,2], Alexey Sorokin[6], Hiroaki Takahashi[7] and Mako Ohzono[7]

[1]*Institute for Applied Mathematics of FEB RAS, Vladivostok, Russia*
[2]*Far Eastern Federal University, Vladivostok, Russia*
[3]*Kamchatka Branch of Geophysical Survey of RAS, Petropavlovsk-Kamchatsky, Russia*
[4]*Institute of Tectonics and Geophysics of FEB RAS, Khabarovsk, Russia*
[5]*Institute of Marine Geology and Geophysics of FEB RAS, Yuzhno-Sakhalinsk, Russia*
[6]*Computing Center FEB RAS, Khabarovsk, Russia*
[7]*Institute of Seismology and Volcanology, Hokkaido University, Sapporo, Japan*

Three years have almost elapsed since the mainshock of the Okhotsk deep focus earthquake occurred on May 24, 2013, at 05:45 UTC in the Sea of Okhotsk near the western coast of the Kamchatka Peninsula. Up to now this seismic event has been remaining the largest deep focus earthquake (Mw = 8.3) in the history of instrumental seismology. The earthquake caused notable and measurable by GNSS technique 3-D coseismic crustal displacements in a wide region around the epicenter. The detected offsets were used by several authors to develop the earthquake source dislocation models. However, despite a significant number of measured coseismic displacements and available a-priory seismological information, the parameters of these models have not been reliably determined.

In this work we analyze coordinate time series of a set of continuous geodetic sites that belong to different geodynamic GNSS networks deployed in the Kamchatka Peninsula, Sakhalin Island and the western coastal areas of the Sea of Okhotsk and the Sea of Japan. The considered time span covers 5 years before and almost 3 years after the earthquake (2008-2015). We have discovered an abrupt annual velocity change after the mainshock at a set of GNSS sites located within the above mentioned region. A coincidence of the beginning of the observed effect with the time of the Okhotsk earthquake occurrence allows us to treat it as a consequence of the earthquake. For most of the network stations, an increase of the western velocity component by 1-4 mm/yr has been observed. Changes in the vertical GNSS site velocities have also been detected, but their quantification is difficult due to limited accuracy of the vertical displacement measurements by GNSS technique. It should be noted that almost all of the obtained postseismic time series retain their linear behavior in contrast to the known examples of postseismic time series caused by shallow earthquakes. Probably, the discussed annual velocity changes detected after the deep focus earthquake have been obtained for the first time.

The physical mechanism of the observed phenomenon has not been clearly determined yet. The deep (> 600 km) location of the Okhotsk earthquake hypocenter precludes us from considering the poroelastic rebound mechanism as a possible candidate to explain the observed effects. The afterslip impact on the observed surface displacements should also be small and rather rapidly decreasing with time. The viscoelastic relaxation and/or some other geodynamic processes seem to provide a more appropriate explanation of the long-term annual velocity changes which are observed in the Russian Far East after the Okhotsk earthquake.

This work was partially supported by FEFU grant No. 14-08-01-05_m and RFBR grant No. 15-37-20269.

COMPOSITIONAL TRENDS OF AMPHIBOLE IN 2001-2013 YOUNG SHIVELUCH ANDESITES AS EVIDENCE OF MAGMA CHAMBER REPLENISHMENT AND SUBSEQUENT CONVECTION

Natalia Gorbach[1], Maxim Portnyagin[2,3], Tatiana Philosofova[1]

[1] *Institute of Volcanology and Seismology FED RAS, Petropavlovsk-Kamchatsky, Russia, n_gorbach@mail.ru*

[2] *GEOMAR Helmholtz Centre for Ocean Research Kiel, Kiel, Germany*

[3] *V.I.Vernadsky Institute of Geochemistry and Analytical Chemistry RAS, Moscow, Russia*

Hornblende-plagioclase andesites of the Young Shiveluch volcano erupted from 2001 to 2013 show minor variations of whole rock and matrix glass compositions but large variations of mineral phenocryst compositions. We focused this work on the composition of amphiboles in andesites from the growing Shiveluch lava dome, pumiceous rocks from pyroclastic flows and rare mafic inclusions. We propose that the shallow magma chamber was replenished during this time that enhances magma convection and caused more frequent eruptions.

2001-2013 eruptive dynamics and whole rocks compositional variations

Intensive growth of the lava dome alternating with episodes of its destruction was observed in 2001-2013. During this period Young Shiveluch had five paroxysmal explosive eruptions (May 2001 and May 2004, February and September 2005 and in October 2010). In the course of these eruptions extensive pyroclastic flows covered the valleys on the southern volcano slopes at a distance of 20-25 km from the eruptive center. In 2007, 2008, 2009 and 2013 more moderate explosions also occurred and were accompanied of small-volume pyroclastic flows. The volume of material erupted during 2001 - 2012 appears to be close to 0.8 km^3 (Shevchenko et al., 2015) even if lavas erupted in 2013 and tephra placed outside of the volcanic edifice are not taken into account.

SiO_2 content in lava dome samples and pumice fragments from pyroclastic flows is 60.5–64.0 wt.% and varies unsystematically over time. The andesites contains 15-20 to 45 vol.% phenocrysts which are represented by plagioclase with An in cores ranging from 30 to 83-88 mol. %, low- and high-Al amphiboles, and rare orthopyroxene and clinopyroxene with Mg# 69-74. Rare olivine (Fo_{80-88}) with reaction rim of orthopyroxene, Fe-Ti oxides and amphibole are presents in most samples. Groundmass is composed by plagioclase, subordinate pyroxene, magnetite and rare amphibole microliths. Matrix glasses are rhyolitic (SiO_2 =74 - 80 wt.%) in all samples. Mafic inclusions, which were found in a block in pyroclastic deposits of 2005 eruption (Gorbach, 2006) are olivine-hornblende basaltic andesite (SiO_2 = 56.3 wt. %).

Amphibole texture and chemistry

Phenocrysts, microphenocrysts and rare microliths of amphiboles in the 2001-2013 eruptive products show a wide range of major element compositions (in wt.%: SiO_2=40.46-50.13; TiO_2=0.56-3.54, Al_2O_3=6.18-14.06, FeO*=6.07-15.24, MgO=11.56-19.31, CaO=10.62-12.59, Na_2O=1.19-3.67, K_2O=0.09-0.75). This compositional range corresponds to masnesiohornblende (*Mg-Hbl*), pargasitic (*Prg*) and magnesiogastingsitic (*Mg-Hst*) amphibole after Leake et al. (1997). Most crystals are idiomorphic. Opacitized amphiboles are rare in 2001-2013 andesites. Two main amphibole generations have been distinguished on the basis of their textural and chemical features: 1) Middle-sized phenocrysts of *Mg-Hbl* (≥1-1.2 мм) with simple chemical zoning (Al, Fe, Na decrease, Si and Mg increase from core to rim); 2) Large phenocrysts (≥1.5-2 mm) with patchy, chemically very heterogeneous, especially with regard to Al and Mg, core compositions containing abundant inclusions of melt, plagioclase and magnetite. In addition to these generations, subphenocrysts (0.3-0.5 mm) and microlites (0.1-0.2 mm) of *Prg* and *Mg-Hst* hornblende were found in some samples erupted in 2004, 2007 and

2013. Amphiboles phenocrysts and microliths from mafic inclusions correspond mainly to *Mg-Hst* composition.

The most of zoned phenocrysts studied exhibit inverse correlation between Mg, Si (on the one side) and Al, Ti, Fe, Na (on the other side), corresponding to edenite - Al-tschermakite substitution. However, this correlation is disrupted in some crystals. For example, simultaneous increase of Al and Mg is observed in amphiboles from mafic inclusions and on the crystal rims at the contact of a host andesite with the inclusion, in some crystals from 2001, 2004, 2007 and 2013 eruptions. The positive trend of Al and Mg (or of Al_{IV} and Mg#, Fig.1) is interpreted in a series of papers as trend magma replenishment (e.g., Sato et al, 2005; Kiss et al., 2014).

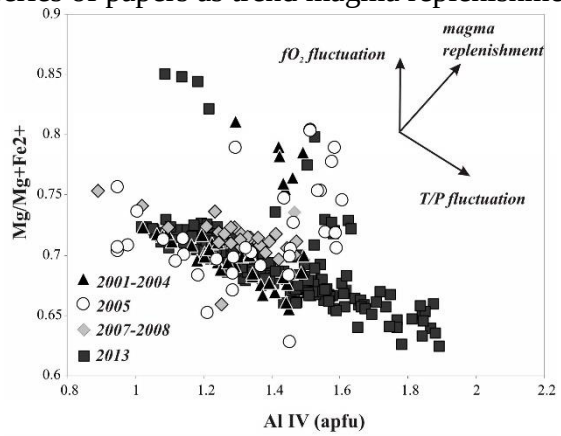

Fig. 1. Al_{IV} (a.p.f.u.) vs. Mg# variations in amphiboles from 2001-2013 Young Shiveluch rocks.
In result of mafic magma replenishment, the silica content in magma decreases that leads to increasing Al_{IV} values in amphiboles. Mafic input also increases $Mg/Mg+Fe^{2+}$ ratio in the mixed magma. Thus, simultaneous increase in Al_{IV} and Mg# of amphibole is expected to reflect magma replenishment (Kiss et al., 2014).

Dirksen et al. (2006) proposed on the basis of olivine reaction rim study that mafic replenishment preceded two months to four years the 2001 eruption. The data on amphibole compositions are consistent with this conclusion and indicate that a part of the crystals of amphiboles from 2001-2013 Young Shiveluch andesites crystallized from hotter magma. According to Ridolfi et al. (2010) and Holland, Blundy (1994) thermometers, the predominant association of *Mg-Hbl* and plagioclase An_{40-50} crystallized at temperature of 847 ± 18 °C and pressure of about 150 MPa (~5 km depth). Some amphibole phenocrysts crystallized under higher temperature conditions (T av. = 917º ± 23 °C, T max = 970 °C). The temperature increase is identified not only in the cores of complexly zoned crystals but also in the rims of individual crystals and microphenocrysts, more rarely microliths (e.g., from andesite pumice of 2013 eruption).

Heterogeneity of amphibole composition and crystallization conditions, the varies of the crystals amount with small variations in bulk rocks and matrix glasses composition in 2001-2013 andesites are in good agreement with the mechanism of convective mixing. Mafic magma replenishment should result in the formation of heated boundary layer in the lower levels of shallow magma chamber and cause convection in its upper levels (Sparks et al., 1977). As a result, portions of magma with different contents of crystals having a contrasting thermal history and different amount of dissolved volatiles can reach the surface (e.g., Couch et al. 2001). Convective processes in a shallow magma chamber also may explain the Young Shiveluch eruptive dynamics in 2001-2013. The overpressure in the magma chamber due to the mafic magma input and intense emission of volatile components may cause an increase in volume and frequency of eruptions.

This work was supported by a Russian Foundation for Basic Research (grant # 15-05-06640).

Referenses: Dirksen et al., 2006. J Volcanol and Geotherm Res, 155: 201-206; Couch et al., 2001. Nature, 411:1037–1039; Gorbach, 2006. Abstracts volume of JKASP-5:133–137; Holland, Blundy, 1994. Contrib Mineral Petrol, 116: 433-447; Kiss B. et al., 2014. Contrib Mineral Petrol, 167: 986; Leake B.E. et al., 1997 Mineral Mag, 61. (3): 295 – 321; Sato et al., 2005 J Petrol, 46 (2): 339-354; Shevchenko A.V. et al., 2015. J Volcanol and Geotherm Res, 304: 94-107; Sparks et al., 1977. Nature, 267: 315–318; Ridolfi et al., 2010. Contrib Mineral Petrol, 160. P: 45-66.

LANDSLIDE AT ZHUPANOVSKY VOLCANO (KAMCHATKA) IN JULY 2015: DISTRIBUTION OF THE DEPOSITS AND POTENTIAL PRECURSORS

Natalia Gorbach[1], Anastasiya Plechova[2] , Dmitry Melnikov[1] and Sergey Samoilenko[1]
[1] – Institute of Volcanology and Seismology FED RAS, Petropavlovsk-Kamchatsky, Russia, n_gorbach@mail.ru
[2] – V.I.Vernadsky Institute of Geochemistry and Analytical Chemistry RAS, Moscow, Russia

Zhupanovsky volcano, situated 70 km north of Petropavlovsk-Kamchatsky, resumed its activity in October 2013 (Samoilenko et al., 2014). The volcano consists of four late Pleistocene to late Holocene cones (Fig. 1a) ranging in composition from basalts to dacites. Current activity is associated with the youngest Priemysh cone which started to form ~3.5 ^{14}C ka BP (Bazanova et al., 2009). Six historical explosive eruptions from Priemysh are known in 1776, 1882, 1925, 1929, 1940, and 1956-57 (Masurenkov et al., 1991). In 2014 and in the first half of 2015 episodic explosions occurred with ash columns up to 6-8 km above sea level (a.s.l) (http://www.kscnet.ru/ivs/kvert/volc.php?name=Zhupanovsky) .

On July 12, 2015 Zhupanovsky produced a strong explosive eruption, accompanied by a series of seismic events (http://www.emsd.ru/~ssl/monitoring/main.htm). The height of explosive plumes reached 10 km a. s. l. (Senyukov et al., 2015). A smaller explosive event took place on July 14. A few days later, on July 16, it appeared that the southern sector of Priemysh cone had collapsed covering the slopes of the volcano with a large field of landslide and lahar deposits (Gorbach et al., 2015).

A 250-300 m-wide and ~500 m deep landslide crater was formed on the southern slope of the Priemysh cone. The eastern wall exposes hydrothermally altered rocks and unconsolidated pyroclastic deposits while the western wall exposes fragments of lava flows, covered the slopes of the cone. The northern wall exposes a lava plug formed during previous stages of activity (Fig. 1b).

Landslide deposits extended to southwest from the crater and covered an area of ~20 km^2. Two sectors of the landslide and related deposits, western and eastern, can be clearly seen on the satellite image (Fig. 1c). The western sector is composed of debris avalanche deposits. At a distance of ~5 km from the crater piles of blocks of different size (from a few tens of cm to 4 m) have formed a complex topography (Fig. 1d). On July 16 the debris material in this sector was cold and had monotonous composition corresponding to the apical part of Priemysh lava flows.

The deposits of the eastern sector have more complex structure. Closer to the crater the surface of the deposits is smooth and composed of a layer of fine-grained gray material (fig. 1e). Such deposits are confined to depressions and to the current streams and have signs of redeposition. In this sector the field of landslide deposits is surrounded by extensive lahar deposits, which reach the length of ~10 km and thickness of ~5 m. On July 16 lahar deposits in places were soaked with water. Most likely, some of these deposits represent mixed facies of the debris avalanche deposits (Gliken, 1991).

At the terminal parts of the lahar deposits the mixture of blocks, ragged trunks and branches with moistened material and the remnants of melting snow have formed a ~4 m thick steep front. Near the front trees and bushes have been crushed, and some of them felled down. The vegetation surrounding the landslide and lahars fronts was covered with a very thin layer of light gray ash. No signs of burning were observed on the vegetation (fig. 1f).

Landslide was not directly observed or recorded by video cameras installed near Zhupanovsky volcano due to adverse weather conditions. However, the presence of thermal anomaly on the satellite image TERRA ASTER (NASA, JPL) from 11:23 UTC 13 July 2015 in the southwestern sector of the volcano, coinciding with the main field of landslide deposits

suggests that the collapse occurred in July 12 and was triggered by explosive and seismic activity, registered on this day. The heterogeneous structure of the Priemysh cone could have caused its edifice instability. Another factors contributing to cone instability and formation of the water- saturated lahars may have been abundant precipitation during the month preceding this event and presence of buried ice and snow in the saddle between the Second and Priemysh cones.

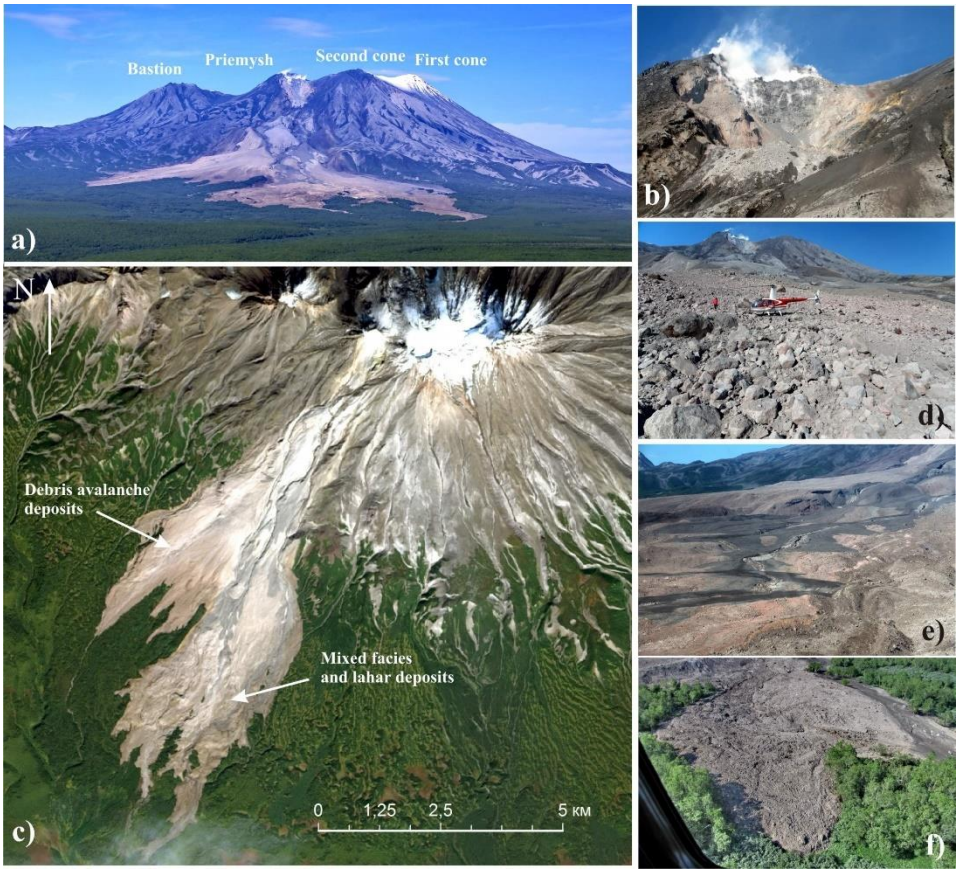

Fig. 1. Landslide at Zhupanovsky volcano: a – view of the collapsed cone and its deposits from south; b – collapsed crater and lava plug in its detachment scarp; c – landslide deposits in the Western foot sector; d – debris avalanche deposits; e – mixed facies deposits; f – one of the lahar flows.

References:

Bazanova L.I., Dirksen O.V., Kulish R.V. and Kartasheva E.V., 2009. Evolution of recent volcanism of Zhupanov ridge (Kamchatka) // In Gordeev E.I. (eds), Proceedings of the IV All-Russian Symposium of Volcanology and Paleovolcanology, Petropavlovsk-Kamchatsky, pp. 265-268.

Glicken H., 1991. Sedimentary architecture of large volcanic-debris avalanches. In: R.V. Fisher and G.A. Smith (eds), Sedimentation in Volcanic Settings. Sot. Econ. Paleontol. Mineral., Spec. Publ., 45: 99-106.

Gorbach N.V., Samoilenko S.B., Plechova A.A. and Melnikov D.V., 2015 // Landslide at Zhupanovsky volcano (Kamchatka) in July, 2015: first data and observation // Bulletin of Kamchatka Regional Association "Educational-scientific Center". Earth Sciences. 3/27:5–11.

Masurenkov Yu. P., Florensky I.V., Melekestsev I.V., 1991. Zhupanovsky volcano In: Fedotov SA, Masurenkov YP (eds) Active volcanoes of Kamchatka, vol 1. Nauka Press, Moscow, pp 84–103

Samoilenko S.B., Melnikov D.V., Chirkov S.A. et al., 2014. Activation of Zhupanovsky volcano in 2013-2014 // Bulletin of Kamchatka Regional Association "Educational-scientific Center". Earth Sciences. 1/23:21-26.

Senyukov S. L., Nuzhdina I.H., Droznina C. Ya., et al. 2015. Seismicity of Zhupanovsky volcano region in 2000-2015 // Materials of the conference "Problems of integrated geophysical monitoring of the Russian Far East", September 27 - October 3, 2015, Petropavlovsk-Kamchatsky; http://www.emsd.ru/conf2015lib/pdf/mon/Senyukovetc.pdf

GEOLOGY AND PETROLOGY OF TAISETSU VOLCANO GROUP, JAPAN; EVOLUTION OF MAGMA AND ACTIVITY AGES.

Kosuke Ishige[1], Mitsuhiro Nakagawa[1], Seiko Yamasaki[2], Akikazu Matsumoto[2]
[1]Earth and Planetary System Science Department of Natural History Sciences, Graduate School of Science, Hokkaido University, Sapporo, Hokkaido, JAPAN.
[2]Geological Survey of Japan, AIST, Tsukuba, Ibaraki, JAPAN.

Taisetsu volcano group, located in central Hokkaido, is the northern part of the Taisetsu-Tokachi volcanic chain, which is situated at the southern end of Kuril arc. The volcanic activity in central Hokkaido started ca. 12 Ma. Large eruptions associated with caldera formation had repeated several times from 5 to 1 Ma. After the last caldera-forming eruption occurred 1 Ma, the volcano group started its activity ca. 1 Ma and is composed of andesitic lava domes and stratovolcanoes. We performed a detailed geological survey combined with K-Ar dating for representative samples. In addition, petrological and geochemical studies for the rocks of the volcano group are also carried out. These reveal not only the structure and eruption history of the volcanic group but also the temporal change of eruptive magma during 1 My.

The activity of the volcano group can be divided into two stages, Older and Younger ones, associated with a long dormant period for ca. 0.5 million years. In the Older stage (ca. 1 - 0.7 Ma), fluidal andesite lavas were effused from several eruption centers to form flat-shaped volcanic edifices extending in N-S direction, such as Takanegahara, Chubetsu-dake and Goshiki-dake. The Younger stage began ca. 0.2 Ma. According to the location of eruption centers and the eruption style, the stage can be divided into three sub-stages, Y1, Y2 and Y3. In the Y1 sub-stage (ca. 0.2 Ma - ca. 34 ka), stratovolcano and several lava domes, such as Nagayama-dake, Haku-un-dake, Ryoun-dake and Keigetsu-dake, were formed in the northwestern - central part. In the Y2 sub-stage, the most explosive and voluminous pyroclastic eruption occurred ca. 34 ka to produce an eruption column and pyroclastic flows, resulting to the formation of Ohachidaira caldera, 2 km in diameter. Pumice and ash fall deposits were widely distributed at eastern Hokkaido. In addition, pyroclastic materials flowed down mainly two directions, northeast and southwest. After the formation of the caldera, the activity has continued mainly at southwestern flank of the caldera (the Y3 sub-stage) to form the Asahidake volcano group. The Asahidake volcano is the largest edifice of the volcano group and started its activity ca.20,000 years ago. The activity continued explosive eruption with lava effusion ca. 5,000 years ago to form a stratovolcano. After that, edifice collapse occurred ca. 2,500 years ago, resulting to the formation of a horseshoe crater, Jigokudani crater. Phreatic eruptions have continued since then to form many small explosion craters. The latest phreatic eruption occurred ca. 250 years ago. Fumarole activity has continued within the crater until now. Although the average eruption rate during the Older stage can be estimated to be >0.08 km^3 /ky, the eruption rate was 0.36 km^3 /ky in the period from 0.82 Ma to 0.74 Ma. In the Younger stage, the eruption rate of each sub-stage is as follows; >0.20 km^3/ky for Y1, >1.2 km^3/ky for Y2, and >0.30 km^3/ky for Y3.

Petrological features of the rocks of Taisetsu volcano group are largely different between the Older and Younger stages. All of the rocks of the both stages are basaltic-andesite to dacite, containing plagioclase, clinopyroxene, orthopyroxene and Ti-magnetite as phenocrysts, associated with minor amounts of olivine and quartz phenocrysts in some rocks. In addition,

the rocks of the Older stage do not contain hornblende phenocrysts, while those of the Younger stage usually include hornblende phenocrysts. The whole-rock SiO_2 contents range from 54 to 69 wt.% for host rocks and from 52 to 59 wt.% for the inclusions. The host rocks from the Older stage are characterized by higher contents of incompatible element such as P_2O_5, Zr, Y and Nb. The rocks show higher $^{87}Sr/^{86}Sr$ and lower $^{144}Nd/^{143}Nd$ ratios, compared with those of the Younger stage. On the other hand, mafic inclusions in the rocks of the Older stage are the same as those of the Younger stage. Although the same mafic magma has existed in the Taisetsu volcano, the silicic magma had largely changed during the long dormancy.

THERMAL SUPPLY OF HYDROTHERMAL SYSTEM, A CASE STUDY OF THE BOGDANOVICH VOLCANIC CENTER HYDROTHERMAL SYSTEM (PARAMUSHIR ISLAND, THE KURIL ISLANDS)

Olga Khubaeva, Antonina Nikolaeva
Institute of Volcanology & Seysmology, Petropavlovsk-Kamchatsky, Russia

Paramuchir Island is located at the north-east end of the Kuril-Kamchatka Arc (Fig.1). The north part of the island forms the Vernadsky Volcanic Ridge with the adjusting North Paramushir magmatic hydrothermal convection system. [Belousov, 2002] It is closely related to the Vernadsky Ridge magmatic structure and belongs to an andesitic type of volcanic hydrothermal system [Henley, 1983].

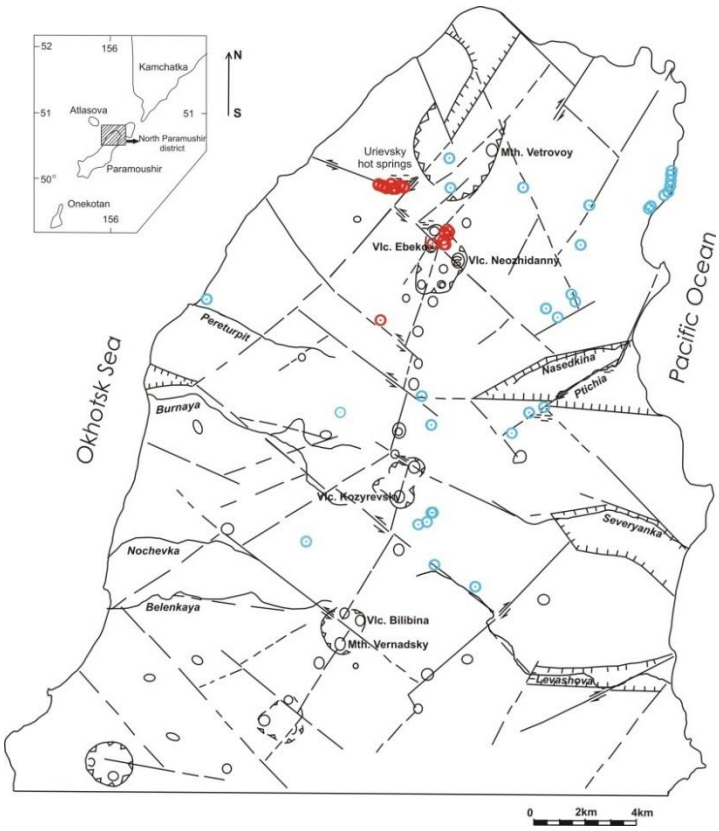

Fig.1 Shematical structural scheme of th Northen part of Paramushir island

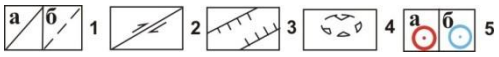

1 - Prospective fouls a) more sure b) less shure; 2- Displacement; 3 - Graben depression; 4 – Caldera border; 5 - Sourses a) thermal b) cold Gas and hydrothermal sources within Ebeko and Bogdanovich Volcanic Centers are surface manifestations of this system.

Ptichy Sourse (T=20-45^{o} C) with mineralization up to 0.5 g/l are discharging at two hypsometric levels, on the east flank of Bogdanovich Volcanic Center, at the edge of one of the tongues of the last lava flow from the crater of Krasheninnikov Volcano. The waters are slightly acidic or nearly-neutral (pH=4-6.7) with Cl-SO_4-Na-Ca composition. The water of Ptichy Hot Springs is of mixed origin. Although the water of these springs are much diluted we fix elevated, compared to other springs of this group, concentrations of Na, Cl and others chemical elements in two springs' outlets. (Na + K)/Cl dependence diagram obviously shows that most solutions from these hot springs are on the line II (Fig. 2). Fumarole thermal sources are shown on the line I. Probably these solutions were formed due to condensation of volcanic gas-steam jets (HCl, HF, SO_2, H_2S) under subsurface conditions of hydrothermally altered rocks. We compared the solutions from several springs (Verkhne-Yurievskie and Ebeko Volcano), discharging within Ebeco Volcanic Center, and revealed a tendency to the shift towards magma water (line III). Ivanov, 1961 reveals that atmospheric, gas and depth components of fluid flow were involved during formation of Yurievskie Mineral Springs. Ptichy Hot Springs probably were formed by the same components. Elevated concentrations of Cl, Na, SO_4, B and H_4SiO_4 in water of Ptichy Hot Springs may evidence for hydrothermal system located within the dipped block of Paramushir Island block system.

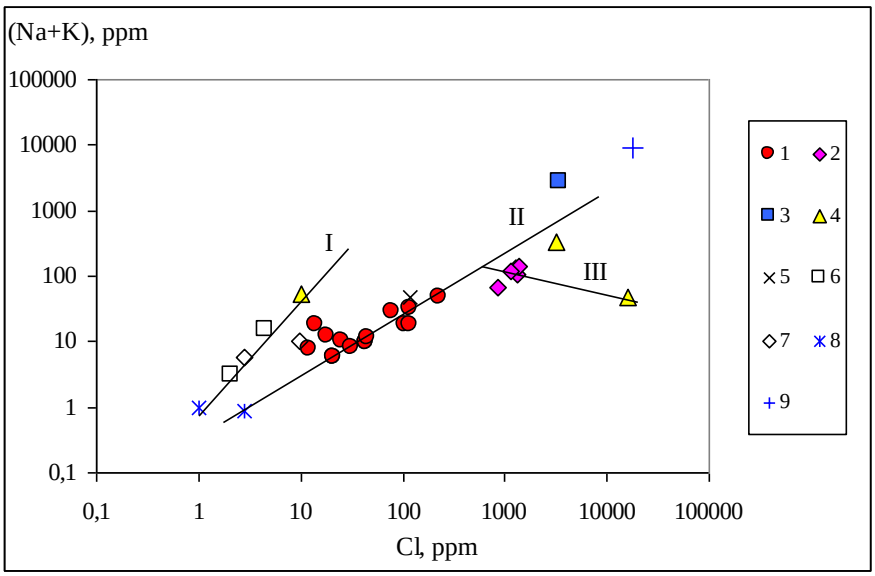

Fig 2. The Na - Cl ratio (mg / l) in hot springs in the northern part of Paramushir Island.
1 – the source of the Ptichya River basin; 2 – Urievsky hot springs; 3 – P2 borehole; 4 –the source of Ebeko Volcano; 5 – the source of the Severyanka River head; 6 – the source of the Levashova River head; 7 – the source of the Nasedkina River head; 8 – atmospheric precipitation; 9 – seawater.

Since no geophysical works have been carried out on the island until present, the heat source of the Bogdanovich hydrothermal system is not completely revealed. Thus, we have to use indirect indicators and study similar systems in other parts of the planet. For example feathering fractures [Gorshkov, 1967] on the island provides increased permeability of the crust and the possibility of manifestation of magma generation processes.

There are many dikes and explosive craters within the Vernadsky Ridge. This may be the evidence for the basaltic heat source in the depth of the hydrothermal system. Volcanoes on Iceland, Kamchatka, the Kuril Islands and others show that the network of basaltic dikes is often located in long-lived volcanic centers, which are associated with contemporary hydrothermal systems. Often basaltic dikes are the main structure, through which melt and heat are transfered. [Belousov, 2002., Gudmundsson, 1995].

Volcanic clusters on Paramushir island [Gorshkov, 1967] with their peculiarities such as long life, geology, morphology, petrographic and chemical composition of lava and fragmental materials from volcanic eruptions suggest that magmatic feeding system has evolved throughout their formation. Apparently, the dikes are the main structures that provide heat for hydrothermal systems of Paramushir Island.

References:

1. Belousov V.I., Rychagov S.N., Sugrobov V.M. *Severo-Paramushirskaya*…(The North-Paramushir Hydrothermal-Magmatic System: Geological Structure, Conceptual Model, Geothermal Resources// Vulkanologiya i Seismologiya, 2002. № 1. Pp. 34-50.
2. Henley R.W. and Ellis A.J. Geothermal systems ancient and modern: a geochemical review. Earth Sci. Rev. 19, 1983.
3. Gorshkov G.S. VulkanismKurilskoy… (Volcanism of the Kuril Island Arc).M.: Nauka, 1967. Pp. 288.
4. Gudmundsson A. Infrastructure and mechanics of volcanic systems in Iceland/Journal of Volcanology and Geothermal Research 64 (1995). Pp. l-22.
5. Ivanov, V.V., *Osnovnye geologicheskye usloviya*… The Basic Geological Conditions and Geochemical Processes in the Formation of Thermal Waters in Present-Day Volcanic Areas, Tr. Laboratorii Vulkanologii AN SSSR, 1961, issue 19, Pp. 58–68.

MUTNOVSKY AND GORELY VOLCANOES IN KAMCHATKA: A PERFECT CLASSROOM FOR TEACHING VOLCANOLOGY

Olga Khubaeva[1], Pavel Izbekov[2], Sergey Samoylenko[1], and John C Eichelberger[2]
[1]Institute of Volcanology & Seismology, Petropavlovsk-Kamchatsky, Russia
[2]University of Alaska Fairbanks, Fairbanks, USA;

Unique natural objects of Kamchatka have always attracted the attention of researchers from all over the world. Joint international field works take place in the territory of Kamchatka for many years.

Since 2003 the International Volcanic Field School is held in Kamchatka students, PhDs and young scientists from international research community can participate in it. The school is held annually in the first half of August, thanks to the collaboration of the Institute of Volcanology and Seismology (Petropavlovsk-Kamchatsky), the Vitus Bering Kamchatka State University (Petropavlovsk-Kamchatsky) and the University of Alaska (Fairbanks, United States).

Since 2003, over 200 people from different countries of the Russian Federation, the United States, France, England, Belgium, Turkey, etc attended the school.

The scientific program of the school includes lectures by leading scientists, geological excursions and oral presentations by young participants.

The main task of the school is to improve the school participants notion of modern volcanology and associated earth sciences (geology, petrology, geophysics, seismology), develop students' and graduate students' research capacity.

Active Mutnovsky and Gorely Volcanoes is a traditional venue of the school. On a compact territory these volcanoes give an extremely broad insight into different types of volcanism, one can observe the whole range of volcanic rocks (from dacite to rhyolite) and different stages of volcanic process.

Mutnovsky produced more than 15 eruptions in historical time. The strongest of these occurred in 1848 and 1927. Its last eruption had been occurring from 1960 to 1961, and had an explosive character. Gorely Volcano produced 8 eruptions in historical time. Its last eruption occurred at the beginning of 1985 and was characterized by weak phreato-magmatic activity. At the summit crater of both volcanoes intensive fumarolic activity is still prevailing.

One of the most powerful deposits of steam hydrotherms in Kamchatka was discovered in the area of Mutnovsky Volcano.High temperature crater fumaroles (up to 800 ° C) effuse to the surface steam and gas mixtures of typical for magmatic gases chemical composition. The earth surface temperature of singular parts of the crater is more than 100 ° (Vakin et al., 1976). The heat efflux from North Crater comprises more than 89400 kcal/s. Mutnovsky Volcano is located within the North Mutnovsky volcano-tectonic zone, forming a series of large faults, along which numerous dikes and extrusions of acid composition have been intruding since Pliocene till presence. At the same time acidic and basic magmatism within this volcano tectonic zone also occurs (Selyangin, 2009)

Various volcanic forms and eruptive products - lava flows, cinder cones, crater lakes were revealed on Gorely. Thus, thanks to the variety of landscapes, forms and eruptive products, Mutnovsky and Gorely Volcanoes are unique observation objects for young scientists, participating in field researches (Vakin et al., 1976).

The base camp of the International Volcanic Field School is located near the observatory at the foot of Mutnovsky Volcano and allows making circle geological routes to the crates of Mutnovsky and Gorely Volcanoes, Mutnovsky geothermal power station, other geological objects.

Geological excursions are accompanied by lectures and field trainings on volcanology, mineralogy, petrography, geomorphology, seismology.

Basic geological routes on Mutnovsky and Gorely Volcanoes are led by the PhD at the University of Alaska Fairbanks Pavel Izbekov. These research excursions allow discussing tectonic and geodynamic setting of the Kamchatka Peninsula, catastrophic caldera-formation volcanic eruptions, considering the role of water in geothermal and magmatic processes, as well as many other basic and specific subjects. Lectures are co-taught by leading researchers from the Institute of Volcanology and Seismology, the Space Research Institute, the Moscow State University, the University of Alaska Fairbanks (USA), and other world universities such as: Tohoku University (Japan), Université Joseph Fourier, Grenoble, France, Paris Institute of Earth Physics, France et al. lecture.

References:

1. Vakin Ye.A., Kirsanov I.T., Kirsanova T.P. Termal'nyye polya i goryachiye istochniki Mutnovskogo vulkanicheskogo rayona./Gidrotermal'nyye sistemy i termal'nyye polya Kamchatki. Vladivostok. 1976. S. 85-115. Thermal fields and hot springs in the area of Mutnovsky Volcano. /Hydrothermal systems and thermal fields in Kamchatka.

2. Selyangin O.B. K Vulkanam Mutnovskiy i Gorelyy. Petropavlovsk-Kamchatskiy. Kholdingovaya kompaniya «Novaya kniga». 2009. Mutnovsky and Gorely Volcanoes. Petropavlovsk-Kamchatsky.

FIRE AND LIFE: MICROBIAL MEDIATION OF DEEP CARBON CYCLING ALONG THE "RING OF FIRE", A SUBDUCTING OCEANIC LITHOSPHERE, WESTERN ALEUTIAN ISLANDS

Heather Miller[1], Jake Roush[2], Taryn Lopez[3], Tobias Fischer[4], Matt Schrenk[1,2]
[1]Department of Microbiology and Molecular Genetics, and [2]Department of Geological Sciences, Michigan State University, East Lansing, MI, USA; [3]Geophysical Institute, University of Alaska Fairbanks, Fairbanks, AK, USA; [4]Department of Earth and Planetary Sciences, University of New Mexico, Albuquerque, NM, USA

In collaboration with geoscientists from the Alaskan Volcano Observatory (AVO) and the Deep Carbon Observatory (DCO), we are beginning to investigate the roles that microbial communities play in the cycling of deep carbon reservoirs released through volcanic activity. As the Pacific Plate subducts along the Aleutian Trench, the mantle is subjected to intense pressures and high temperatures, resulting in the release of volatile compounds and water vapor throughout the Aleutian island arc. We hypothesize that volcanic arc environments associated with subduction zones sustain unique communities of microorganisms able to utilize these volatiles to sustain their growth, potentially impacting the global carbon cycle.

Volcanic soil samples from four Aleutian Islands (Gareloi, Kanaga, Kiska, Little Sitkin) were collected in September 2015, and DNA from resident microbial communities was extracted and quantified (Table 1). Using universal primer sets for the 16S rRNA gene, we were able to confirm the presence of bacterial cells in all samples, however archaeal species were not detected (data not presented). When we compared this general microbial diversity and abundance data to the environmental and gas composition measurements taken at the fumarole, no obvious correlations could be made. As a result, we submitted our extracted DNA samples for 16S rRNA sequencing (MSU Genomics Core Facility), which we hope will reveal a pattern in microbial community composition related to the volcanic gas composition and flux. We are also conducting shotgun metagenomic analyses of the extracted DNA to identify the metabolic potential of the volcano-hosted microbial communities to consume or assimilate volcanic gases. This information will guide experiments aimed at the enrichment and isolation of microorganisms from the volcanic environment, which may yield information on rates and processes in such systems. To date, we have been able to isolate a microorganism from the Gareloi volcanic soil, initially enriching for sulfur-oxidizing microbes using minimal media (pH 3.0) then plating 300mL on nutrient agar (pH 7.0), both being incubated at 40°C. Further culturing and microbial characterization activities are underway.

The outcomes of the current study are expected to provide valuable insight into the utilization of volcanic gases by microorganisms. Resident microbial communities may be preferentially consuming the gases being emitted to increase biomass production, or they may be altering the gas composition currently attributed to tectonic activities. Through ongoing work, we aim to expand this initial survey to other volcanic island arc sites along the "Ring of Fire", with the goal of incorporating these data into current models of the global carbon cycle.

Table 1. Volcanic soil sample data, including geochemistry, geography, temperature, and DNA yield

	Little Sitkin	Kiska	Gareloi	Kanga
Sample Collection Date	9-Sep-15	10-Sep-15	12-Sep-15	20-Sep-15
Fumarole Location	51.96117°N, 178.49226°E	52.10575°N, 177.599194°E	51.7646°N, 178.80697°E	51.9230167°N, 177.161083°E
Fumarole Elevation (m)	166	1030	1326	1237
Fumarole Temp (°C)	98	NA	101.6	94.6
Soil Sample Location	same as fumarole	52.105833°N, 177.598861°E	~10 cm from fumarole vent	fumarole vent adjacent
Elevation (m)	166	1047	1326	-
Temperature (°C)	98	7	89.1	49-94
DNA concentration (µg/g-soil)	***8.9***	***5.05***	***4.7***	***5.65***
Background Soil Location	1 m from fumarole	52.105833°N, 177.598861°E	~0.5 m away from fumarole	~4 m away from fumarole
Elevation (m)	166	1047	1326	-
Temperature (°C)	24	7	40.5	16.4
DNA concentration (µg/g-soil)	***4.75***	***11.6***	***ND***	***47.75***
Gas Fluxes				
SO_2 (t/d)	ND	3.6	306	70
CO_2/SO_2 (molar)	95	7	PS	PS
Fumarole Gas Composition(%)*				
CH4	26.3	ND	0.41	0.03
H2	2.77	ND	51.5	0.65
Ar+O2, N2	70.9	100	48.1	99.3

ND – none detected; PS - poorly constrained; sensor saturation; NA – not available; * - Preliminary data

THE EFFECT OF THE AD 1611SANRIKU EARTHQUAKE ON VOLCANIC ACTIVITY IN HOKKAIDO, JAPAN

Mitsuhiro Nakagawa[1]
[1]Earth and Planetary System Science Department of Natural History Sciences, Graduate School of Science, Hokkaido University, Sapporo, Hokkaido, JAPAN.

After several thousand years dormancy, three active volcanoes in southwestern Hokkaido (SW Hokkaido), Hokkaido-Komagatake, Usu and Tarumai volcanoes, started their eruptive period with large eruptions of VEI=5 during AD 1640 to 1667. It has been discussed that these could be caused by the 1611 Sanriku earthquake (M>8). It has been recently proposed that the source of the earthquake was distributed widely from off the eastern coast of Hokkaido to the Sanriku area. In this research, I compile the eruptive history of active volcanoes in Hokkaido to clarify the regional difference of the eruptive activity around 17th century. In addition, I also compile the structure and eruptive processes of magma plumbing system of these three volcanoes to discuss the relationship between earthquake and volcanic eruption. Relatively large eruptions occurred in Hokkaido from end of Plesitocene to early Holocene. In E Hokkaido belonging to Kuril arc, two large eruptions of Me-Akandake (VEI=5) and Mashu volcanoes (VEI=6) occurred 13 and 7 ka, respectively. Nigorikawa and Tarumai volcanoes in SW Hokkaido belonging to NE Japan arc occurred a large eruption (VEI=5) 9 and 7 ka, respectively. Since then, volcanoes in E Hokkaido, such as volcanoes in the Shiretoko peninsula, Masu, Atosanupuri, Me-Akan and O-Akan volcanoes, had been active until ca. 1000 years ago. On the other hand, in SW Hokkaido, although a large eruption of VEI=5 occurred in Tarumai volcano, smaller eruptions of VEI<3 sporadically occurred in other volcanoes. In summary, eruptive activity in SW Hokkaido had been quite lower than that of E Hokkaido since ca. 5000 years ago. In contrast, the eruptive activity of volcanoes in central Hokkaido belonging to the boundary between the two arcs has been relatively low. A large eruption of VEI>4 has not occurred in the region. In 17th century, as mentioned above, three volcanoes in SW Hokkaido started vigorous eruptive activity and has continued their activity until now. Other volcanoes adjacent these three volcanoes have also started their activity since then. In contrast, although two relatively large eruptions occurred in Mashu and Me-Akandake volcanoes ca. 1ka, and Rausu volcano ca. 0.7ka, eruptive activity of volcanoes in E Hokkaido has been quite weak since then. Although small magmatic eruption have sporadically occurred in Tokachidake volcano in central Hokkaido, no magmatic eruptions have occurred in E Hokkaido at least since 17th century. Considering temporal change of eruptive activity of active volcanoes in Hokkaido during Holocene, if 1611 Sanriku earthquake affected the volcanic activity, it should be emphasized that the earthquake had reduced eruptive activity in E Hokkaido, whereas it had caused sequential eruptions in SW Hokkaido. In other word, the earthquake caused distinct influences to southwestern and eastern part of Hokkaido, respectively.

Eruptive history, the structure of magma plumibing system and its eruption processes of these three volcanoes in SW Hokkaido are summarized as follows. 1) Each volcano started its eruptive activity after a long dormancy. 2) Although whole-rock chemistry of major eruptive magma is silicic, ranging from dacitic andesite to rhyolite, whereas their melt compositions are similar rhyolite. 3) Each initial eruption had been caused by the injection of mafic magma into the above silicic magma less than several years before eruption. These features suggest that enough volume of silicic magma had been accumulated in each volcano. Thus, a large earthquake could affect the activity of a volcano to cause mafic injection and/or activation of a voluminous silicic magma chamber. However, there existed the interval of 30 years between the earthquake and the initial eruption in AD 1640. This would not be consistent with the 1611 Sanriku explanation that the earthquake caused sequential large eruptions in SW Hokkaido.

SUMMARY OF 20-YEARS' SURVEY OF MINERAL COMPOSITION OF THE KARYMSKOYE CALDERA LAKE AFTER ITS 1996 HAZARDOUS ERUPTION

A.G. Nikolaeva, G.A. Karpov, A.F. Sashenkova
Institute of Volcanology and Seismology FEB RAS, Petropavlovsk-Kamchatsky, Russia, ocean@kscnet.ru

Karymskoye Lake is located within the Akademii Nauk Caldera, which is an integral part of the Karymsky Volcanic Center (KVC) (Fig. 1). KVC is peculiar for its repeated seismic-tectonic, tectonic and volcanic activation [Volcanic Center…, 1974]. Early in January 1996, two almost simultaneous events took place in KVC: eruption of the Karymsky volcano and underwater phreatomagmatic eruption in the north part of the caldera lake (Fig. 1, 2). Karymsky volcano outburst was preceded by the changes of seismic and tectonic environments [Fedotov, 1997], while the eruption of the lake was considered sudden and unexpected. Later, however, we distinguished the changes of hydrochemical environment that could be interpreted as the precursors of the lake eruption. Thus, three years before the event, the lake water showed increased salinity. S content was also gradually elevating, as well as pH (7.20-7.45). Probably, prior to the outburst, activation of fault zones at the lake bottom caused the supply of volatiles (HCl, HF, CO, SO_2, CO_2, H_2S, as well as H_2 and He). We reported those volatiles within the explosion funnels in the newly formed Novogodny Peninsula and in the Tokarev underwater crater immediately after the 1996 events (see Fig. 1). Lake eruption was accompanied by the supply of abundant heat (which melted down the ice cover of the basin) and powerful explosions ejecting huge amounts of steam-gas mixtures and scoria-bomb materials [Fedotov, 1997]. Karpov et al. [2006] reported on enormously abundant endogen matter (about 27200t of Cl and 203456 t of SO_4) supplied to the lake and diluted in it during the underwater eruption. Waters sampled close to the submerged eruption center showed high contents of Na, K, Mg, Cl, F, B, H_4SO_4, SO_4, Zn, Ni, Mn, Fe, Cu, Al, Sr. The outburst caused the formation of the Tokarev underwater crater in the north part of the lake, artificial Novogodny Peninsula, break in the northeastern rim of the caldera and powerful discharge of high-temperature thermal waters (Piipovskiye and Plyazhnye Springs, vents in the Novogodny Peninsula, bottom discharges we found in the Tokarev crater). This discharge source traced a narrow surface zone of submeridional strike in the central part of the peninsula.

Color of the lake water dramatically changed from grayish-blue to turquoise-blue. Chemical composition of the lake water also suffered drastic changes. Once fresh pond (pH=7.2, Cl-HCO_3–Na composition, salinity 130 mg/l) inhabited by salmon species Oncorhynchus nerka (Walb.) suddenly turned acidic (pH=3.2, Cl-SO_4–Ca-Na, salinity ≈ 1 g/l). Immediately after the eruption lake water reached the temperature of 20°C being well-mixed and lacking O_2 [Karpov et al., 2006; Fazlullin et al., 2000]. Later on, using a catamaran, we yearly sampled the lake water at two hydrochemical sites – S_1 located in the center of the Tokarev underwater crater, and S_2 in the middle of the lake – along standard profiles of 0-10-20-30-40-50-60 m (see Fig. 1). Deep hydrochemical sampling was carried out by means of reversing water bottles.

The phenomenon observed was the first example of surveying the process of recovering the mineral composition of the lake water after a hazardous event in it. The following significant changes were observed in the course of the 20-year hydrochemical monitoring of the Karymskoye Lake. By the year of 1998, lake water already showed signs of stratification by some hydrochemical parameters (T^oC, pH, $O_{2dissolved}$). In 2000 there appeared a weak trend towards the recovery of the water chemical composition (alkalization), which became quite distinct by 2001 [Nikolaeva et al, 2005]. Suggested was total recovery of the lake water composition back to the initial state (that of 1984) during the complete cycle of flushing (8-10 years). But this failed to happen. In contrast, slow alkalization of the lake water occurred as

well as monotonic increase of pH (Fig. 2). Water salinity was gradually decreasing down to the depths of 40 meters, while at deeper levels this process was even slower. In 2001 water salinity near the Tokarev crater was reported to increase by 1/3 with depth.

Our routine surveys of the area allowed distinguishing two representative groups of elements whose behavior could account for the hydrochemical evolution of the lake water consisting in the mere drop of SO_4, Ca, Mg, and slow decrease of (Na+K) and particularly Cl. The first group is postvolcanic-fumarolic, typical of acidic SO_4–Cl waters occurring in volcanic areas. It appeared in the lake water as a result of the 1996 underwater eruption. It includes Ca, Mg and S whose sources were igneous pyroclastics (1996), wall rocks of the caldera and dissolved acidic gasses. The second group is the hydrothermal one, typical of deep thermal waters of Cl–Na composition occurring within watered hydrothermal systems (such as Uzon, Geyser Valley, Yellowstone). Its elements (Cl, Na+K) were supplied by the surface and bottom discharges of thermal waters within the lake basin. Piper's triangular diagram shows the evolution of the salinity of the Karymskoye Lake waters as monitored for 20 years (see Fig. 2). For this period, total salinity of the lake water decreased almost three-fold. Concentrations of bulk saline composition elements dropped as follows: Ca, Mg and SO_4 > 4 times, Na and K – 3 times, Cl – twice. The data obtained show that only in recent years the lake water has entered the initial stage of intensive mixing. We consider the factors suppressing the lake water alkalization to be insufficient mixing of the water body (seasonal), lack of storm winds, and contribution of bottom saline solutions along the fractures from the lake bottom.

References:

1. Volcanic center: structure, dynamics, matter (Karymskaya setting). Moscow: Nedra. 1974. 260 p.
2. *Karpov G.A., Nikolaeva A.G., Lupikina E.G., Bortnikova S.V., Ushakov S.V.* Paculiarities of hydrochemical and geochemical composition of the matter in the Karymskoye Lake basin during the post-hazard period (1996-2005) / Reports on geophysical monitoring of Kamchatka. Proceedings of the scientific-technical conference, January 17-18, 2006. Petropavlovsk-Kamchatsky. 2006. Pp. 207-217.
3. *Nikolaeva A.G., Karpov G.A., Lupikina E.G., Ushakov S.V.* Evolution of mineral composition of thermal spring waters and Karymskoye Lake after the 1996 eruption // Proceedings of the Annual Conference dedicated to the Volcanologist's Day, March 30 – April 1, 2005, Petropavlovks-Kamchatsky. 2005. Pp. 37-47.
4. *Fazlullin S.M., Ushakov S.V., Shuvalov R.A., Aoki M., Nikolaeva A.G., Lupikina E.G.* Underwater eruption in the Akademii Nauk Caldera (Kamchatka) and its effects: hydrologic, hydrochemical and hydrobiological studies // Vulkanologiya i Seismologiya. 2000. № 4. Pp. 19-32.
5. *Fedotov S.A.* On the 1996 eruptions of the Akademii Nauk Caldera and Karymsky volcano in Kamchatka: researches and mechanism // Vulkanologiya i Seismologiya. 1997. № 5. Pp. 3-38.

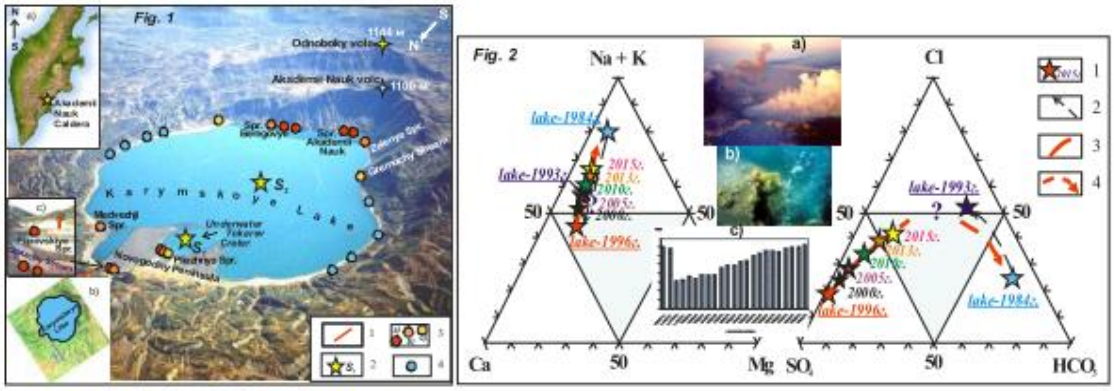

Fig. 1. View of Karymskoye Lake. Insets: **a** – location of Akademii Nauk Caldera in Kamchatka; **b** – Karymskoye Lake prior to the hazard (1996); **c** – view of the newly formed Piipovskiye Springs. **1** – 1996 fissure; **2** – hydrological regime sites; **3** – thermal water discharges with temperatures of 80-100ºC (a), 40-60ºC (b), 10-20ºC (c); **4** – cold water discharges (2-4ºC). ***Fig. 2.*** Evolution diagram of mineral composition of the Karymskoye Lake waters (1984-2015). Inset: **a** – simultaneous eruptions of the two centers within KVC (1996), **b** – bottom discharges within the underwater Tokarev crater, **c** – evolution of pH at the head of the Karymskaya River. **1** – figurative points of lake water sampling sites (by years); **2** – evolution of the lake water prior to the hazard (1984-1993…1996); **3** – evolution of the water mineral composition during the post-hazard period (1996-2015); **4** – anticipated trend of lake water recovery back to its initial state.

NEW DATA ON THE EOPLEISTOCENE CATASTROPHIC CALDERA-FORMING ERUPTION IN KAMCHATKA

A.N. Rogozin, V.L. Leonov
Institute of Volcanology and Seismology, Petropavlovsk-Kamchatsky, Russia
alekseiras@yandex.ru

The work presents new data on the giant caldera. **A new large caldera** (15×25 km), the Karymshina caldera, has been discovered in 2006 in southern Kamchatka [1]. Three complexes are distinguished according to consecutive stages of the caldera development: pre-calderian, caldera-forming and post-calderian. The pre-calderian stage (complex I) is assumed to have mid-Pleiocene age (3.4 – 2.6 myr). The caldera-forming stage (complex II) has Eopleistocene age (1.78 – 1.2 myr). The post-calderic stage (complex III) is dated to Lower and Middle Pleistocene (0.5 – 0.8 myr). An approximate **volume of material erupted** during the caldera generation was estimated to be **about 825 km^3**, which makes **a weight of 2×10^{15} kg**. This eruption should therefore be considered as the largest so far known to have occurred in Kamchatka and to be among the great eruptions worldwide [2]. **A tectonic uplift** (4 × 12 km × 200 m) interpreted as a resurgent dome has been reconstructed in the northwestern part of this caldera, bounded by straight northeast and northwest trending faults. Also **the boundary of a lake**, which had existed in the caldera to the South from the resurgent uplift, has been reconstructed.

During fieldwork in 2012-2015 **a vast field of ignimbrites**, **traces of a large pyroclastic flow** associated with caldera Karymshina, **was mapped for the first time (fig. 1)**. Ignimbrites were found at a distance up to 35-40 km from the edge of the caldera. The maximum thickness of the flow exceeds **500 m**, the area of the pyroclastic flow deposits is **about 298 km^2**, and their total volume is **84 km^3**. It is mainly represented by ignimbrites and crystalloclastic tuffs related to the caldera-formation, which side with volcanic relics shaped the border of the structure at the pre-calderic stage. At the central part of the depression the total observed thickness of ignimbrite deposits reaches 1000 m.

It has been unambiguously established that the volcanoes of mounts Goryachaya, Yagodnaya, Levaya Karymchina, etc., located out of the caldera, but close to the boundaries of the caldera, are older and must be considered as **evidence of a major volcanic phase that proceeded the caldera generation**. It proved by the fact that the Karymshina rocks (mostly acid tuffs and ignimbrites) that fill the caldera in some cases lay on the lavas that compose the above volcanoes.

New data were obtained on the setting of the rhyolite domes widely abundant in the area of study. It was shown that they are mostly confined to the boundaries of the caldera and to the boundary of the resurgent dome situated in it. Most of the domes were emplaced much later following caldera generation, they have ages of 0.5--0.8 Ma, and they should be regarded as **a consequence of post-caldera volcanism**. The Karymshina caldera is found to have the largest scale in high-siliceous volcanism. Total volume and area of extrusions and related lava flows reaches 2.68 km^3 and 26.44 km^2, correspondingly.

The structural setting of the **present-day hydrothermal systems** in the area of study has been revised. It was observed that all larger hydrothermal systems (the Bol'she-Bannaya, Karymshina, and Verkhne-Paratunka ones) **are confined to the boundaries of the Karymshina caldera**.

This work was carried out within the projects of the Far Eastern Branch, Russian Academy of Sciences (project no. 15-I-2-031), and was supported by the Russian Science Foundation (project no. 16-17-10035).

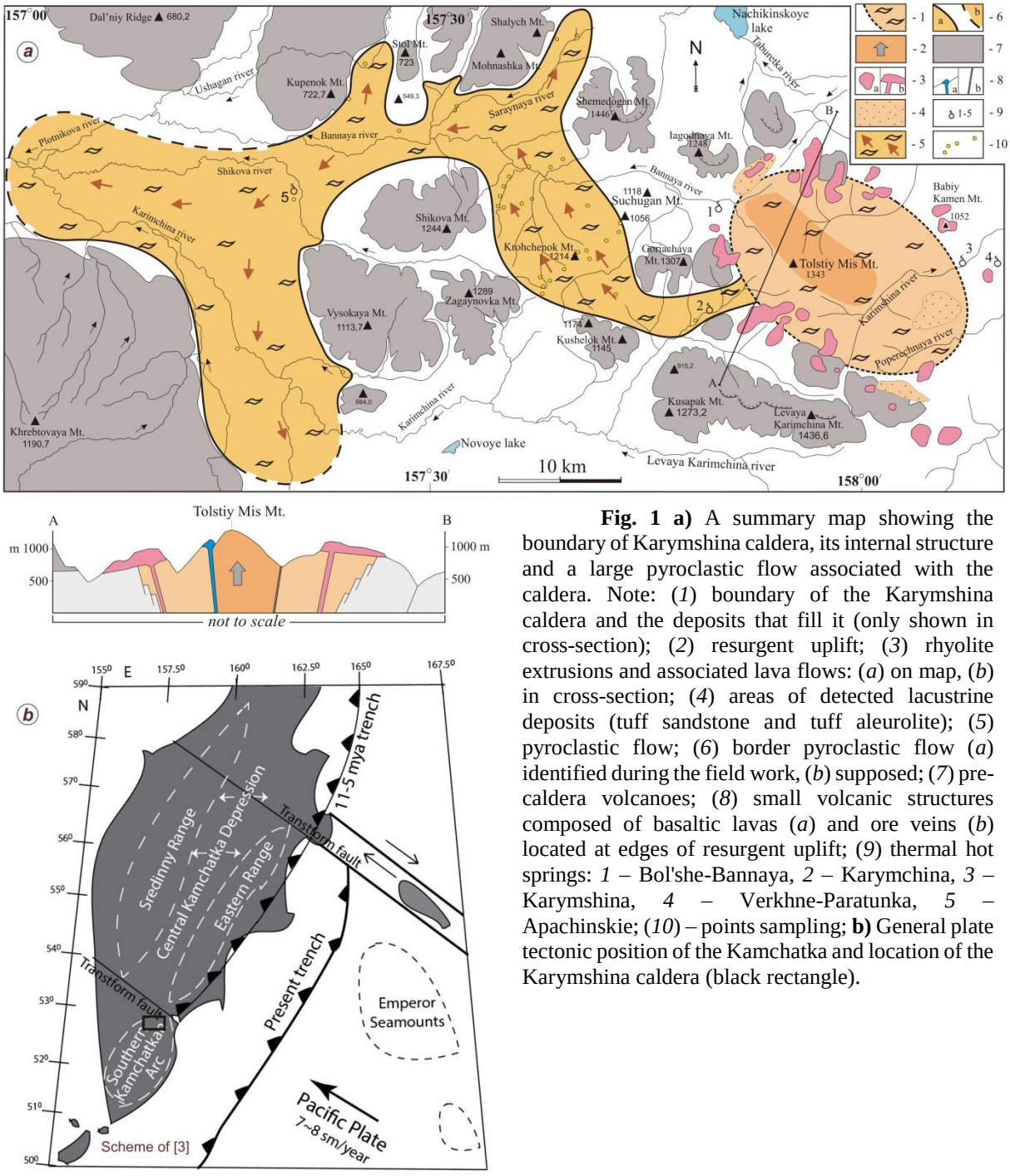

Fig. 1 a) A summary map showing the boundary of Karymshina caldera, its internal structure and a large pyroclastic flow associated with the caldera. Note: (*1*) boundary of the Karymshina caldera and the deposits that fill it (only shown in cross-section); (*2*) resurgent uplift; (*3*) rhyolite extrusions and associated lava flows: (*a*) on map, (*b*) in cross-section; (*4*) areas of detected lacustrine deposits (tuff sandstone and tuff aleurolite); (*5*) pyroclastic flow; (*6*) border pyroclastic flow (*a*) identified during the field work, (*b*) supposed; (*7*) pre-caldera volcanoes; (*8*) small volcanic structures composed of basaltic lavas (*a*) and ore veins (*b*) located at edges of resurgent uplift; (*9*) thermal hot springs: *1* – Bol'she-Bannaya, *2* – Karymchina, *3* – Karymshina, *4* – Verkhne-Paratunka, *5* – Apachinskie; (*10*) – points sampling; **b)** General plate tectonic position of the Kamchatka and location of the Karymshina caldera (black rectangle).

REFERENCES

1. *Leonov V.L., Rogozin A.N.* Karymshina, a giant supervolcano caldera in Kamchatka: boundaries, structure,volume of pyroclastics // J. Volcanology and Seismology. 2007. V. 1. № 5. P. 14-28.

2. *Bindeman I.N., Leonov V.L., Izbekov P.E.,et al.* Large-volume silicic volcanism in Kamchatka: Ar-Ar, U-Pb ages, isotopic, and geochemical characteristics of major pre-Holocene caldera-forming eruptions // J. Volcanol. Geotherm. Res. 2010. V. 189. № 1-2. P. 57-80.

3. *Bergal-Kuvikas O.V.* Geochemical studies of volcanic rocks from the northern part of Kuril-Kamchatka arc: Tectonic and structural constraints on the origin and evolution of arc magma. Ph.D. thesis. Hokkaido University. 2015. p. 190.

FRAGMENTS OF CRETACEOUS SEAMOUNTS IN ACCRETIONARY STRUCTURE OF THE KAMCHATSKY MYS PENINSULA (KAMCHATKA, RUSSIA)

Dmitry Savelyev[1], Olga Savelyeva[1] , Maxim Portnyagin[2, 3]
[1]Institute of Volcanology & Seismology, Petropavlovsk-Kamchatsky, Russia.
[2] GEOMAR Helmholtz Centre for Ocean Research Kiel, Kiel, Germany.
[3]V.I. Vernadsky Inst. of Geochemistry and Analytical Chemistry, Moscow, Russia

The geological structure of the Kamchatsky Mys peninsula is determined by its position at the junction of major structures in the NW Pacific - the Kuril-Kamchatka island arc, Aleutian island arc and submarine Emperor Ridge. The southern part of the peninsula is composed by the accretionary prism of the Kronotsky paleoarc (Khotin and Shapiro, 2006). A significant part of the accretionary complex is comprised by rocks of ophiolite association, namely mantle peridotites, gabbro, dolerites, basalts, hyaloclastites, jaspers and limestones. Our many-year studies showed that some Cretaceous volcanic and sedimentary rocks of the ophiolite complex can represent fragments of an intraplate seamount, which could belong to the Emperor Ridge.

Volcanic rocks in the ophiolites are represented by basalts ranging geochemically from trace element depleted MORB-type to enriched OIB-type (Savelyev, 2003). Trace element and isotopic composition of a peculiar type of rocks from the ophiolite, enriched tholeiites, are particularly close to basalts of the northernmost Emperor Seamounts, Meiji and Detroit (Portnyagin et al., 2008). Depleted tholeiites with ultradepleted melt inclusions in spinel were also found among the volcanic rocks of the Kamchatsky Mys peninsula. The extremely depleted compositions of the rocks and melt inclusions were interpreted to originate by high degrees of melting under the influence of mantle plume (Portnyagin et al., 2009). Highly depleted mantle peridotites from the ophiolites appear to have genetic link to these ultra-depleted magmas and were interpreted to be formed under influence of a mantle plume (Batanova et al., 2014). The most recent finding are cumulative picrites with MgO up to 20 wt% which were found in the serpentinite melange zone fringing the ultramafic massif in its south-western part. Their geochemical characteristics also indicate an origin under the influence of mantle plume [Savelyev, 2014]. The groundmass of these rocks and olivine phenocrysts contain abundant sulphide globules with micro inclusions of native gold, platinum and palladium compounds [Savelyev et al., 2015]. We interpret the strong enrichment in Au and PGE as additional evidence of plume-related origin of the rocks.

Paleoceanic sedimentary rocks exposed on the Kamchatsky Mys peninsula are represented by limestones and jaspers of the Albian-Cenomanian age according to their radiolarian assemblage (Palechek et al., 2010). The rocks were formed at seamount surface at a depth of 2-2.5 km. Two beds enriched in carbonaceous material were identified in the sedimentary sections. The formation of these beds is likely related to the oceanic anoxic events MCE and OAE2 (Savelyev et al., 2012). During the anoxic events, the seamount surface fell in the oxygen minimum zone, which led to the accumulation of rocks enriched in organics. Anoxic conditions promoted the accumulation of many ore elements in carbonaceous beds, including the platinum group elements, the source of which can be synchronous volcanic eruptions (Savelyeva et al., 2015).

Tectonic structure of the southern part of the Kamchatsky Mys peninsula corresponds to accretionary prism. Fragments of basalt flows and carbonate-siliceous sections occur as faulted blocks and olistoliths in siliceous tuff matrix of island-arc origin. The mantle peridotites and gabbro compose tectonic slices (Khotin and Shapiro, 2006). This structure was formed in the Paleogene, before the accretion of the Kronotsky paleoarc to Kamchatka in Pliocene (Lander and Shapiro, 2007). The peculiarity of this terrane is large diversity of paleoceanic

rocks that may be related to a complex structure of the subducted oceanic plate complicated by seamounts of the Hawaiian-Emperor chain.

Lander A. V. and Shapiro M.N. The Origin of the Modern Kamchatka Subduction Zone // Volcanism and Subduction: The Kamchatka Region (J. Eichelberger, E. Gordeev, P. Izbekov, J. Lees editors). Geophysical Monograph 172. American Geophysical Union, Washington, DC, 2007. P. 57-64.

Khotin M. Yu. and Shapiro M. N. Ophiolites of the Kamchatsky Mys Peninsula, Eastern Kamchatka: Structure, Composition, and Geodynamic Setting // Geotectonics, 2006, Vol. 40, No. 4. P. 297-320.

Batanova, V. G., Lyaskovskaya Z. E., Savelieva G. N., and Sobolev A. V. Peridotites from the Kamchatsky Mys: evidence of oceanic mantle melting near a hotspot, Russian Geology and Geophysics, 2014. V. 55 (12). P. 1395-1403.

Palechek, T.N., Savel'ev, D.P., Savel'eva, O.L., 2010. Albian-Cenomanian Radiolarian Assemblage from the Smaginsk Formation, the Kamchatsky Mys Peninsula of Eastern Kamchatka // Stratigraphy and Geological Correlation, 2010. V. 18 (1). P. 63-82.

Portnyagin M., Hoernle K., Savelyev D. Ultra-depleted melts from Kamchatkan ophiolites: Evidence for the interaction of the Hawaiian plume with an oceanic spreading center in the Cretaceous? // Earth and Planetary Science Letters, 2009. Vol. 287. Iss. 1-2. P. 194-204.

Portnyagin M., Savelyev D., Hoernle K., Hauff F. and Garbe-Schönberg D. Mid-Cretaceous Hawaiian tholeiites preserved in Kamchatka. Geology, 2008. Vol. 36. № 11. P. 903-906.

Saveliev, D.P. Intraplate alkali basalts in the Cretaceous accretionary complex of the Kamchatkan Peninsula (Eastern Kamchatka) // Volcanology and Seismology, 2003. Vol. 1. P. 14–20. (Rus).

Savelyev D.P. Plagioclase picrites in the Kamchatsky Mys Peninsula, Eastern Kamchatka // Journal of Volcanology and Seismology, 2014. Vol. 8. Iss. 4. P. 239-249.

Savelyev D., Botcharnikov R., Filosofova T., Portnyagin M., Danyushevsky L. Platinum Group and Chalcophile Elements in Sulfides from Picrites of Ophiolite Complex from Kamchatsky Mys Peninsula (Kamchatka, Russia) // Goldschmidt Abstracts, 2015. 2778.

Savelyeva O., Palesskiy S., Savelyev D. PGE in Carbonaceous Beds in the Cretaceous Carbonate-Siliceous Section of the Kamchatsky Mys Peninsula (Russia) // Goldschmidt Abstracts, 2015. 2779.

Savelyev D.P., Savelyeva O.L., Palechek T.N., Pokrovsky B.G. Carbon isotope curve and iridium anomaly in the Albian-Cenomanian paleoceanic deposits of the Eastern Kamchatka // Geophysical Research Abstracts, Vol. 14, EGU2012-1940, EGU General Assembly 2012.

GEOLOGICAL STUDY ON CALDERA-FORMING ERUPTION OF SHIKOTSU VOLCANO, SOUTH-WESTERN HOKKAIDO : SPECIAL REFERENCE TO VENT FORMATION PROCESS AND MAGMA SYSTEM

Chiharu Tomijima[1], Mitsuhiro Nakagawa[1]
[1]Earth and Planetary System Science Department of Natural History Sciences, Graduate School of Science, Hokkaido University, Sapporo, Hokkaido, JAPAN.

Shikotsu caldera, 14 km long and 12 km wide, is located in southwestern Hokkaido, Japan, and was formed ca. 40 ka. It has been widely recognized that the caldera-forming eruption, the 40 ka Shikotsu eruption, started with a plinian eruption to form Spfa-1 tephra, Shikotsu pumice fall 1, and was followed by voluminous Spfl tepra, Shikotsu pyroclastic flow (Katsu, 1959). Thus, the sequence has been widely believed to be a typical for caldera-forming eruption. On the other hand, Yamagata (1992) described the sequence of the 40ka Shikotsu eruption at several proximal sites and reported the presence of large scaled lag breccia layer in the pyroclastic flow, which suggests caldera widening during Spfl eruption. However, the eruption sequence and the precise lithofacies characteristics related to temporal change of eruptive magma have not been clearly clarified. We carry out field works and boring exploration at several sites to reinvestigate the eruption sequence and temporal change of eruptive materials during the caldera-forming eruption of the Shikotsu volcano.

In proximal area, tephra deposits can be divided into many geological units. Based on lithofacies characteristic of these units, the caldera-forming eruption can be divided into five phases, Phase 1 to 5 in ascending order. Phase 1 deposit consists of the alternation of fine ash with accretionary lapilli and pumice fall layers (Unit 1), suggesting that the eruption strated with phreatomagmatic eruption. The tephra unit of Phase 2 is composed of three sub-units, thick pumice fall (Unit 2-1), fine ash and thin pumice fall (Unit 2-2), and pyroclastic flow (Unit 2-3) deposits in ascending layers. These deposits suggest that large scaled plinian column was formed and had become unstable to form pyroclastic flows (Phase 2). In Phase 3, voluminous pyroclastic flows were generated. Phase 4 started with effusion of the lithic rich pyroclastic flows with lag breccia , followed by pyroclastic flows. In Phase 5, the scale of eruption had extremely decreased to produce small scaled pumice fall and pyroclastic flow deposits. There exists the erosional gap between layers of Phase 2 and 3, indicating possible interval. Thus, the eruption can be divided into two stages with the time gap. Although Phase 2 could be considered as typical plinian eruption, component analysis and size distribution of units of the phase suggest that vent widening and newly vent opening possibly occurred in the later phase. Phase 3 and 4 are climactic activity of the caldera-forming eruption. However, the occurrence of the lithic concentrated pyroclastic flow deposits strongly suggests that caldera collapse occurred during Phase 4. Juvenile materials of the caldera-forming eruption are mainly phenocryst poor rhyolite pumice (aphyric type pumice: A-type). However, strongly porphyritic dacitic to andesitic pumice (porphyritic type pumice: P-type) was also recognized since the activity of Phase 4. This suggests that caldera collapse was strongly related to the activity of P-type magma.

GEOCHEMISTRY OF NEOGENE-QUATERNARY MAGMATISM OF THE SOUTHERN PART OF SREDINNY RANGE, KAMCHATKA

Anna Volynets [1], Maria Pevzner [2], Andrey Babansky [3]
[1]Institute of volcanology and seismology FEB RAS, Petropavlovsk-Kamchatsky, Russia
[2]Geological Institute RAS, Moscow, Russia
[3]IGEM RAS, Moscow, Russia

Sredinny Range of Kamchatka (SR), the largest volcano-tectonic structure of the peninsula, is composed from the old (Cretaceous-Paleogene) metamorphic massif and the volcanic belt, built in Neogene-Quaternary times. According to its structure and geomorphology, SR can be divided to the northern and southern parts. SR_N (northern part of SR) is a narrow range stretching from Alney volcanic massif to the NE (to Tobeltsen cone or even further) and is composed by Miocene-Quaternary volcanic rocks. SR_S (southern part of SR) has more complicated structure with two principal elements: (1) eastern flank, or main watershed (Bystrinsky and Kozyrevsky Ridges), which is the southern continuation of SR_N; and (2) "western" flank, that has NNE strike; it begins around Sredinny metamorphic massif and continues to the N and NE. "Western" flank is marked by the large stratovolcanoes: Khangar, Ichinsky, Kekuknaysky, Bolshaya Ketepana, composed by Pliocene-Quaternary rocks. Geochemistry of the SR_N rocks was studied in detail by (Volynets et al., 2010). It was demonstrated that all rocks in SR_N may be divided to two groups according their age. During Neogene, when SR was a frontal part of the corresponding subduction system, typical island-arc rocks were erupted within SR_N, with high fluid-mobile/immobile ratios (f. ex. Ba/Nb), and very low HFSE concentrations. That has changed in Quaternary times when SR became a rear part of the subduction system and rocks with hybrid signature started to erupt. They combine island-arc and within-plate affinities, have lower Ba/Nb (and other fluid-mobile/immobile element ratios) and elevated HFSE content. Average amount of the enriched mantle component in the source of Q_{3-4} SR_N magmas was estimated as 30% (lowest (14%) at Alney volcano and highest (55 %) at Sedanka monogenetic zone (Volynets et al., 2010)). Geochemical characteristics of the SR_S volcanic rocks are not so well-studied. (Churikova et al., 2001) included in their research Ichinsky volcano, which is located within SR_S. They described two types of rocks here: IAB-type and WPT-type. Rocks of both types have variably elevated fluid-mobile/immobile element ratios and are enriched by HFSE to different extent, i.e. all of them combine island-arc and within-plate signatures (from 5% enriched mantle in IAB-rocks to 35 % in WPT) and may be classified as hybrid type rocks, in analogy with SR_N. (Perepelov et al., 2006; Flerov et al., 2009) described Pliocene volcanic rocks, located at the northern flanks of Ichinsky, also composed by hybrid type rocks. Therefore, rocks of Neogene age with typical island-arc signatures were not described in SR_S. The goal of our regional work was to establish the location and time of hybrid-type and island-arc-type volcanism within SR_S. This work includes Neogene-Quaternary rocks of the following volcanic centers in SR_S: at the eastern flanks, within the main watershed - Akhtang volcano, Anaun volcano, Kostina mt. area, Kozyrevka mt. area; at the "western" flank - Yurtinaya mt., Khangar volcano, Ichinsky volcano, Kekuknaysky volcano; and Uksichan volcano, which is located between these two belts. At each volcanic massif we sampled rocks of the basement, stratovolcanoes and monogenetic centers; for Kekuknaysky we use published data from (Koloskov et al., 2011). At the current stage of research we used mostly elements that can be determined by XRF to include in this study as many sampled sites as possible.

Large volcanic centers, located in the "western" belt – Khangar, Ichinsky, Kekuknaysky - have a long eruptive history (f. ex., K-Ar age of the initiation of volcanic activity at Khangar caldera – 7 Ma (Pevzner et al., 2016)). They demonstrate differentiated geochemical trends (trachybasalts to pantellerites at Ichinsky; basalts and trachybasalts to trachyandesites at

Kekuknaysky, and basalts to rhyolites at Khangar). All volcanic rocks of these centers, including old basement rocks, have elevated Ti, Zr, Nb, low Ba/Nb, typical for Q hybrid rocks of the SR_N. Difference between older and younger rocks is clearly observed only at Kekuknaysky area, but even here all analyzed edifices have hybrid signature, with increasing amount of enriched OIB-type component in young rocks. Plateau-effusives of Yurtinaya mt., located at the southernmost part of SR_S (6 Ma, Volynets et al., 2016) also have hybrid signature, similar to Ichinsky basalts with ~5% of OIB-mantle in the source. Volcanic rocks, erupted within the eastern flank of SR_S, in Bystrinsky and Kozyrevsky Ridges, demonstrate quite different compositions. All studied centers have similar geochemical characteristics: medium-K basalts to andesites (in Neogene – to rhyolites), with low to moderate Ti and HFSE concentrations. Within the eastern flank we found typical island-arc plateau-basalts of Neogene age (Kostina mt. area), which are practically identical to the N_{1-2} plateau basalts of SR_N. Quaternary rocks of the eastern flank have slightly elevated HFSE content, similar to the rocks of IAB-type of Ichinsky volcano (Churikova et al., 2001) and rocks of Alney-Chashakondzha massif (Volynets et al., 2010) with minimal amounts of OIB-type mantle component in the source. Rocks of Uksichan massif can't be divided to groups according their geochemistry and age: most of the samples have hybrid signature with elevated HFSE; the concentrations are lower than in neighboring Ichinsky and Kekuknaysky volcanic massifs ("western" flank), but higher than in Anaun volcano (eastern flank). Some of the monogenetic centers, superimposed on the old Pliocene caldera, produced low-K, -Nb, -Ti basalts with high Ba/Nb, while underlying basement rocks have hybrid signatures. Thus, rocks of Uksichan volcano have geochemical characteristics intermediate between typical island-arc rocks and hybrid type rocks of the "western" flank of SR_S and SR_N.

Conclusions. Preliminary research of the geochemical features of the N-Q volcanic rocks of SR_S shows that this part of SR has complicated geological history, with simultaneous participation of different types of the mantle sources in magma generation within the different, spatially separate areas. "Western" flank of SR_S is characterized by the enriched mantle in the source from at least Miocene times. Eastern flank of SR_S, from Kostina mt. to Alney-Chashakondzha massif, demonstrates two age groups, different by their geochemistry, as it was reported for SR_N, but the amount of the enriched mantle component in the source of Quaternary magmas is substantially lower in SR_S than in SR_N or in the "western" flank.

Financial support by RAS Presidium Program №18, IVS FEB RAS (research theme № 01201354689), GIN RAS (research theme № 0135-2014-0068), RFBR projects № 08-05-00932 и 14-05-00549. The authors are grateful to V. Rodin, M. Tolstykh, B. Tugarinov, S. Zakharov, Yu. Novikov for the help in the field, sampling and sample preparation.

Churikova T., Dorendorf F., Wörner G. (2001) Sources and fluids in the mantle wedge below Kamchatka, evidence from across-arc geochemical variation // Journal of Petrology. 2001. Vol. 42. № 8. P. 1567-1593.

Flerov G., Philosofova T., Puzankov M. (2009) Series of rocks of Belogolovsky volcano as a reflection of the magmagenesis of the sources at the different depths (Sredinny Range of Kamchatka) // IV Russian Symposia on volcanology and paleo-volcanology. Petropavlovsk-Kamchatsky, 2009. V. 1. P.208-211.

Koloskov A., Flerov G., Perepelov A., et al. (2011) Stages of evolution and petrology of Kekuknaysky volcanic massif as reflection of rear zone magmatism of the Kurile-Kamchatka island arc system. Part 1. Geological position and geochemical composition of the volcanic rocks // Volcanology and seismology. 2011. №5. P. 17-41.

Perepelov A., Chaschin A., Martynov Yu. (2006) Sredinno-Kamchatskaya zone (Pliocene-Holocene) // Geodynamic, magmatism and metallogeny of the Eastern Russia. Vladivostok: Dalnauka. V. 1. P.382-398.

Pevzner M., Volynets A., Kostitsin Yu., et al. (2016) First data on the time of volcanism initiation in Khangar caldera (Sredinny Range, Kamchatka) // Proceedings of the annual conference on Volcanologists Day "Volcanism and related processes". IVS FEB RAS, Petropavlovsk-Kamchatsky, p.125-128.

Volynets A., Pevzner M., Kovalenko D., et al. (2016) First data on age, geochemistry and mineralogy of Yurtinaya mt. plateau-effusives (Sredinny Range, Kamchatka) // Proceedings of the annual conference on Volcanologists Day "Volcanism and related processes". IVS FEB RAS, Petropavlovsk-Kamchatsky, p.21-23.

Volynets A., Churikova T., Wörner G., et. al. (2010) Mafic Late Miocene - Quaternary volcanic rocks in the Kamchatka back arc region: implications for subduction geometry and slab history at the Pacific-Aleutian junction // Contributions to mineralogy and petrology. 2010. № 159. P. 659–687.

REAL-TIME EARTHQUAKE MONITORING FOR TSUNAMI WARNING IN KAMCHATKA DURING 2011-2015

Victor N. Chebrov, Anna A. Skorkina, Danila V. Chebrov, Dmitry V. Droznin, Dmitry A. Ototuk
Kamchatka Branch, Geophysical Survey, Russ. Ac. Sci., Petropavlovsk-Kamchatsky, Russia.

Tsunami Warning System in Kamchatka was established in Petropavlovsk-Kamchatsky, Russia in 1956–1959 years as a direct result of the great earthquake and tsunami that occurred in the Kuril Islands and Kamchatka on November 05, 1952 (M = 8.5). This earthquake alerted Federal officials to the need for a facility to provide timely and effective tsunami warnings and information for these coastal areas.

In 2006–2010 Tsunami Warning System in the Russian Far East was deeply modernized as the response of Federal officials to the tragedy of December 26, 2004 (Sumatra earthquake). The task of the Kamchatka Branch of Geophysical Survey, Russian Academy of Sciences, was to develop and implement the seismological component (Chebrov et al., 2009, 2012).

In this paper we shortly describe the concept of the Tsunami Warning System (TWS) and real-time earthquake monitoring system in Russian Far East and report on its present status in Kamchatka.

In 2014 Kamchatka Branch of GS renewed collaboration with Local officials. And in autumn of the same year there were 5 new strong ground motions instruments installed around the city. Since then a new service appeared in real-time earthquake monitoring system, such as mapping of instrument intensity for the (1) Petropavlovsk-Kamchatsky city and (2) Kamchatka region. These two documents are formed automatically in real time using strong ground motion data and supposed to be sent within 15–20 minutes since the event origin time in cases of $I \geq 1$ in the city and $I \geq 3$ in the region.

To date the system of seismological observations developed by the Kamchatka Branch of GS RAS includes:

(1) three regional processing centers (PCs in Petropavlovsk-Kamchatsky, Yuzhno-Sakhalinsk and Vladivostok) equipped with satellite communication system. All of them have complete access to the data of all seismic stations of SSO TWS, analyze seismic data and determine earthquake parameters in real time in 24/7. Processing centers obtained two types of estimations: interactive (preferred, human-controlled) and automatic (as an auxiliary alarm signal which turns on when 7 onsets are detected);

(2) seismic network, consisting of 55 strong motion instruments, 31 among them are in seismic groups around 6 principal stations, and 18 auxiliary digital stations. All stations are equipped with both accelerometers and broadband velocimeters (T_c = 120 sec). Principal stations are located near the towns on the coast. Also data of Global Seismographic Network and a few regional GS stations are incorporated in the data processing;

(3) real time data acquisition system.

PC "Petropavlovsk-Kamchatsky" is mainly responsible for the offshore zone within the circle area with the radius of 1000 km around PET station. The "tsunami" alert should be released when within the area an earthquake with $M_S \geq 7.0$ occur.

Let cover the main results for 2011–2015.

41 regional events have $K_S \geq 13.5$ and/or $M_S \geq 6$, which are the threshold estimates when the Urgent Message Survey "Petropavlovsk" starts to operate as TWS. Traditionally, tsunami alerts are formed on the basis of earthquake epicenter coordinates and magnitude. The only "tsunami" alert was sent in 2012 which turned out to be false due to depth factor. After that the hypocenter criteria was checked.

SSO TWS is capable to release the first alert about the fact of a strong earthquake ("possible tsunami" alert) not later than 4 minutes after its origin time. For the near-fields (with radius of 200 km from PET), estimates of earthquake parameters are supposed to be sent within 7 minutes from the time of registration at the first station. In fact in 2011–2015, the average response time to an earthquake within this area is 4 minutes 25 seconds after its origin time (*Table*). The discrepancy of epicentral assessment, comparing to NEIC solutions, equals 40 km in average.

The Urgent Message Survey "Petropavlovsk" for the same period has sent 2411 information messages including 1694 urgent messages (*Table*). From them there were 75 earthquakes felt in Petropavlovsk. It also should be noted that since 2015 solutions obtained with $K_S < 10$ are also used to reflect the current seismicity in the region. And currently the number of solutions produced by PC "Petropavlovsk" has increased, what is mainly the result of saving solutions which are turned out to be after processing not strong enough to be sent as urgent messages.

To summarize, since 2015 year PC "Petropavlovsk-Kamchatsky" has been on-stream as (1) a seismological component in Tsunami Warning System, (2) Urgent Message Survey and (3) local real-time seismological information center.

Table. Distribution of solutions numbers and average response times in different zones by years for PC "Petropavlovsk-Kamchatsky".

	Number of messages	Δ ≤ 200 km	Average $t_{response}$	Δ ≤ 1000 km	Average $t_{response}$	Δ ≤ 2000 km	Δ > 2000 km
2011	247	39	4 min 55 sec	90	5 min 53 sec	124	123
2012	347	44	4 min 09 sec	162	6 min 35 sec	207	140
2013	414	116	4 min 16 sec	209	4 min 54 sec	256	158
2014	329	30	4 min 15 sec	116	5 min 49 sec	151	178
2015	357	23	3 min 57 sec	122	6 min 30 sec	166	191
*2015**	*1074*	*183*	*5 min 47 sec*	*498*	*7 min 27 sec*	*726*	*348*
Total	1694	252	4 min 25 sec	698	5 min 51 sec	904	790
*Total**	*2411*	*412*	*5 min 03 sec*	*1075*	*6 min 31 sec*	*1464*	*947*

* The numbers reflect the quantity of both urgent and information messages. The rest results are for urgent messages only.

References

Chebrov, V.N., Gusev, A.A., Gusiakov, V.K., Mishatkin, V.N., Poplavsky, A.A. 2009. A concept of development of a system for seismological observations with the purpose of tsunami warning in the Far East of Russia // Seismic Instruments. V. 45. №4. P. 41-57.

Chebrov, V.N., Gusev, A.A., Droznin, D.V., Mishatkin, V.N., Sergeev, V.A., Shevchenko, Y.V., Chebrov, D.V. 2012. Renewed system of seismic observations for the tsunami warning in the Russian Far East // 33rd ESC General Assembly, Russia.

TSUNAMI SIMULATION AND LANDSLIDE MODEL OF THE 1741 OSHIMA-OSHIMA ERUPTION

Kei Ioki[1], Yuichiro Tanioka[2], Gentaro Kawakami[3], Yoshihiro Kase[3], Kenji Nishina[3], Wataru Hirose[3], Satoshi Ishimaru[3], Hideaki Yanagisawa[4]

[1] *National Institute of Advanced Industrial Science and Technology, Japan*

[2] *Institute of Seismology and Volcanology, Hokkaido University, Japan*

[3] *Geological Survey of Hokkaido, Japan*

[4] *Department of Regional Management, Faculty of Liberal Arts, Tohoku-gakuin University, Japan*

The 1741 tsunami occurred near Oshima-Oshima in Hokkaido caused great damage along the coast of Japan Sea in Oshima and Tsugaru peninsula. Assuming that the tsunami was generated by flowing a landslide into the sea with a sector collapse in Oshima-Oshima, the landslide was simulated. Distribution of debris deposits, topography before the sector collapse, and landslide volume were re-calculated from a bathymetry survey data (Satake and Kato, 2001) in the north part of Oshima-Oshima. Based on these data, the landslide was simulated using the integrated model of landslide and tsunami (Yanagisawa et al., 2014). As a result, distribution of computed debris deposits agrees relatively well with the distribution of debris deposits made out from bathymetry. However, the computed debris deposits spread to north part than debris deposits made out from bathymetry and not reach to the east and west part compared to debris deposits made out from bathymetry in detail. The thickness of computed debris deposits was thicker to the north part than debris deposits made out from bathymetry. Further, model parameters and topography before the sector collapse are needed to be improved for more realistic tsunami simulation.

CHARACTERIZATION OF ELECTRIC CONDUCTIVITY, PH, AND ORGANIC-WALLED MICROFOSSILS FOR IDENTIFYING TSUNAMI DEPOSITS: AN EXAMPLE OF MODERN TSUNAMI AND PALEOTSUNAMI DEPOSITS IN PACIFIC COAST LOWLANDS, HOKKAIDO AND TOHOKU, JAPAN

Yoshihiro Kase[1], Keiichi Hayashi[1], Gentaro Kawakami[1], Kenji Nishina[1], Atsushi Urabe[2], Yasuhiro Takashimizu[2]

[1]Geological Survey of Hokkaido, Hokkaido Research Organization, Sapporo, Hokkaido, Japan

[2]Niigata University, Niigata, Japan

Introduction

For the recognition of tsunami deposits in coastal lowlands, some distinctive criteria have been proposed based on sedimentological analyses of modern tsunami deposits (e.g. Peters and Jaffe, 2010; Goff et al., 2012). In particular, the discrimination between tsunami- and flood-origin deposits is crucial for clarifying inundation areas, occurrence ages, and recurrences (cycles) of paleotsunamis. Although analyses of sediment geochemistry and organic-walled microfossils are potentially crucial for the identification of tsunami deposits, they have only been undertaken in a small number of studies (Minoura et al., 1994; Chagué-Goff et al., 2012; GSH, 2015). Therefore, we performed geochemical analysis, namely, analysis of electric conductivity (EC) and pH, and organic-walled microfossil analysis for previously identified tsunami deposits to verify the effectiveness of these methods in the coastal lowlands along the Pacific Ocean in Hokkaido and Tohoku, Japan.

Results and discussion

We collected several samples from both modern (the 2011 Tohouku-oki tsunami) and historical tsunami deposits (Nanayama et al., 2003; Sawai et al., 2012) along the Pacific Coast in Japan.

(1) Geochemical analysis

The supernatant solutions of the tsunami deposits, in general, showed high EC and low pH values compared with those of peats (Fig. 1). The high EC and low pH values correspond to high SO_4^{2-} and Ca^{2+} contents (Fig. 1). Some samples also showed high values of Mg^{2+} contents. However, these EC and pH values are not applicable to surficial deposits, up to depths of 60–70 cm (Fig. 1).

The high EC (high SO_4^{2-} and high Ca^{2+}) and low pH absolute values of the supernatant solutions of the tsunami deposits are indicative of seawater inundation, although the levels of Na^+ and Cl^-, the most significant components of seawater, are low (Na^+; *ca* 44–95 ppm, Cl^-; *ca* 9–19 ppm) and do not correspond with the EC and pH values. The SO_4^{2-} may originate from sulfides, and the low Na^+ and Cl^- contents probably reflect chemical leaching of soluble species. Although the precise geochemical processes are unclear, this characterization could be a useful method to identify tsunami deposits.

(2) Organic-walled microfossils

Some modern tsunami and paleotsunami deposits contain dinoflagellate cysts and foraminiferal linings characteristic of coastal areas, indicating shallow marine sources for the clastics. However, other tsunami deposits do not contain organic-walled microfossils. It is suggested that differences in organic residue composition are related to variations in geographical location and distance from the sea.

In addition, in 2011 Tohoku-oki tsunami deposits, foraminiferal linings are concentrated only in the base of the sand beds, while dinoflagellate cysts are found both in the base of sand beds and in the top of muddy beds (mud drapes) (Fig. 2). These results suggest density separation of the foraminifera and dinoflagellate cysts occur through sedimentation processes.

Hence, it is effective to examine muddy layers (mud drapes) of tsunami deposits to locate dinoflagellate cysts.

Acknowledgement

This research was supported by the Collaborative Research Project (2015-7) of the Research Institute for Natural Hazards and Disaster Recovery, Niigata University

References

Chagué-Goff et al., 2012, *Sed. Geol.*; Geol. Sur. Hokkaido, 2015, *Special Rep. No. 42.*; Goff et al., 2012, *Sed. Geol.*; Minoura et al., 1994, *Sed. Geol.*; Nanayama et al., 2003, *Nature.*; Peters and Jaffe, 2010, *U.S. Geol. Sur. Open-File Rep.*; Sawai et al., 2012, *Geophy. Res. Lett.*

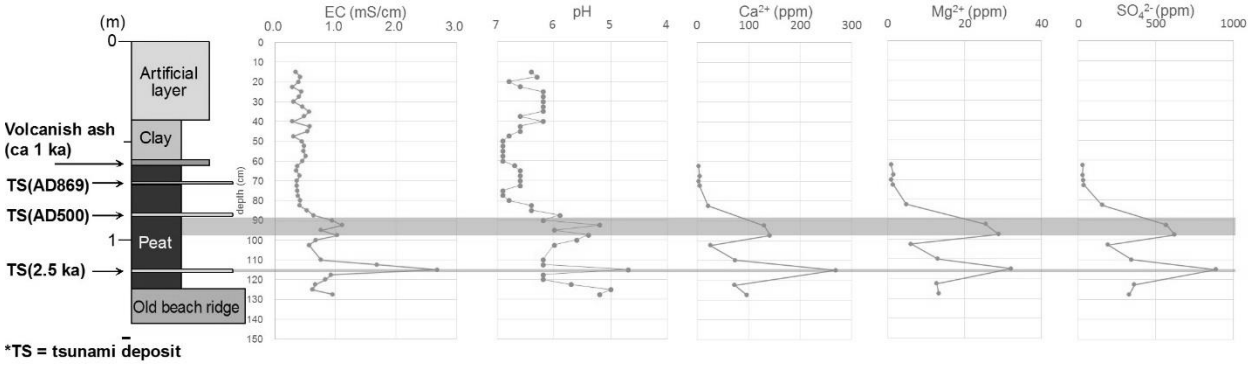

Fig. 1. An example of stratigraphy and vertical variations in electric conductivity (EC), pH, and Ca^{2+}, Mg^{2+} and SO_4^{2-} of a core sample from Yamamoto-cho, Miyagi Prefecture, Japan. Ages of tsunami deposits are compiled from Sawai et al. (2012).

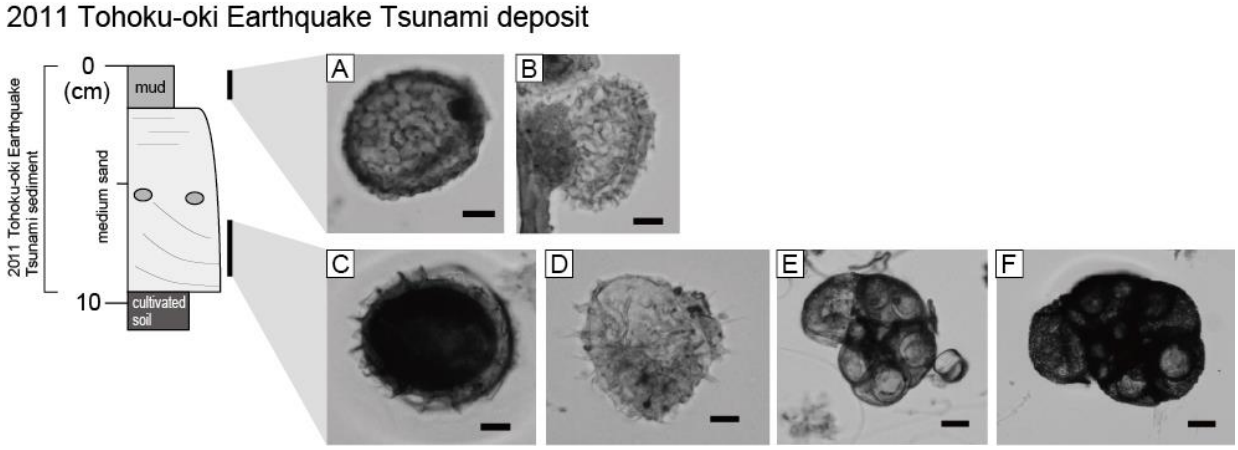

Fig. 2. Stratigraphy of the 2011 Tohoku-oki tsunami deposit and associated organic-walled microfossils. A and B were from muddy layers of the deposit (mud drapes) (A, B: dinocysts gen. et sp. indet.). C–F were from basal part of the sand (C: dinocyst gen. et sp. indet. D: *Cleistosphaeridium* sp., E, F: foraminiferal linings). Scale bar is 20 μm long.

2015-2016 ACTIVITY OF KAMCHATKAN AND NORTHERN KURILES VOLCANOES (RUSSIA) AND DANGER TO AVIATION

Evgenii Gordeev, Olga Girina, Alexander Manevich, Dmitry Melnikov, and Anton Nuzhdaev
Institute of Volcanology & Seismology FEB RAS, Petropavlovsk-Kamchatsky, Russia.

There are 36 active volcanoes in Kamchatka and Northern Kuriles with several of them being continuously active. In 2015-2016, four of the Kamchatkan volcanoes (Sheveluch, Klyuchevskoy, Karymsky, and Zhupanovsky) and two volcanoes of Northern Kuriles (Alaid and Chikurachki) had strong and moderate explosive eruptions. Moderate gas-steam activity was observed at Bezymianny, Kizimen, Avachinsky, Koryaksky, Gorely, Mutnovsky, and other volcanoes.

Strong explosive eruptions are the most dangerous for aircrafts because they can send to atmosphere up to several cubic kilometers of volcanic ash and aerosols during a few hours or days. Ash clouds can propagate for thousands of kilometers away from a volcano remain in the air for several days, and pose a continuous threat to aircrafts, as the melting temperature of ash particles is below operating temperatures of jet engines.

The eruptive activity of *Sheveluch volcano* resumed in 1980 and is continuing at present. In 2015 strong explosive events at Shiveluch occurred on January 7, 12, and 15; February 1, 17, and 28; March 4, 8, 16, 21-22, and 26; April 7 and 12. Each time ash plumes rose up to 7-12 km a.s.l. and extended for more than 900 km to different directions from the volcano [3]. Ashfalls occurred in Ust'-Kamchatsk on March 16, and in Klyuchi on October 30. In the second half of 2015 and early 2016, an intensive growth of the northern block of lava dome was observed, accompanied by strong and moderate hot avalanches. Aviation color code of Sheveluch was Orange during 2015-2016. Activity of the volcano was dangerous to international and local aviation.

Explosive-effusive eruption of *Klyuchevskoy volcano* lasted from January 1 to March 24, 2015 [1]. Strombolian explosive volcanic activity began on January 1, 2015. On January 8-9 a lava flow was detected at the Apakhonchich chute on the SE flank of the volcano. Vulcanian activity of the volcano began on January 10. Ashfalls occurred on January 11 and 28, and on February 7 in Kozyrevsk, as well as on January 21 and 27, on February 5, 11, and 13-16 in Klyuchi. Paroxysmal phase of the eruption occurred on February 15 when continuous series of explosions sent ash up to 8 km a.s.l. during five hours of eruptive activity. Ash plumes drifted for about 1000 km mainly to the east from the volcano. A thermal anomaly was observed in satellite images again on August 28 and it was registered time to time till December 31. Aviation color code of the volcano was Yellow during January 1-11; Orange during January 11 – February 15; Red on February 15; Orange during February 15 – March 25; Yellow during March 25 April 6; Green during April 6-14; Yellow during April 14-18; Orange during April 18-26; Yellow during April 26 – May 5; Orange during May 5-13; Yellow during May 13 – July 20; Green during July 20 – August 28; Yellow during August 28 – December 31, 2015. Next Strombolian explosive eruption began on March 3, 2016 and continues at the time of this writing. Volcanic explosions send bombs up to 500 m above the volcanic crater. The volcano sometimes produces strong gas-steam plumes containing small amounts of ash. Aviation color code of the volcano is Yellow at present. Eruptive activity of Klyuchevskoy poses a continuous threat to international and local aviation.

Karymsky volcano has been in a state of explosive eruption since 1996. Moderate ash explosions at Karymsky volcano were observed during 2015-2016 with ash plumes rising up to 5 km a.s.l. and extending for more than 300 km mainly to the east from the volcano [3].

Aviation color code of the volcano was Orange. Activity of the volcano was dangerous to local aviation.

Explosive eruption of *Zhupanovsky volcano* began on June 6, 2014, and continues in unstable regime at present time. In 2015, explosions sent ash up to 8-11 km a.s.l. on March 7-8 and 25, July 12, and November 30; and up to 3.5-6 km a.s.l. on other days [3]. Ash plumes extended for about 1200 km mainly to the east from the volcano. During January 26 - February 6, February 9-15, February 23 – March 01, March 25 - April 03, April 4 to May 20, May 21 – June 8, June 16 – July 12, and July 15 – November 27 the volcano was in a state of relative quiescence. The activity culminated in explosions and flank collapses of Priemysh active cone on July 12 and 14, and November 30, 2015. Aviation color code of the volcano was Orange from January 1 to May 16; Yellow from May 16 to June 8; Orange from June 8 to July 19; Yellow on July 19-20; Green from July 20 to November 27; Orange from November 27 to December 10; Yellow on December 10-17; and Green on December 17-31. In 2016, explosions sent ash up to 8-10 km a.s.l. on January 19, 21, and 24, February 5, 7, 9, and 12, and on March 24 [2]. Ash plumes extended for about 600 km in different directions from the volcano. Aviation color code of the volcano was Orange from January 19 till April 13, and then Yellow till present. Activity of the volcano was dangerous to international and local aviation.

The eruption of *Chikurachki volcano* occurred on February 15-18, 2015 and March 28-31, 2016. In 2015, ash plumes rose up to 7.5-8 km a.s.l. and extended for nearly 280 km to the west and to the east of the volcano [3]. In 2016, ash plumes rose up to 4 km a.s.l. and extended for about 570 km to the NE, south, and SW from the volcano. Aviation color code of the volcano was Orange during February 16-22, Yellow on February 22-26 in 2015; Yellow on March 29 – April 05 in 2016. Activity of the volcano was dangerous to local aviation.

The intensive thermal anomaly at *Alaid volcano* was observed in satellite images from October 1, 2015 [3], till present. In 2016, strong gas-steam plumes containing ash rose up to 3 km a.s.l. on March 03, from March 30 till April 1 (simultaneously with eruption at Chikurachki Volcano), and on April 9. Aviation color code of the volcano was changed to Yellow on October 1, 2015, and then to Orange on March 3, 2016. The volcano remains at Orange at present. Activity of the volcano was dangerous to local aviation.

References

1. Girina O.A., Demyanchuk Yu.V., Mel'nikov D.V., Manevich A.G., Manevich T.M, Nuzhdaev A.A., Muraviev Ya.D. 2015 Eruption of Klyuchevskoy Volcano and it Danger for Aviation. In: Materials of XVIII Volcanol. Conf. “Volcanism and Processes involve with it”, 30 March – 01 April, 2015, Petropavlovsk-Kamchatsky: IVS FED RAS, 2016, pp. 16-20 (in Russian)

2. Girina O.A., Manevich A.G., Mel'nikov D.V., Manevich T.M, Nuzhdaev A.A., Lungul O.A., Sorokin A.A. 2016 Explosive Activity of Zhupanovsky volcano. In: Materials of XIX Volcanol. Conf. “Volcanism and Processes involve with it”, 29-30 March, 2016, Petropavlovsk-Kamchatsky: IVS FED RAS, 2016, pp. 24-34 (in Russian)

3. Girina O.A., Manevich A.G., Mel'nikov D.V., Nuzhdaev A.A., Demyanchuk Yu.V. 2015 Activity of Volcanoes of Kamchatka and Northern Kuriles and Danger for Aviation. In: Materials of XIX Volcanol. Conf. “Volcanism and Processes involve with it”, 29-30 March, 2016, Petropavlovsk-Kamchatsky: IVS FED RAS, 2016, pp. 35-45 (in Russian)

TEMPORAL VARIATION OF THE ACROSS SIGNALS DURING A PERIOD FROM JANUARY TO AUGUST, 2015 IN SAKURAJIMA VOLCANO, JAPAN.

Hiroki Miyamachi[1] , Koshun Yamaoka[2] , Hiroshi Yakiwara[1] , Yuta Maeda[2] , Toshiki Watanabe[2] , Takahiro Kunitomo[2] , Takeshi Tameguri[3] , Masato Iguchi[3]

[1] Graduate school of Science and Engineering, Kagoshima University, Kagoshima, Japan.
[2] Earthquake and Volcano Research Center, Graduate School of Environmental Studies, Nagoya University, Nagoya, Japan.
[3] Disaster Prevention Research Institute, Kyoto University, Kyoto, Japan.

Quantitative monitoring of magma transport process is essentially important for understanding the volcanic process and prediction of volcanic eruptions. To realize this monitoring, an active monitoring system using a vibration source called ACROSS has been operated in Sakurajima Volcano since September 2012 (Yamaoka et al., 2014; Miyamachi et al., 2013, 2014). From our previous observational studies, we obviously found that the amplitude and travel times of the daily transfer functions (the ACROSS signal) vary temporally. In particular Maeda et al. (2015) revealed that the amplitude of the ACROSS signals in the later phases became small in several hours before and after explosive eruptions. In this report, we show a long-term temporal change for the ACROSS signals observed with the remarkable volcanic activity that occurred in Sakurajima volcano on August 15, 2015.

Our ACROSS system is composed of two vibrators: one vibrator (SKR1) with a signal frequency range of 7.510Hz +/- 2.50Hz and the other (SKR2) with the range of 12.505Hz +/- 2.50Hz. The seismic signals from the ACROSS sources are routinely monitored with more than 20 permanent and 5 temporal seismic stations in and around Sakurajima volcano. The signals recorded at the seismic stations are deconvoluted with the ACROSS source function to obtain the transfer function between the source and the receivers. In 2015, the ACROSS system started operation at the beginning of January 2015, but the operation was suspended on 18 August, because of the signal contamination to a monitoring seismic station for the volcano. We use the data in 2015 to check the temporal change of transfer functions between the ACROSS source and the seismic stations in Sakurajima island.

We calculated the daily transfer functions for each station by every 1 day stacked data during a period of January to August 2015. Transfer functions in Sakurajima volcano indicate large temporal variation especially in later phase part comparing to the other site such as Awaji or Tokai area where ACROSS system is being operated. In many of the transfer function connecting between the ACROSS source and the stations remarkable change can be seen at the end of July, 2015, though causal relationship to the volcanic event on 15 August is not clear. We also need to make a quantitative investigation on the meteorological effect to the transfer functions.

Reference

Yamaoka et al. (2014) Earth Planets, Space, Doi:10.1186/1880-5981-66-32.
Maeda et al. (2015) Geophys. Res. Lett., Doi: 10.1002/2015GL064351.

REVISITING COSEISMIC AND POSTSEISMIC DEFORMATION FROM THE 2002 DENALI, ALASKA EARTHQUAKE

Hugh Harper[1], Jeff Freymueller[1]
[1]*Geophysical Institute, Univ. of Alaska Fairbanks. Fairbanks, AK, USA.*

Given the multi-decadal temporal scale of postseismic deformation, predictions of previous models for postseismic deformation resulting from the 2002 Denali Fault earthquake (M 7.9) do not agree with longer-term observations. In revising the past postseismic models with what is now over a decade of data, the first step is revisiting coseismic displacements and slip distribution of the earthquake. Advances in processing allow us to better constrain coseismic displacement estimates, which will affect slip distribution predictions in modeling.

Previous studies have shown that two primary processes contribute to postseismic deformation: afterslip, which decays with a short time constant; and viscoelastic relaxation, which decays with a longer time constant.

By fitting continuous GPS time series, we have optimized postseismic relaxation time constants, which will be used in future studies. The time series can be fit using either two exponential decay terms (one for each postseismic process) or both a logarithmic and exponential decay term. We use a simple grid search to minimize model WRSS and find optimal relaxation times of: 0.625 years and 8.5 years for two exponentially decaying terms; and 0.075 years and 10.083 years, for logarithmic and exponential decay, respectively.

VOLCANO MONITORING
(ORAL PRESENTATIONS)

RECENT ADVANCES IN GEOPHYSICAL MONITORING AT MOUNT CLEVELAND VOLCANO, ALASKA

John Lyons[1], Matthew Haney[1], David Fee[2], Cindy Werner[3], Christoph Kern[3], Diana Roman[4], and John Power[1]
[1]Alaska Volcano Observatory, U.S. Geological Survey, Anchorage, Alaska, USA,
[2]Geophysical Institute, Alaska Volcano Observatory, University of Alaska Fairbanks
[3]Cascades Volcano Observatory, U.S. Geological Survey, Vancouver, Washington, USA,
[4]Department of Terrestrial Magnetism, Carnegie Institution for Science, Washington, D.C., USA

Mount Cleveland volcano (1730 m) is one of the most active volcanoes in the Aleutian Arc, having had eruptive activity recorded every year since 2005. Eruptive activity is typically characterized by dome growth in the central crater, followed by minor explosive activity that often destroys the domes. In recent years, minor lava flows have extended as much as to 2-3 km down slope on the flanks of the volcano. While the majority of activity is minor, major ash producing eruptions are a constant aviation hazard in the region and most recently occurred at Mount Cleveland in 1998 and 2001.

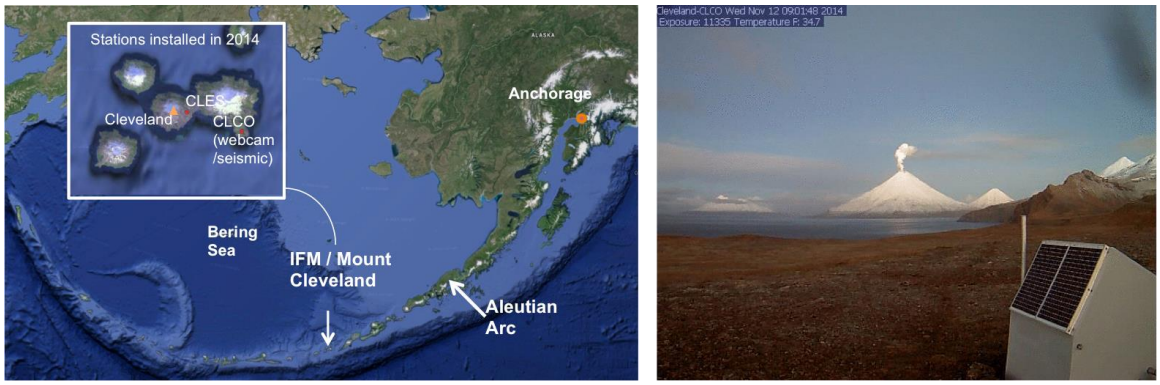

Figure 1. Location map and web cam image from November 2014.

Mount Cleveland last erupted at 16:58 UTC on 16 April 2016. This short-lived explosive event was the 40th explosion detected by the Alaska Volcano Observatory since 25 December 2011. Although the volcano is frequently active, its remote location makes observations and access difficult and costly. Prior to 2014, Mount Cleveland was only monitored by satellite observations or with distal seismic stations or infrasound arrays. Collaboration between the Alaska Volcano Observatory (AVO) and the National Science Foundation (NSF) in 2014 provided the opportunity to install the first local monitoring stations. Two real-time seismic stations, an infrasound array, and a web cam now provide significantly improved monitoring capabilities to AVO. The time to detect explosions has been greatly reduced, and frequent small earthquakes (including a small swarm) have been observed for the first time.

Scientifically, Mount Cleveland has been minimally studied geophysically despite strong interest in relating monitoring observations to processes at depth. Research into what makes Cleveland tick was given a boost in 2015, when two proposals were funded to investigate the linkages between deep and shallow earthquakes in and around the volcano and eruption dynamics (Roman et al., NSF GeoPRISMS), and the geochemistry of gas emissions (Werner et al., Deep Carbon Observatory). A network of 12 campaign broadband seismic stations was

deployed in August 2015 and will be recovered in July 2016. The first volcanic gas measurements were made in August 2015, and will be repeated in July 2016. Measurements of SO2 column concentrations were made using an upward-looking DOAS spectrometer mounted to the helicopter skid (a FLYSPEC was also initially used). In situ gas concentrations (H2O, CO2, SO2, H2S) were measured using a USGS Multi-GAS unit. Low molar C/S ratios derived from these data (<3) are consistent with the presence of shallow magma in the system and the observed growth of a new lava dome.

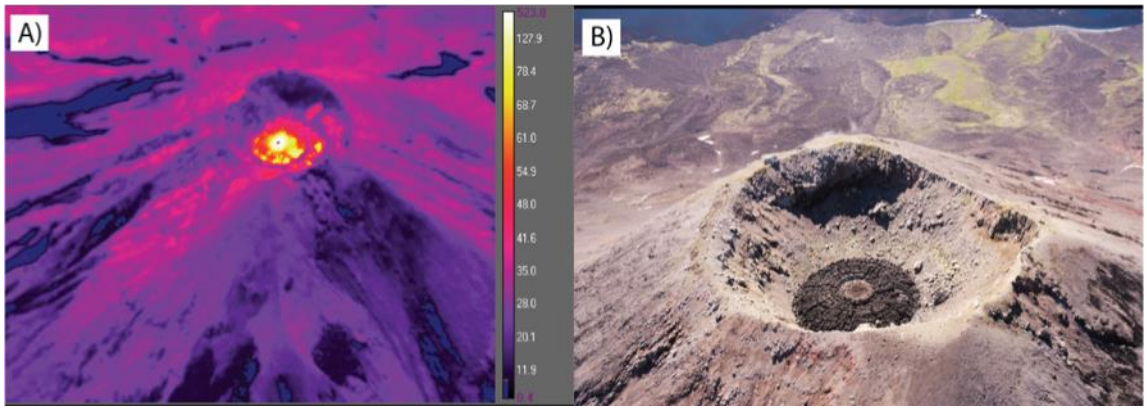

Figure 2. A) Thermal (IR) and B) visual observations of a new lava dome growing in the summit crater of Mount Cleveland on 4 August 2015.

CONSTRAINING THE SPATIAL AND TEMPORAL VARIABILITY OF ATMOSPHERIC CONDITIONS TO EXPLORE THE INFRASOUND DETECTION OF VOLCANIC ERUPTIONS IN ALASKA

Alex M. Iezzi [1, 2], Hans F. Schwaiger [2], David Fee [1], Matthew Haney [2]
[1] *Geophysical Institute, Alaska Volcano Observatory, University of Alaska Fairbanks*
[2] *U.S. Geological Survey, Alaska Volcano Observatory, Anchorage, Alaska*

Alaska's over 50 historically active volcanoes span 2,500 kilometers, and their eruptions pose great threats to the aviation industry and local populations. This makes both prompt observations of explosion onsets and changes in intensity a necessity. These volcanoes are predominantly monitored by local seismic networks in the best case, and augmented by remote observations including satellite imagery and infrasound arrays. Infrasound, or acoustic energy below 20 Hz, is an especially crucial tool because it is not obstructed by frequent cloud cover (as in satellite imagery) and infrasound waves from large sources can travel hundreds to thousands of kilometers. However, infrasound station coverage is relatively sparse and strong wind and temperature gradients in the atmosphere create multiple waveguides and shadow zones where the propagation of infrasound is enhanced and diminished, respectively. To accurately constrain volcanic source information and the long-range propagation of infrasound waves, a detailed characterization of the spatial and temporal variability of the atmosphere is vital. These properties can be constrained using a ground-to-space model similar to that of Drob et al. (2003) that is based upon numerous meteorological observations and applied to the propagation of infrasound waves. Here we present the first results of an atmospheric condition re-analysis system constructed by the Alaska Volcano Observatory (AVO-G2S) to accurately characterize and model long-range infrasound propagation from volcanic eruptions.

We select a number of case studies to examine infrasound detections (or lack thereof) from recent eruptions of Alaskan volcanoes, including the November 2014 and March-April 2016 eruptions of Pavlof Volcano and July 2015 explosion of Cleveland Volcano. During the November 2014 eruption of Pavlof Volcano, it was found that discrepancies between seismic and infrasound detection may be due to marginal wind changes, which influences the appearance and disappearance of both weak tropospheric and stratospheric waveguides. Strong tropospheric ducting during the 21 July 2015 Cleveland eruption produced favorable propagation conditions that likely contributed to the trigger of the alarm at a remote infrasound array. This was compared with weak stratospheric ducting for the 6 November 2014 explosion of similar size that did not trigger the alarm. Detailed examination of the acoustic propagation conditions will provide additional insight into detection capability, eruption dynamics, and array location with future work aiming to implement real-time long-range infrasound propagation modeling in Alaska.

Drob, Douglas P., J. M. Picone, and M. Garces. "Global morphology of infrasound propagation." *Journal of Geophysical Research: Atmospheres (1984-2012)* 108.D21 (2003).

ANALYSIS OF FUMAROLE ACOUSTICS AT ASO VOLCANO, JAPAN

Kathleen McKee[1], David Fee[1], Akihiko Yokoo[2], Robin Matoza[3]
1. Wilson Alaska Technical Center, Alaska Volcano Observatory, Geophysical Institute, University of Alaska Fairbanks, Fairbanks, AK, United States
2. Aso Volcanological Laboratory, Institute of Geothermal Sciences, Graduate School of Science, Kyoto University, Kumamoto, Japan
3. Department of Earth Science, University of California, Santa Barbara, CA, United States

The lowermost portion of a large volcanic eruption column is dominated by momentum-driven, fluid flow processes, and is termed the volcanic jet. The perturbation of the atmosphere from this region produces infrasound resembling jet noise. Recent work has shown that infrasonic volcanic jet noise has similar characteristics to audible sound from jet and rocket engines. The study of volcanic jet noise has gained much from laboratory jet-engine studies; however, laboratory jet studies have primarily focused on pure-air jets, thereby limiting their use as a comparison tool to the complex (i.e., hot, multiphase) volcanic jet. Jet noise is highly directional, which makes sampling the acoustic wavefield at a varying angle relative to the jet access necessary to determine jet parameters. This task is achievable with a laboratory jet engine, but presents another challenge in the volcanic case, as our observations are usually ground based. Previous studies have noted that fumaroles, vents in volcanic environments that issue volatiles at temperatures greater than 100°C, produce jet noise without further detailed investigation. The goal of this work is to enhance our understanding of large-scale volcanic jets by studying an accessible, less hazardous fumarolic jet. We aim to characterize the acoustic signature of fumaroles and evaluate if fumarolic jets scale to that of large volcanic jets. On July 13 a new small vent opened on the southwest flank of the partially collapsed pyroclastic cone within Naka-dake crater of Aso Volcano, Japan. The vent was several meters in diameter and had consistent gas jetting which produced audible jet noise. We deployed a 6-element acoustic array along the southwestern edge of the crater to capture the acoustic signature of the gas jetting. The array was ~230 meters from the vent and was positioned 54 degrees from the vertical jet axis, a recording angle usually not feasible in volcanic environments. We used Mean Cross Correlation Maxima (MCCM) to determine times of highly correlated signal across the array elements with a threshold of 0.8. Periods of highly correlated waveforms are characterized by sustained, low-amplitude signal with a spectral peak around 8-10 Hz. The signal is easily buried in wind noise and in the infrasound as well as audible bands. We have also observed a reduction in power and decrease in correlation between certain array elements suggesting the influence of topography along the propagation path.

ERUPTION TRENDS IN THE KURILE, KAMCHATKA, AND ALASKAN ARCS

Jonathan Dehn[1,2], Peter Webley[1,2], Anna Worden[1]
[1] *Geophysical Institute University of Alaska Fairbanks, Fairbanks, Alaska, 99775, USA.*
[2] *V-ADAPT Inc., 903 Koyukuk Dr. Fairbanks Alaska, 99775, USA.*

Volcanic activity in the Northern Pacific Arcs have been recorded consistently over the last 40 years. Taking activity reported in eruption logs and satellite data, including thermal activity as well as plumes, the database was divided up into quarters (Jan-Feb-Mar, Apr-May-Jun, Jul-Aug-Sep, Oct-Nov-Dec) from January 1986 to present showing volcanic activity. This should help account for gaps in coverage and not preferentially weight volcanoes with better monitoring coverage. It also picks out larger eruption events and overlooks small periods of unrest. The analysis of the 40 years of eruption data show over 400 sequences of ash producing eruptions with some volcanic activity occurring 83% of the time. A total of 35 volcanoes have produced this activity, but the top 6 volcanoes (in order, Shiveluch, Bezymianny/Cleveland, Kliuchevskoi, Karymsky, and Pavlof) are responsible for 65% of all the volcanic activity. Shiveluch is active nearly a third of this time, and continually since 2011 (over five years at this time). Shiveluch is also most responsible for air traffic disruption. Dome building volcanoes are slightly more active that stratocones in this region, due to the activity at Shiveluch and Bezymianny (77 total quarters combined). The 4 stratocones typically have very symmetrical eruption cycles around the climax, long lead-ups leading to protracted eruptions (e.g Kliuchevskoi 2010-2011), and sudden eruptions being very brief (e.g. Pavlof, 2016). The Kamchatka Peninsula is more active by nearly a third over the Alaska/Aleutian Arc (148 to 105 volcano quarters), yet has only 10 active volcanoes during this period compared to the 20 in Alaska. The Northern Kurile Arc is an order of magnitude less active that the Alaska/Aleutian Arc.

Overall the number of quarters with plumes detected has remained stable over the time period, suggesting that the monitoring effort is catching most if not all of the ash-producing explosions that provide a risk to air travel. However, the precursory activity, in the form of thermal anomalies, fluctuates over the years, and generally are greater in recent years likely representing more attention being paid to this phenomena. There is some indication in the last three years little thermal activity was missed and we have reached effective monitoring levels. Over 66% of the thermal activity was followed by an ash-producing explosion, however almost one half of the ash producing eruptions showed no thermal warning prior to the event.

Fully a third of the quarters had air travel disruption due to volcanic activity in the last 40 years. This was rare in the early years but as monitoring and level of air traffic have increased, in the last 5 years fully 50% of the quarters have air travel disruption. Since the global awareness of air travel disruption from Eyjafjallajökull in 2010, even more quarters have shown air travel disruption.

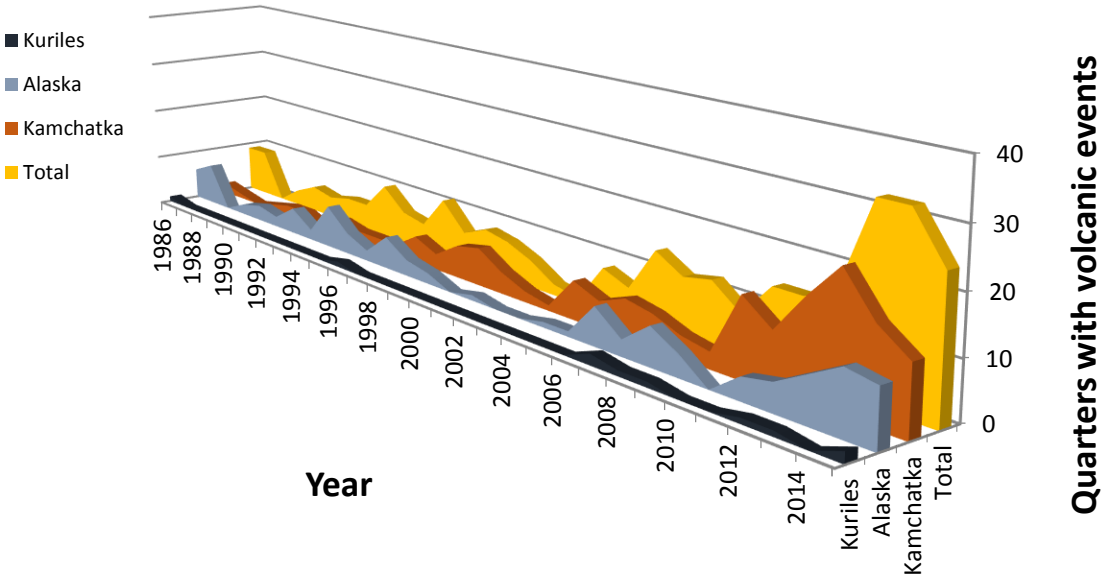
Kuriles
Alaska
Kamchatka
Total
1986
1988
1990
1992
1994
1996
1998
2000
2002
2004
2006
2008
2010
2012
2014
Year
0
10
20
30
40
Kuriles
Alaska
Kamchatka
Total
Quarters with volcanic events

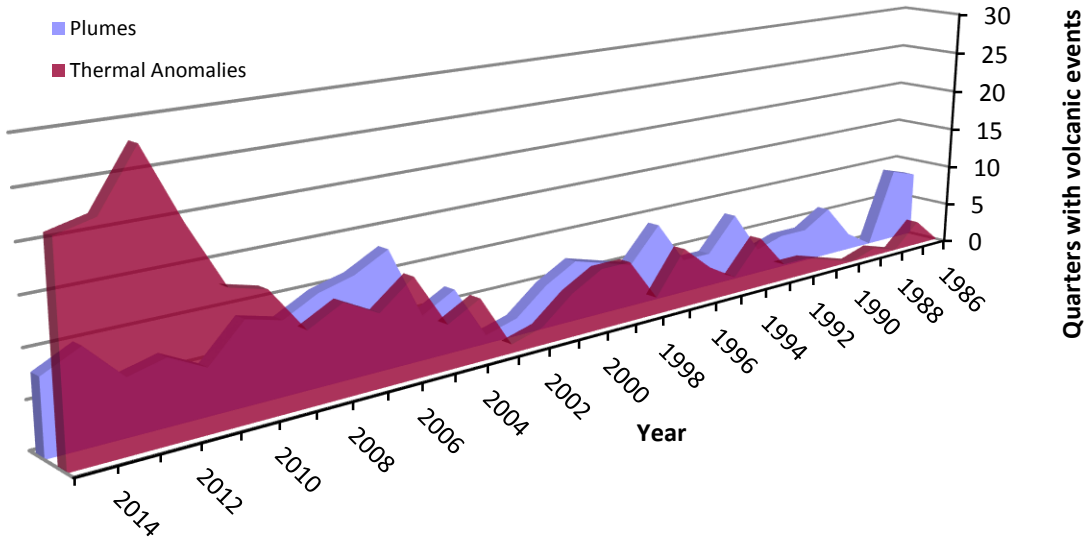
Plumes
Thermal Anomalies
0
5
10
15
20
25
30
1986
1988
1990
1992
1994
1996
1998
2000
2002
2004
2006
2008
2010
2012
2014
Year
Quarters with volcanic events

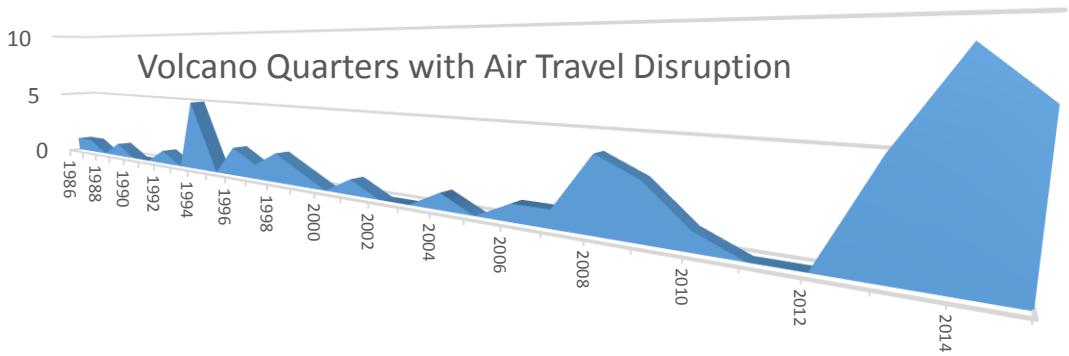
Volcano Quarters with Air Travel Disruption
0
5
10
1986
1988
1990
1992
1994
1996
1998
2000
2002
2004
2006
2008
2010
2012
2014

INCREASING OF GAS BUBBLINGS AT WARIISHI FLOWING SPRING, CENTRAL JAPAN, PRIOR TO THE 2014 ONTAKE VOLCANO ERUPTION

Shigeki Tasaka∗ †, Masaya Matsubara†, Yasuhiro Asai∗, and Fumiaki Kimata

[1] *Tono Research Institute of Earthquake Science, ADEParth & Space Sciences, Japan.*
[2] *Information and Multimedia Center, Gifu University, Gifu, Japan.*

Wariishi flowing spring is located in Niigata-Kobe Tectonic Zone (NKTZ) in central Japan, and artesian aquifer of 45 degrees are flowed from the 850 m underground with periodic spring. Continuous monitoring of temperature and discharge volume was started at Wariishi Spa, to make clear their change by seismic and ground deformation activities in the NKTZ in 1998 by Gifu University. An electromagnetic flowmeter is employed to measure the discharge with sampling rates 1 to 20 Hz.

As results, hot springs of about 40 litters per minute is discharged including of two intermittent spring with periods of about two hours and three minutes. Co-seismic raising discharges few to 35 litter/minutes are observed 72 times at the big earthquakes in Japan and large earthquakes in the world in the late 12 years since 2004 (Fig.1). Raising discharges are decreasing gradually with time. In contrast to discharge, the frequencies of intermittent spring are shortening to be 20-minute at the co-seismic rising discharge, and they are coming buck to be 120-minute gradually.

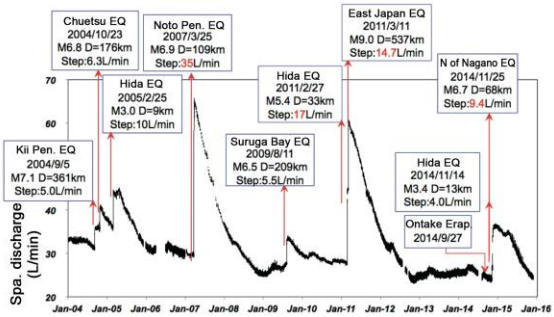

Fig.1 Time series of hot spring discharge at Wariishi

On September 27, Ontake volcano, an active volcano locates 50 km southward from Wariishi spa, was erupted. There is no change of discharge volume and intermittent spring frequencies at the eruption. Discharges are steady about 25 L/min, and it is increasing up to 38 L/min at the M6.7 Earthquake in Northern Nagano on November 25. The frequency of intermittent spring was also steady about 100 to 120 minutes in the period.

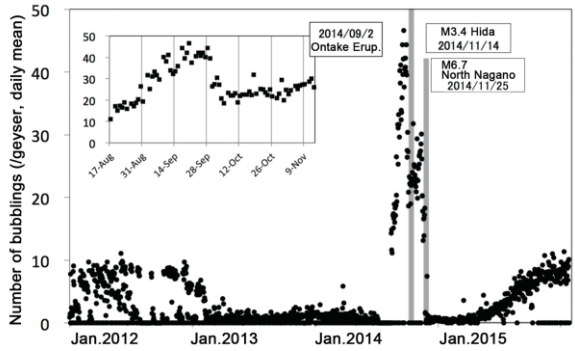

Fig.2 Number of bubbling between intermittent spring at Wariishi

Additionally, small bubbling was detected few times between main intermittent spring with a period of two hours by an electromagnetic flowmeter. Nevertheless, bubbling was increasing in August 2014, and it raised over 40 times in the middle of September 2014 (fig.2). After then bubbling was decreasing, and it was few times at the end of November. It is the most remarkable changes since 2012. As it is no definite change of discharge volume and frequency of intermittent spring in Warisihi flowing spring, it is suggested that a bubbling system is provided as the different process from the discharge and spring frequency. In addition, there some changes in the strain field around Ontake volcano and Wariishi spa, and it triggered the bubbling.

REMOTE SENSING ANALYSIS OF THE 2015-2016 SHEVELUCH VOLCANO ACTIVITY

P. W. Webley[1], O. Girina[2], J. S. Shipman[1]

[1]*Geophysical Institute, University of Alaska Fairbanks, Fairbanks, Alaska, 99775, USA*

[2]*Institute of Volcanology and Seismology, Petropavlovsk-Kamchatsky, 683006, Russia*

E-mail: pwwebley@alaska.edu Phone: +1 907 474-1542 Fax: +1 907 474-7290

Sheveluch is one of the most active volcanoes of Kamchatka. Sheveluch volcanic edifice has a complex structure, including the Late Pleistocene Old Sheveluch stratovolcano (3.283 km) complicated on its western flank with a later lava field (Baidarny ridge) and the 9-km-wide caldera enclosing Holocene active Young Sheveluch (2.8km) eruptive center. In addition, several Holocene domes have been emplaced at the western slopes of Old Sheveluch.

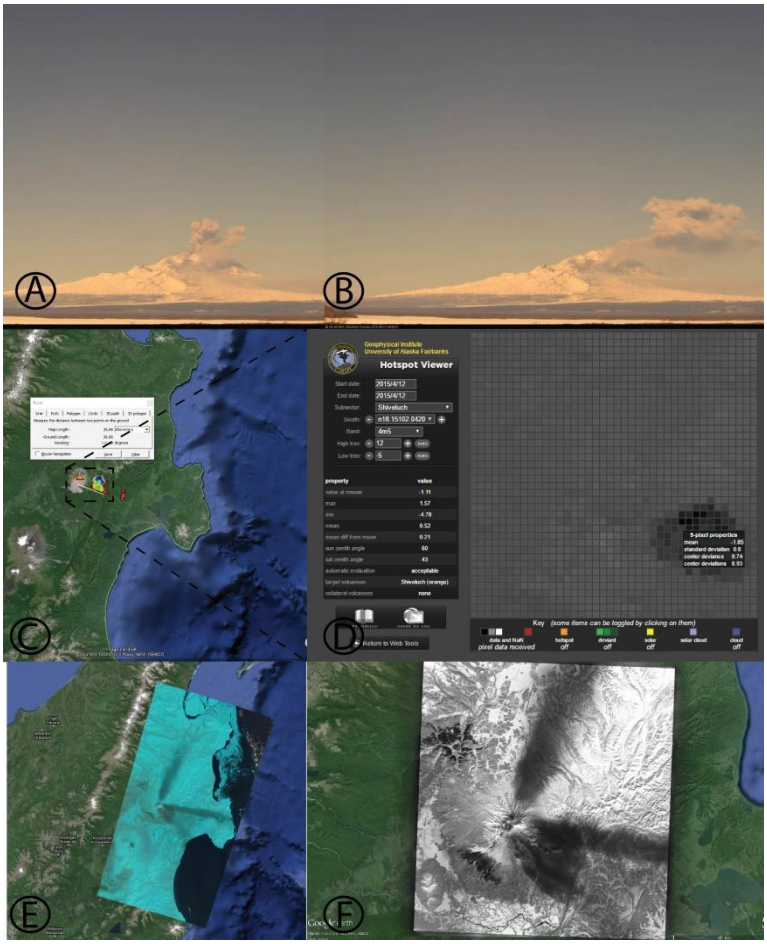

Figure 1. *Webcam snapshots of the eruption on April 12, 2015 at 03:48 (A) and 03:59 UTC (B) respectively, as well as the NOAA AVHRR BTD from 04:20 UTC (C) and zoomed in around the volcano (D). Also included is an example of the high spatial resolution data from LANDSAT 8 on April 17, 2015(Band 7, E and Band 3, F).*

Two large Plinian eruptions of Sheveluch occurred in 1854 and 1964 [1]. In 1980, a new lava dome began growing into the 1964 explosive crater and continues at present. Strong paroxysmal explosive eruptions connected with a growth of the lava dome, occurred in 1993, 2001, 2004, two in 2005, 2007, and 2010 [2].

Significant explosive activity of Sheveluch volcano occurred in the first half of 2015 with explosions sending volcanic ash up to 7-12 km above sea level (ASL), and ash plumes extended more than 900 km from the volcano [3]. These events occurred on January 7, 12, and 15; February 1, 17, and 28; March 4, 8, 16, 21-22, and 26; and April 7 and 12, see Figure 1A - 1D, with ashfall seen in high resolution data from April 17 (Figure 1E and 1F). Ashfall also occurred at Ust'-Kamchatsk on March 16, and Klyuchi on October 30, 2015. Strong and moderate hot avalanches, mainly from the lava dome, were observing in the second half of 2015.

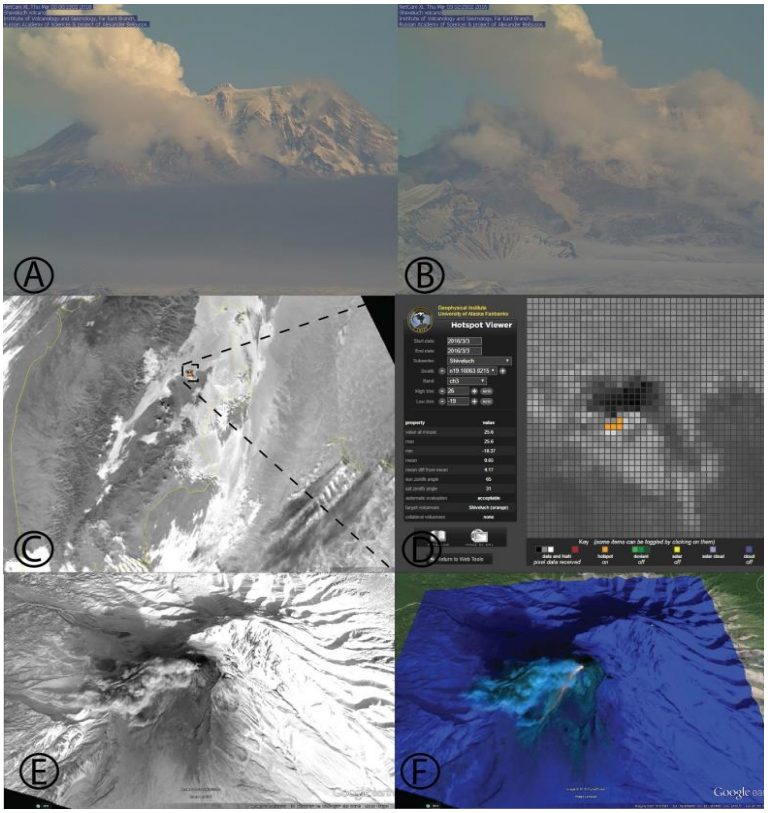

Figure 2. *Webcam snapshots of on March 3, 2016 activity at 00:13 (A) and 02:15 UTC (B) respectively, as well as the NOAA AVHRR MIR from 02:15 UTC (C) and zoomed in around the volcano (D). Also included is an example of the high spatial resolution data from LANDSAT 8 at 00:13 UTC (Band 8, E and RGB of Bands 765, F).*

In 2016, Sheveluch is still very active as the large lava block continues to grow on the northern part of the dome over the past 11 months (since April 2015). Hot avalanches are continually observed from the western and eastern flanks of the lava dome. Figure 2 shows an example of the finer spatial resolution data from LANDSAT 8 that illustrates a significant thermal signal from a volcanic flow as compared to the coarser spatial resolution advanced very high resolution radiometer (AVHRR) data at 02:15 UTC. The AVHRR data only shows a weak signal while the LANDSAT 8 data clearly captures the flow. Combining these two datasets together can help us to better understand the ongoing activity at Sheveluch.

We will present on how remote sensing data has and is being used to analyze the volcanic plumes and clouds along with the surface activity within the summit crater and at the lava dome. We will show both the coarse spatial, high temporal frequency data often used in real-time monitoring as well as the coarser temporal, higher spatial resolution data to map out the thermal activity at the summit dome. We will illustrate how by combining the datasets together along with ground observations that volcano scientists can obtain a better understanding of the volcanic eruption and evaluate the impact to the local region.

Acknowledgments

We would like to thank the V-ADAPT, Inc. team for access to their MIR and TIR derived products and time series data, as well as the USGS GloVis website for access to ASTER sensor data and the Earth Explorer site for available LANDSAT-8 data. Also we would like to thank KVERT for their monitoring and field observations and the US National Oceanic and Atmospheric Administration for access to the AVHRR data.

References

1. Fedotov, S. A. et al., 1991. Active volcanoes of Kamchatka / Ed. (1). 302 p.
2. Gordeev, E. I., and Girina, O.A., 2014. Volcanoes and their hazard to aviation, *Herald of the Russian Academy of Sciences*, 84, (1). 1-8. doi: 10.1134/S1019331614010079
3. Girina, O.A., Melnikov, D.V., Manevich A.G., et al, 2016. Kamchatka and North Kurile Volcano Explosive Eruptions in 2015 and Danger to Aviation, *Geophysical Research Abstracts*, **18,** doi: 10.13140/RG.2.1.5179.4001.

INFRASOUND AND SEISMIC OBSERVATIONS OF THE MARCH 2016 ERUPTION OF PAVLOF VOLCANO, ALASKA

David Fee[1], Matt Haney[2], Robin Matoza[3], Dave Schneider[2], Peter Cervelli[2], Alex Iezzi[1]
[1]Alaska Volcano Observatory, Geophysical Institute, University of Alaska Fairbanks, 903 Koyukuk Dr, Fairbanks, AK 99775
[2]Alaska Volcano Observatory, U.S. Geological Survey, 4230 University Drive, Anchorage, AK 99508, USA
[3]Department of Earth Science and Earth Research Institute, University of California, 1006 Webb Hall, Santa Barbara, Santa Barbara, CA 93106

On March 28, 2016, Pavlof Volcano, Alaska erupted with little to no warning. The eruption lasted for ~40 hours and produced a sustained ash plume reaching up to 9.5 km altitude that forced the cancellation of over 100 flights in Alaska and Canada. This eruption produced significant seismicity, as well as infrasound that was recorded up to 1300 km away. Of particular note is that the eruption was recorded on the recently deployed EarthScope Transportable Array (TA), a large continental-scale network of co-located seismic and acoustic sensors. The Pavlof eruption is the first to be recorded on the TA. Two other distant infrasound arrays (460 and 1300 km) also recorded the eruption.

Here we present the main features of the seismic and acoustic recordings of the March 2016 Pavlof eruption, with a focus on the remote observations on the TA and infrasound arrays and the relationship between plume height and amplitudes of seismic and acoustic data. We use a coherence-based processing technique to detect acoustic waves on the TA and a new coherence-weighting technique to reduce noise during periods of low coherence. We also discuss the potential to use the TA and remote infrasound arrays to detect, locate, and characterize large volcanic eruptions in AK. Lastly, we discuss an intriguing hysteresis phenomenon between the plume height and seismic and acoustic amplitudes, where the plume heights are strongly correlated during periods in which the eruption is intensifying and less correlated when it is declining. Similar hysteresis has been observed in seismicity from river discharge events.

THERMAL REMOTE SENSING AND ASH DISPERSION MODELING OF THE 2016 ERUPTION OF PAVLOF VOLCANO

P. Webley [1], J. Dehn[1], M. Harrild[1], A. Worden[1], D. McAlpin[1]
[1]*Geophysical Institute, University of Alaska Fairbanks, Fairbanks, Alaska, 99775, USA*
E-mail: pwwebley@alaska.edu Phone: +1 907 474-1542 Fax: +1 907 474-7290

Pavlof Volcano erupted on March 28, 2016. Alaska Volcano Observatory (AVO) first released a volcanic activity notice (VAN) at 01:12 UTC on March 28 [1] while the first volcanic ash advisory was released at 01:00 UTC [2]. We captured remote sensing data from geostationary and polar orbiting sensors to determine the nature and characteristics of the airborne eruptive products during the eruption. We demonstrate the usefulness of the coarser spatial resolution data (1 km in the infrared) for event detection and that high temporal-resolution brightness temperature data from the mid- (MIR) and thermal- (TIR) infrared time series can be converted into ash cloud mass loadings using the two band retrieval method [3].

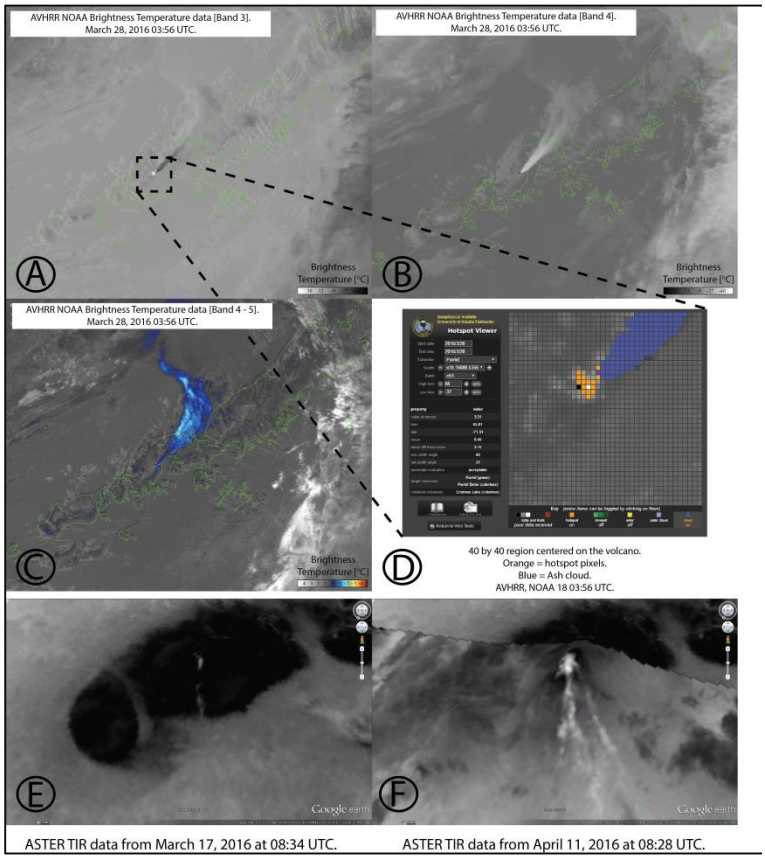

Figure 1. *MIR (A, D), TIR (B), and BTD (C) data from AVHRR on March 28, 2016 at 03:56 UTC along with NASA ASTER emissivity normalized TIR data from March 17 (E) and April 11 (F), 2016.*

Figure 1 shows MIR, TIR, and brightness temperature difference (BTD) data acquired on March 28, 2016 at 03:56 UTC by the Advanced Very High Resolution Radiometer (AVHRR), together with imagery from the Advanced Spaceborne Thermal Emission Radiometer (ASTER) sensor acquired on March 17 and April 11, 2016. The MIR data from 03:56 UTC (1A and 1D) show a thermal signal at the summit while the TIR (1B) and BTD data (1C) show evidence for the dispersing ash plume and cloud. The ASTER data shows weak but elevated temperatures (287K on a background of 260K) on March 17 (1E) and April 11, 2016 (1F) that were unable to elevate the thermal signals seen in the 1 km resolution data in either the MIR or TIR.

In addition to analysis of the remote sensing data we will also evaluate particle size distributions (PSD) and mass eruption rates using the Puff Lagrangian Volcano Ash Transport and Dispersion (VATD) model [4]. We use a default PSD as well as coarse and fine initial PSD's. We will evaluate the best method to determine the mass eruption rate during an eruptive event. Our final modeling output will include a probabilistic approach that illustrates the capability for near real-time simulations. Figure 2 shows a model simulation from the Puff

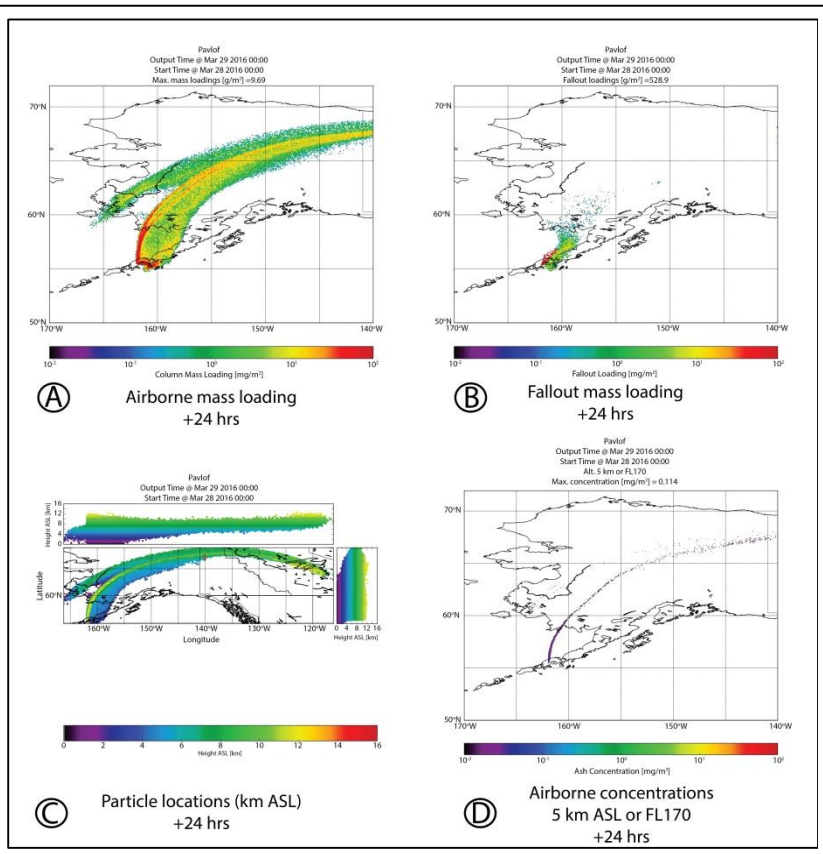

Figure 2. *Puff VATD modeling for Pavlof Volcano, Alaska. (A) Total mass loading (mg/m^2); (B) fallout (mg/m^2); (C) ash particle locations by altitude (km, ASL); and (D) airborne concentrations (mg/m^3) at 5 km ASL or FL17).*

VATD model from March 28 – March 29, 2016. This illustrates how the model can be used to document the ash location, mass loadings, fallout, and ash concentrations at specific altitudes.

In documenting the time series data, we use the BTD data to determine the direction, length, and total mass content of the cloud at the time the first saturated MIR signal is acquired. For the Puff VATD modeling, we illustrate how the choice of initial PSD and eruption rate method are important until more empirical observational data is obtained.

Our work shows how the coarser spatial resolution data can be used to analyze the ongoing volcanic activity and to task the high resolution data for analysis at a finer scale. Our work also illustrates the need for a probabilistic modeling approach to better evaluate the ash mass loadings and ash concentrations.

Acknowledgements

We would like to thank the V-ADAPT, Inc. team for access to their MIR and TIR derived products and time series data, as well as the USGS GloVis website for access to ASTER sensor data and the Earth Explorer site for available LANDSAT-8 data.

References

1. Alaska Volcano Observatory (AVO), 2016. AVO Volcanic Activity Notice, viewed April 13, 2016. https://www.avo.alaska.edu/activity/report.php?type=3&id=82161&mode=hans.
2. Anchorage Volcanic Ash Advisory Center (VAAC), 2016. VAA FVAK21 PAWU 280108, last viewed April 11, 2016 http://vaac.arh.noaa.gov/data/VAA/FVAK21PAWU_1603271710
3. Wen, S., and Rose, W. I., 1994. Retrieval of sizes and total masses of particles in volcanic clouds using AVHRR bands 4 and 5. *JGR: Atmospheres*, **99** (D3), 5421-5431.
4. Searcy, C., Dean, K., and Stringer, W., 1998. PUFF: A high-resolution volcanic ash tracking model. *Journal of Volcanology and Geothermal Research*, **80** (1), 1-16.

ESTIMATION OF VOLUME FLUX OF VOLCANIC ERUPTIONS WITH VERY-LONG-PERIOD ACOUSTIC SIGNALS

Taishi Yamada[1], Hiroshi Aoyama[1], Takeshi Nishimura[2], Masato Iguchi[3], Muhamad Hendrasto[4]
[1]*Graduate School of Science, Hokkaido University, Japan.*
[2]*Graduate School of Science, Tohoku University, Japan.*
[3]*Disaster Prevention Research Institute, Kyoto University, Japan.*
[4]*Center for Volcanology and Geological Hazard Mitigation, Indonesia.*

Volume flux (or mass flux) of volcanic eruptions is a crucial parameter for the eruption dynamics and assessment of eruption scale. There are several methods to estimate the volume flux during volcanic eruptions, including analysis of infrasound data (e.g., Johnson et al., 2004; Vergniolle et al., 2004). The advantage of adopting infrasound data for flux estimation is that most active volcanoes in the world have been monitored with infrasound network at near to middle field and the acquisition of data can be done in real time.

In 2012–2013, we have conducted broadband seismic and infrasound observations of Vulcanian eruptions at Lokon-Empung volcano in Indonesia. The temporal observation network consists of 4 broadband seismometers (Trillium 40, Nanometrics, 0.025–50 Hz) and an infrasound microphone (SI 102, Hakusan, 0.05–1500 Hz). About 80 % of observed vulcanian explosions are followed by the continuous ash emissions, which is recognized as continuous vibration in the seismic and infrasound waveforms. We find a clear pulse at the onset of the continuous vibration consisting of Very-Long-Period (VLP, > 10 s) signals of infrasound and vertical velocity waveforms. The apparent propagation velocity of the VLP pulse at each station can be explained by the sound velocity from the vent. Moreover, the generation of the VLP pulse approximately coincides with the appearance of ash plume from the vent. Hence, it is regarded that the VLP pulse is induced by pressure wave accompanying the formation of the ash plume. Such the VLP signals accompanying eruptions also can be seen in microbarograms of ash emission eruptions at 3 Japanese volcanoes (Shinmoedake, Aso, Kuchinoerabu) in 2011-2016. National research Institute for Earth science and Disaster prevention (NIED) has operated several barometers (AP 270, Koshin; PTB 100, Vaisala) at 2-7 km from the vent at those volcanoes. Since the microbarogram data is recorded at 1 Hz, the VLP signals are properly recorded microbarograms accompanying eruptions.

We estimate the volume flux during those eruptions with the VLP signals on infrasound records and microbarograms. Largely there are two methods to describe the source of infrasound signals accompanying eruptions; monopole and dipole approximations (Johnson et al., 2014; Vergniolle et al., 2004). The volume flux estimated by the monopole approximation and observed plume height show well agreement with the empirical relationship between these two parameters (e.g., Sparks et al., 1997). Our study suggests that the volume flux can be estimated with infrasound and microbarogram data in quasi real time due to its simplicity of waveform processing.

NUMERICAL MODEL OF TEMPORAL CHANGES IN MAGNETIC TOTAL FIELD AND GROUND DEFORMATION DUE TO HYDROTHERMAL SYSTEM IN VOLCANOES (1). - A CASE STUDY ON TOKACHI-DAKE VOLCANO, JAPAN

Ryo Tanaka[1], Takeshi Hashimoto[1], Tsuneo Ishido[2], Nobuo Matsushima[2]

[1]Hokkaido University, Japan
[2]National Institute of Advanced Industrial Science and Technology (AIST), Japan

Localized temporal changes in the magnetic total field and ground deformation are often observed at volcanoes that have hydrothermal system within. At Tokcahi-dake volcano, one of such volcanoes in central Hokkaido, Japan, continuous magnetic field changes accompanying ground inflation at a shallow depth have been observed. At this volcano, small phreatic explosions took place commonly among major magmatic/phreatomagmatic eruptions in recorded history (JMA, 2013). Repeated magnetic total field surveys since 2008 revealed demagnetization beneath 62-2 crater between 2008 and 2009 (Hashimoto et al., 2010). Besides, the baseline changes by GPS suggested a localized inflation beneath the crater after 2007 (JMA, 2015). Assuming the thermomagnetic effect, Hashimoto et al. (2010) proposed a possible mechanism for such changes. They suspected that steam ascending along the conduit experienced phase change at a shallow depth, releasing latent heat and flowing back as liquid to form a hydrothermal reservoir. They also suggested that increase in heat supply from depth is not essential for the demagnetization in case that heat discharge rate from the crater has been reduced for some reasons. In this study, we verify such a conceptual model by using a numerical simulation of hydrothermal system.

In general, phreatic explosions need substantial amount of water, cap-rock structure that confines pressure, heat supply and increase in pressure for a hydrothermal reservoir to flush through an abrupt phase change. However, it remains an open question whether such structure and processes bring about observable magnetic changes and/or ground deformation preceding to a phreatic eruption. We addressed the following working hypothesis to model Tokachi-dake as a case study. (1) There is a cap-rock structure with a narrow crack below 62-2 crater. (2) Gases through the crack are discharged as plumes from the crater. (3) Decreasing permeability of the crack causes increase in temperature and pressure around the cap-rock structure. We tried to examine the hypothesis using the numerical code "STAR" with the equation-of-state "HOTH2O" (Pritchett, 1995). It enabled us to calculate the heat and mass flow rate of H_2O (gas, liquid and two-phase) in porous media. The calculation region was set as approximately the cross-section passing the summit of Tokachi-dake, 62-2 crater and hot spring located on halfway up the mountain. Firstly, we estimated the background permeability of rock constituting the volcano, which gives a plausible water table. As boundary conditions, constant temperature and pressure conditions were applied to the ground surface and downstream vertical boundary, thermally-insulating and impermeable conditions were applied to the bottom and upstream vertical boundaries. A constant rate of precipitation was injected from the ground surface. A constant heat flow was supplied from the bottom. Subsequently, we reproduced the fumarolic discharge from the crater and the hot spring located in the middle of the slope by providing thermal water from the bottom just beneath the crater. We also introduced a high permeability column as a vertical conduit connected from the volcanic input at the bottom to the crater, as well as a horizontal channel connected to the hot spring. In addition, the low permeability cap-rock with a narrow crack was introduced below the crater. Finally, we changed the crack permeability to observe changes in temperature and pressure of the system. We confirmed that the decrease of the crack permeability caused the increase in temperature and pressure around the cap-rock structure. These results suggested that the working hypothesis

was at least self-consistent. In the next step, we will quantitatively investigate the system's responses by comparing the changes in temperature and pressure beneath the crater from the numerical simulation to the observed temporal change in the magnetic total field and ground deformation.

EVALUATING THE INFLUENCE OF DATA GAPS IN THE ANALYSIS OF POSITION TIME-SERIES DERIVED FROM GPS CONTINUOUS STATIONS

Rui Fernandes[1], Machiel Bos[1], Rafael Couto[1], J. Freymueller[2], Maksim Tretyakov[3]
[1] *SEGAL (UBI/IDL), Covilhã, Portugal.*
[2] *University of Alaska, Fairbanks, Alaska, USA.*
[3] *NEFU, Yakutsk, Russia.*

Time-series derived from CORS (Continuous Operating Reference Stations) GPS stations have significant advantages when compared with campaign-type solutions. In addition to reduce the potential error sources (e.g., offsets due to reoccupation accuracy and/or different receivers and antenna), they permit to extract more information concerning the different geophysical signals, like the secular motions, periodical (annual or semi-annual) signals, co-, post-seismic or volcanic deformation.

However, particularly at very remote locations, it is often difficult to ensure the continuous operation of the stations due to logistic and/or financial issues: lack of communication that prevent the early detection of problems; transportation, extreme weather events; equipment failures, etc.

This was the case of the Bezymianny GPS network, which has been installed in 2006. The network consisted of 10 permanent sites distributed around the volcano edifice. However, due to the extreme difficult conditions, most of the time-series contain large periods with no observations (mainly caused by power failures).

In this work, we investigate the influence of such data gaps on the estimation of the geophysical signals, namely secular motions and periodical signals. We use a network of global stations to determine threshold values relative to the percentage of data gaps (in terms of length and number) on the time-series that start to change significantly the estimated parameters.

Finally, we also apply these values to the time-series obtained for the Bezymianny GPS network in order to quantify how much the existing data gaps have influenced the estimated solutions for the data acquired between 2006 and 2010.

TSUNAMI

(ORAL PRESENTATIONS)

HYPOTHETICAL TECTONIC TSUNAMI SOURCES ALONG THE EASTERN ALEUTIAN ISLAND ARC AND ALASKA PENINSULA FOR INUNDATION MAPPING AND HAZARD ASSESSMENT.

Dmitry Nicolsky[1], Elena Suleimani[1], Jeffrey Freymueller[1], and Richard Koehler[2]

[1]Geophysical Institute, University of Alaska Fairbanks, Fairbanks, AK 99775, USA
[2]University of Nevada, Reno, Nevada, USA

The Alaska Earthquake Center conducts tsunami inundation mapping for coastal communities along the Alaska Peninsula and eastern Aleutians. Tsunami threatened communities are distributed along several segments of the Aleutian Megathrust, each segment is characterized by a unique seismic history and tsunami generation potential. A critical component in the tsunami modeling is accurate identification and characterization of potential tsunami sources.

Our study area extends from the eastern half of the 1957 rupture zone to Kodiak Island, covering the 1946 and 1938 rupture areas, the Shumagin gap, and the western part of the 1964 rupture area. We employ data on the slip deficit along the Aleutian Megathrust, based on GPS campaign surveys, analysis of the seismic reflection data across the arc, the Slab 1.0 interface surface, empirical magnitude-slip relationships, and the numerical code that distributes slip among the subfault elements. We define hypothetical asperities along the megathrust and in down-dip direction. We then calculate coseismic deformations and perform a set of sensitivity model runs to identify coseismic deformation patterns resulting in highest runup at a given community. Because of the extra fine discretization of the interface, we prescribe variable slip patterns, both along strike and in the down-dip directions. We show that the near-field tsunami runup in target communities is sensitive to variability of slip along the rupture area.

We perform simulations for each source scenario using AEC's numerical model of tsunami propagation and runup, which is validated through a set of analytical benchmarks and tested against laboratory and field data. Results of numerical modeling combined with historical observations are compiled on inundation maps and used for site-specific tsunami hazard assessment by local emergency planners.

REGIONAL TSUNAMI HAZARD MAP FOR COMMUNITIES ON ALEUTIAN ISLANDS AND ALASKA PENINSULA

Elena Suleimani[1], Dmitry Nicolsky[1], and Richard Koehler[3]
[1]*Geophysical Institute, University of Alaska Fairbanks, Fairbanks, Alaska, USA.*
[2]*University of Nevada, Reno, Nevada, USA.*

The Alaska Earthquake Center conducts tsunami inundation mapping for coastal communities in Alaska by assessing potential tsunami sources and modeling the tsunami wave dynamics. Over the past two decades, high-resolution tsunami inundation maps were developed for more than 20 communities. In these studies, we performed numerical modeling of tsunami waves for each community using high-resolution digital elevation models (DEMs) of combined bathymetry and topography, which have been verified with local real-time kinematic GPS surveys. The potential inundation according to various tsunamis was simulated with the best available high-resolution data with a typical spatial resolution of 15 m. We also performed source sensitivity studies to determine a possible slip distribution for the worst-case credible tsunami events. In addition, multiple constraints such as regional seismicity, tectonic processes, and geodetic and paleotsunami data were taken into account.

In the regional tsunami hazard assessment we use a different approach, because the currently available DEMs of many Aleutian communities lack high-resolution bathymetry and topography data and do not satisfy the requirements for high-resolution numerical modeling of the tsunami inundation. We follow the National Tsunami Hazard Mitigation Program (NTHMP) guidelines for determining tsunami hazard zones in areas that have either low risk due to small population size and minimal infrastructure vulnerability, or are not scheduled to receive high-resolution tsunami inundation maps in the near future.

To develop a regional tsunami hazard map, we consider three potential ruptures with a uniform slip distribution along the strike, which are positioned on the Alaska–Aleutian subduction interface. The three sources differ in the down-dip slip distribution pattern such that the depth range at which the maximum slip occurs varies from the shallow region near to the trench to the deeper parts of the plate interface. All ruptures have the same extent, which is determined by the location of communities and constrained by the seismic moment. For each community, we simulate a limited number of significant potential tsunamis and develop an approximation to a tsunami hazard map, which is needed to support informed decision making in the event of a tsunami, and can also help with advance development of tsunami evacuation strategies.

AUTHORS INDEX